ABSTRACTS

Oral and Poster

Abstracts were presented at the first annual meeting of the Society for Cardiovascular Magnetic Resonance in Atlanta, GA, January 30–February 1, 1998.

NC100150 Injection: A New Intravascular MR Contrast Agent for Morphological and Functional Assessment of the Heart

Kirk S. Tarlo,[1] Michael Jerosch-Herold,[2] Abdul Mansoor,[2] Shoto Gurchumelidze,[2] Myra Unress,[2] Yimei Huang,[2] Ed McFalls,[3] Norbert Wilke.[2] [1]*Nycomed Inc., Wayne, PA;* [2]*University of Minnesota, Dept. of Radiology, Center for MR Research;* [3]*VA Medical Center, MN*

NC100150 injection is a highly intravascular, superparamagnetic iron oxide contrast agent intended for MR angiography and perfusion imaging. It has the advantage of a long blood half-life with minimal toxicity. The agent is completely cleared from blood by tissues in the reticuloendothelial system. After administration at the clinical imaging dose, NC100150 injection has not been shown to induce symptoms of acute or chronic toxicity. The purpose of this study was to demonstrate the preclinical efficacy of NC100150 injection in cardiac imaging. Using a pig model, artificial coronary stenoses were induced at the LAD. Multiple intravenous injections of NC100150 injection (final dosages of 0.5, 1, 2, 3, 4, 5, and 6 mg Fe/kg) were administered to four pigs. The pigs (30–45 kg) were imaged using T1-weighted, quantitative MR first-pass perfusion imaging (TR/TE 8/2.7) with retrospective gating and navigator echoes on a VISION 1.5 T (Siemens) scanner equipped with phased array coils. Similarly treated pigs were evaluated by x-ray angiography, radiolabeled microspheres, and PET imaging. Inductively coupled plasma atomic emission spectroscopy measurements were obtained to correlate iron oxide blood levels to T1 signal changes. At a bolus dosage of 0.5 mg Fe/kg, absolute quantification of the MR perfusion data yields a correlation of $r = 0.96$ when compared with microspheres. A dosage of 1–2 mg Fe/kg (TE dependent) was necessary for optimal signal enhancement during CA equilibrium measurements and coronary angiography. Coronary stenoses of >65% can be detected and signal enhancement increased significantly ($p < 0.001$) postcontrast. For gradient-echo cine MR images (TE 4.8 ms), the optimal blood pool signal enhancement for better endocardial border definition was achieved using a dosage ≤ 4 mg Fe/kg. Larger dosages showed signal decrease. NC100150 injection clearly enhances cardiovascular MR imaging using standard sequences. Absolute quantification of myocardial blood flow and volume is possible. These preliminary preclinical data suggest NC100150 injection is useful and should be further evaluated in clinical trials of the functional and morphological assessment of the heart.

Assessment of Dynamic Cardiomyoplasty Mechanics Using MRI with Tissue Tagging

A.S. Blom, J. Pilla, L. Dougherty, H.J. Patel, S.V. Pusca, Q. Yuan, V.A. Ferrari, M.A. Acker, L. Axel. *Philadelphia, PA*

The beneficial effects of dynamic cardiomyoplasty (CMP) on left ventricular function in congestive heart failure remain incompletely understood, in particular, the relative roles of contraction augmentation and limitation of ventricular dilatation. MRI with tissue tagging (1) can noninvasively assess regional mechanical cardiac function. Using this technique, values for principal strains can be calculated, which much more directly reflect regional function than other methods, such as echocardiography and hemodynamics. Prior studies using tagged MRI to assess CMP have examined only global tag displacements (2). In this study, we used tagged MRI to assess regional strain and displacement in a canine model of CMP.

Three mongrel dogs were rapid ventricular paced (RVP) (230 bpm) for 10 weeks; after 4 weeks of RVP, a left anterior CMP was performed. The muscle wrap was dynamically stimulated for 1 year after RVP, allowing ventricular function to reapproach baseline values. The dogs were then imaged in a 1.5 T whole body clinical MRI system (GEMS). High-resolution images were acquired using the following parameters: TR/TE 8.8/2.1 ms; FOV 16–18 cm; tag spacing 4–5 mm; 256 × 128 acquisition matrix interpolated to 256 × 256. Images were acquired during unstimulated and stimulated states using a custom MRI stimulating system. Quantitative 2-D regional image analysis was performed with a custom program, SPAMMVU (3). The heart was divided into four regions: anterior, posterior, septal, and lateral. Maximal and minimal principal strains (λ_1 and λ_2) and displacement (D) were determined and pooled for each region.

λ_1 and λ_2 were unchanged in any of the regions between unstimulated and stimulated states (p = NS). Values for D did not change for the septal region (p = NS); D increased significantly in the other three regions (posteroseptal, posterolateral, and anterolateral; $p < 0.05$).

We showed no significant strain changes associated with dynamic stimulation in CMP. Therefore, the stimulation seems to result primarily in global translation of the heart rather than augmented contraction.

References

1. Axel L, Dougherty L. MR imaging of motion with spatial modulation of magnetization. Radiology, 1989; 171:841–845.
2. Cho PW, Levin HR, et al. New method for mechanistic studies of cardiomyoplasty: three-dimensional MRI reconstructions. Ann Thorac Surg, 1994; 57:1605–1611.
3. Axel L, Bloomgarden DC, et al. SPAMMVU: a program for analysis of dynamic tagged MRI. Proceedings of the Society of Magnetic Resonance in Medicine, 1993, p. 724.

Measurement of Regional and Transmural Variation in Left Ventricular Myocardial Motion Using 3D Velocity-Encoded Cine MR Imaging

R.J. van der Geest, H.W.M. Kayser, E.E. van der Wall, A. de Roos, J.H.C. Reiber. *Leiden, The Netherlands*

Three-dimensional velocity-encoded cine MRI (3D VEC-MRI) was used to study the left ventricular (LV) wall motion patterns in different anatomical regions and transmural locations in a population of 12 healthy volunteers (mean age 34; one female). In a midventricular short-axis slice, VEC-MRI was performed using velocity encoding in three orthogonal directions with a venc of 30 cm/s. The field of view was 300 mm, the slice thickness 8 mm, the flip angle 20°, whereas the scan matrix of 128 × 256 was reconstructed to an image matrix of 256 × 256. Retrospective gating was used to acquire 29 phases over the complete cardiac cycle.

The LV myocardium was divided into three equally sized anatomical regions. For each pixel within the myocardium, velocity was measured in radial (RAD), circumferential (CIRC), and through-plane direction (Z), whereas the anatomical region and transmural location (on a scale of 0–1; 0 at epicardial and 1.0 at the endocardial margin) of the pixel were recorded. Results were averaged per individual cardiac

phase to construct graphs showing the myocardial velocity as a function of time for each of the three defined velocity directions.

Figure 1 shows the average myocardial velocity in RAD, CIRC, and Z directions as a function of the phase within the cardiac cycle. Figure 2 shows the radial myocardial velocities as a function of time for each of the three anatomical regions separately. The largest transmural differences in velocity were seen for the radial direction as shown in Fig. 3.

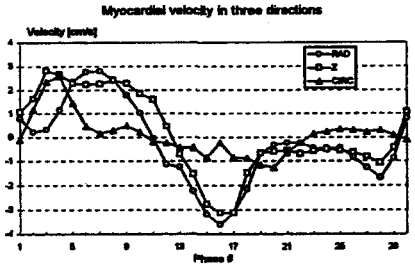

Figure 1

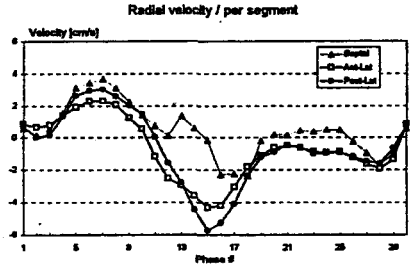

Figure 2

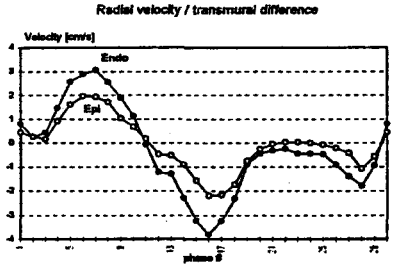

Figure 3

The observed patterns of myocardial velocity clearly demonstrate that the motion of the myocardium in radial and apical directions follows similar patterns. The septal region follows a markedly different radial velocity pattern than the other two anatomical regions. The transmural gradient in radial velocity from epicardium to endocardium observed in this study is in agreement with the known systolic wall thickening and diastolic wall thinning.

20–35% Errors in LV End Diastolic Volume Estimates Using Fastcard

A. Arai, C. Gangireddy, M. Abouasali, S. Wolff. *Bethesda, MD*

Purpose: We describe mechanisms that can distort left ventricular end diastolic volume (LVEDV) estimates by 20–35% using breathhold segmented k-space GRE cine sequences.

Methods: LV time volume curves were measured in 22 patients with hypertrophic cardiomyopathy and 20 normal volunteers. Studies were performed on a 1.5-T GE Echospeed Horizon scanner. The complete cardiac cycle was imaged with a prospectively segmented, retrospectively sorted ECG-gated cine GRE sequence (1). Typical imaging parameters were as follows: flip angle 15, TR 10–12 ms, TE 4–6 ms. Images had 1.9 × 1.9-mm spatial resolution, 60-ms temporal resolution, and 20 images were reconstructed per cardiac cycle. Images were manually traced, or semiautomatic traces were edited manually for each image.

Results: Underestimation of LVEDV occurred in nine normal volunteers and eight patients with HCM when using the first image after the trigger to define end diastole. LVEDV was underestimated on average by 14 ± 3% in the HCM group (maximum 36%) and by 8 + 1% in the normal volunteers (maximum 18%). Most of these underestimations were a result of the first image after the trigger actually representing early systole. In three normal volunteers, apparent loss of LV volume throughout diastole appeared due to loss of contrast between myocardium and blood near the papillary muscles. This effect was eliminated by gadolinium contrast. A time volume curve from a volunteer is shown in Fig. 1 before and after contrast.

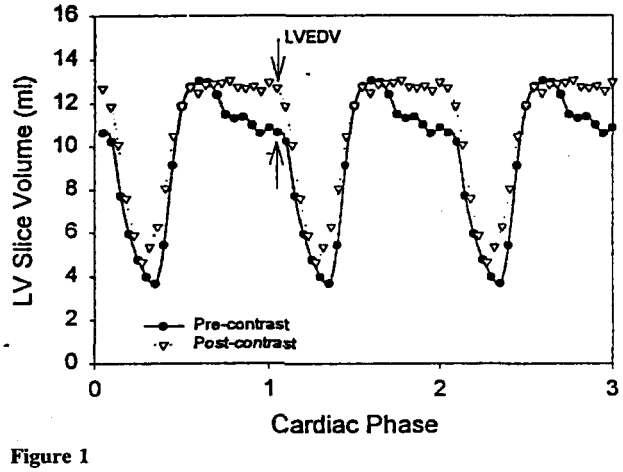

Figure 1

Discussion: Breathhold segmented k-space GRE imaging underestimates LVEDV in 39% of studies when using the first image after the trigger. The magnitude of these errors ranges up to 36% of LVEDV and thus can lead to large errors in basic measurements, such as ejection fraction. Most of these errors are related to trigger delays. A less common mechanism was seen in three normal volunteers with low heart rates. Because the T1 of blood and myocardium are relatively close, blood–myocardial contrast significantly depends on inflow of nonsaturated blood. Because of the restriction of blood movement between the mitral valve and the LV wall, there is substantially less inflow-related contrast in this part of the blood pool.

Reference

1. Feinstein JA, Epstein FH, Arai AE, Foo TKF, Balaban RS, Wolff SD. Using cardiac phase to order reconstruction (CAPTOR): a method to improve diastolic images. JMRI (in press).

Comparison Between 2D and 3D Methods for Noninvasive Assessment of Left Ventricular Ejection Fraction

M.L. Chuang, R.A. Beaudin, M.F. Riley, M.G. Hibberd, P.S. Douglas, W.J. Manning. *Boston, MA*

Accurate and reproducible measurement of left ventricular ejection fraction (LVEF) is important for clinical assessment of cardiac disease and in monitoring the progress of patients. Breathhold cine MRI has been shown to be accurate and reproducible for LVEF determination, when multiple thin slices are used to cover the left ventricle (LV) in the cardiac short-axis orientation (1), as has three-dimensional (3D) echocardiography (2). In contrast to 2D approaches for measurement of LVEF, these 3D methods do not depend on the validity of geometric formulas for determining the volume of the LV. This study was performed to determine the limits of agreement (and hence 95% confidence intervals) between biplane 2D methods and 3D methods for measurement of LVEF in patients with enlarged and distorted ventricles.

Methods: Fifteen patients (4 women, 11 men, ages 29–65) with dilated cardiomyopathies were evaluated by MRI and echocardiography. For each subject, 2D and 3D echo and biplane (2D) and short-axis stack (3D) MRI examinations were all performed within the space of 3 hr. MRI examination used a segmented k-space breathhold cine sequence (TR 11 ms, TE 5.2 ms, FA 25°, 112 × 256 matrix, 224 × 320-mm² FOV, 6.0–7.5 mm slice thickness) on a Philips Gyroscan NT 1.5-T system using either a 20-cm diameter surface coil or cardiac array coil for RF reception. Echo was performed using a modified Hewlett Packard Sonos 1500 scanner, with custom software for the 3D exam. Volumes by short-axis stack MR (3dMR) were determined by summation of disks and by a minimum-energy deformable shell model for 3D echocardiography (3dE). Biplane MR (2dMR) and echo (2dE) methods used $V = 8A_2A_4/(3\pi L_{min})$, where A_2 and A_4 are the planimetered 2- and 4-chamber LV cross-sectional areas, respectively, and L_{min} is the shorter of the apex-to-base lengths of the two views. Comparisons between imaging methods were assessed by limits of agreement. Group differences were assessed with correction for multiple comparisons at the 0.05 level by two-tailed *t*-test.

Results: There were no significant differences ($p > 0.05$) in LVEF between any methods, which yielded (mean ± SD) 3dMR (43.2 ± 14.8%), 3dE (43.2 ± 4.6%), 2dMR (42.5 ± 15.0%), 2dE (41.2 ± 15.0%). Limits of agreement between the various methods are shown below:

	3dMR vs. 3dE	2dMR vs. 2dE	3dMR vs. 2dMR	3dE vs. 2dE	3dMR vs. 2dE
Mean bias (%)	0.0	1.2	0.7	2.0	2.0
95% ConfInt(%)	5.2	19.8	11.0	13.6	12.4

Conclusions: The mean bias, or systematic over- or underestimation, between the various 2D and 3D MR and echo methods is small, but the 95% confidence intervals are wide when comparing 2D with 3D examinations, regardless of whether MR or echo is used, and very wide (spanning a range of nearly 40 percentage points) when comparing 2dMR with 2dE. Differences between 2D and 3D MRI methods appear to be smaller than the differences between 2D and 3D echo. This may in part be due to the ability of MR to provide any selected image plane, whereas echo can be limited by poor acoustic windows that force the sonographer to select a suboptimal off-axis view in 2dE examinations, leading to poorer estimates of LV volume. Agreement is best (suggesting that the likelihood that a small change in LVEF can be more reliably detected is greater) when comparing serial 3D examinations and worst between the two 2D methods. However, there are benefits to be accrued even when only one of the serial measurements of LVEF in dilated cardiomyopathies uses a 3D technique.

References

1. Sakuma et al. Radiology, 1993; 188:377.
2. Hibberd et al. Circulation, 1966; 94(Suppl):I-687.

Magnetic Resonance Imaging in Diagnostic of Arrythmogenic Right Ventricular Dysplasia: Correlation to Other Diagnostic Modalities

M.G. Lentschig, T. Wichter, P. Reimer, E. Rummeny, G. Breithardt. *Muenster, Germany*

Purpose: We assessed the accuracy of magnetic resonance imaging (MRI) in the evaluation of patients with suspected ARVD, correlated to findings in echocardiography, angiocardiography, myocardial biopsy, and electrocardiographic (ECG) or invasive electropysiological studies.

Methods: Fifty-six patients with ARVD were examined by plain ECG-triggered SE T1-weighted MRI and GE cine MR studies (Siemens Magnetom SP 1.5 T, Siemens Impact Expert 1.0 T). Twenty-six patients showed an extensive disease (type 1, with inducible ventricular tachycardia during programmed ventricular stimulation), and 30 patients had a localized ARVD (type 2, without inducible ventricular tachycardia). All patients subsequently underwent cardiac angiography, ECG and/or electropysiological studies, echocardiography, and in most cases myocardial biopsy. MR images and cine MR studies were reviewed without knowing the results of the other image modalities.

Results: In 44 patients (79%) we found abnormalities of the right ventricle in the MRI studies. Comparing the results with angiocardiography in patients with ARVD, the concordance of MRT was 82%, with endomyocardial biopsy 80%, with the origin of ventricular tachyarrhythmias (ECG, invasive electrophysiological studies) 72%, and with echocardiography 50% in patients with ARVD.

Conclusion: MRI can be used to assess myocardial tissue abnormalities and functional changes of the right ventricle. It is a useful supplementary technique to angiocardiography, invasive electrophysiological studies, and myocardial biopsy. Especially in cases of localized ARVD, MRI is helpful in planning of myocardial biopsy. Because there is no imaging modality commonly regarded to the standard of reference in the diagnosis of ARVD, MRI is considered to be an accurate and reliable modality in evaluating ARVD.

Automated Monitoring of Diaphragm End-Expiratory Position for Real-Time Navigator Echo MR Coronary Angiography

A.M. Taylor, P. Jhooti, D.N. Firmin, D.J. Pennell. *London, UK*

In this study, we describe the results of an automated program that monitors the diaphragm end-expiratory position (DEEP) and moves the navigator echo (NE) acceptance window if there is a significant change in the mean DEEP. This maintains scan efficiency (SE) and keeps the DEEP within the NE acceptance window.

Fifteen subjects with known ischemic heart disease underwent continuous monitoring of the dome of their right hemidiaphragm with an NE for 30 min while lying supine.

The NE diaphragm trace was monitored for 30 s at the beginning of the scanning period, and a mean DEEP was calculated by the monitoring algorithm. The algorithm looks for inflections of the diaphragm trace, establishes a maximum value for the inflection, and averages these values over the monitoring period. A 5-mm NE acceptance window is then placed such that the upper limit lies on the calculated DEEP. The algorithm then ran until 16 NE had been accepted. The DEEP was then calculated for this theoretical acquisition. If this calculated DEEP changed from the previous DEEP by >1 mm, the NE acceptance window was prospectively shifted for the next theoretical acquisition.

The drift in the DEEP (Fig. 1a) was mirrored by a fall in the SE

from 46% to a plateau of 39% at 10 min, if a static 5-mm NE acceptance window was used (Fig. 1b). If, however, the automated DEEP monitoring algorithm was used, the SE was maintained at >49% throughout the 30-min monitoring period (SE static vs. SE automated, $p < 0.001$).

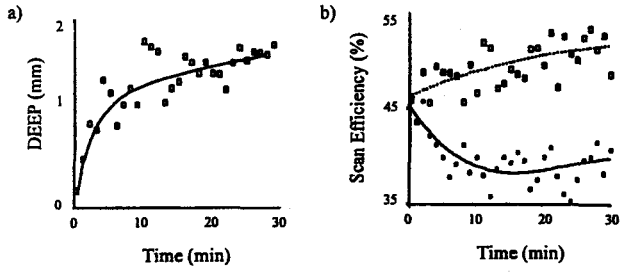

Figure 1. (a) The DEEP (calculated by the monitoring algorithm) was plotted against time at 60-s intervals. (b) SE calculated for a static window (●) and SE calculated with automated DEEP following (□).

In conclusion, we developed a method of monitoring the DEEP and automatically repositioning the NE acceptance window if the DEEP changes significantly. This repositioning of the NE window maintains scan efficiency and allows data acquisition around end expiration (the most stable part of the respiratory cycle), which reduces artifact.

Noninvasive Assessment of Different Flow Patterns in the Left Anterior Descending and Right Coronary Artery by MR Velocity Quantification

J.T. Marcus,[1] A.C. Van Rossum,[1] M.J.W. Götte,[1] J.P.A. Kuijer,[1] R.M. Heethaar,[1] R.J. Van der Geest.[2] [1]*Vrije Universiteit, Amsterdam;* [2]*Leiden University, The Netherlands*

Purpose: We quantified noninvasively the blood flow patterns in the left anterior descending (LAD) and right coronary artery (RCA) (1), corrected for through-plane myocardial motion.

Methods: MRI was on a 1.5-T whole body system (MAGNETOM VISION, Siemens, Erlangen, Germany) using a phased-array body coil. In healthy males, 10 LADs and 10 RCAs were evaluated. MR phase-contrast velocity quantification was applied with prospective ECG triggering, pixel size 1.25 × 0.98 mm², through-plane velocity sensitivity 40 cm/s; temporal resolution was 64 ms for the LAD (3 k_y lines per heartbeat) and 24 ms for the more vigorously moving RCA (nonsegmented). Acquisition was in multiple expiration breathholds.

Analysis was with the FLOW software package (Dept. of Radiology, Leiden University, The Netherlands [2]). The region of interest on the velocity map was adjusted to the artery cross-section in each temporal frame. The area-averaged velocity was corrected for background motion (3) by subtracting the velocity on a reference contour surrounding the artery's cross-section with a three-pixel distance. This reference contour is thus a ring of pixels. Volume flow (ml/s) was calculated as the product of cross-sectional area and area-averaged velocity. The peak and mean values of the volume flow were calculated during systole and during diastole. Systolic versus diastolic values were compared by paired-samples t-testing.

Results: Results for all subjects are summarized in the table. In systole the LAD showed a smaller peak and mean flow than in diastole ($p < 0.001$). The RCA, however, showed systolic peak and mean flow values that were not different from the diastolic values. Stroke volume was smaller in the RCA (0.59 ± 0.16 ml) than in the LAD (0.94 ± 0.20 ml; $p < 0.001$).

	Peak Flow (ml/s)		Mean Flow (ml/s)	
	Systole	Diastole	Systole	Diastole
LAD	0.88 ± 0.42	2.71 ± 0.61	0.22 ± 0.28	1.56 ± 0.33
RCA	1.60 ± 0.59	1.52 ± 0.53	0.67 ± 0.22	0.65 ± 0.23

Conclusion: The LAD showed a predominantly diastolic flow; the RCA, however, showed about equal flow values in systole and diastole. The different flow patterns in the LAD and RCA may be explained by the different pressures in the perfusion beds.

References

1. Post JC, Hofman MBM, Galjee MA, et al. Circulation, 1996; 94:I-122.
2. Van der Geest RJ, Buller VGM, Reiber JHC. Comput. Cardiol., 1995; 29–32.
3. Polzin JA, Korosec FR, Wedding KL, et al. JMRI, 1996; 1:113–123.

Trade-offs Between Applications of Echocardiography (Transthoracic and Transesophageal) and MRI in Children and Adults with CHD

David J. Sahn. *Oregon Health Sciences University, Portland, OR*

Despite its robust capabilities for noninvasive characterization of anatomy, physiology, and flow in congenital heart disease (CHD), (MRI) sees little application in the care provided by most centers. In infants and young children, certainly, the quality of ultrasonic imaging, the portability of the instrumentation, and the wide availability of expertise for performance and interpretation of studies will make it hard to displace as the primary definitive diagnostic technique. Very unusual chamber morphology, the need for quantitation of chamber volume and mass, and the need for characterizing complicated systemic or venous anatomy and the anatomy of the pulmonary arteries and aorta outside of the bounds of the traditional echo windows remain indications to use MRI when angiography is to be avoided. In older patients, adult patients, and postoperative patients with poor echo windows, the requirements for sedation involved in TEE versus agitation of patients that can occur in the MRI environment may or may not indicate one test over another. TEE, however cumbersome in awake patients, has incredibly improved spatial resolution and is the front line for perioperative, intraoperative, and cath lab procedural monitoring. Although elegant work in flow volume computation, shunt determination, and fluid dynamics evaluation of the Fontan circulation has been accomplished by experts in CHD applications, the lack of expertise in advanced MRI methods in many regional centers remains an obstacle. The evolution of ultrasound toward real-time 3D volume imaging is in competition with the faster, almost "real time," interactive implementations of MRI in certain research centers. Access and expertise, and the gradual disappearance of the specialty previously called Cardiovascular Radiology, have hampered applications of MRI in CHD strategy and protocols. The development of the Society for Cardiovascular Magnetic Resonance and possibility of the Society fostering expertise, a forum for multicenter studies, and education within the cardiovascular community about accessibility and efficacy of MRI are as important as the incredi-

ble pace of advances in MRI methods to its wider application in the CHD population.

Quantification of Heart Valve Regurgiation with Velocity-Encoded Magnetic Resonance Imaging

G.P. Chatzimavroudis,[1] J.N. Oshinski,[1] P.G. Walker,[2] R.H. Franch,[1] A.P. Yoganathan,[1] R.I. Pettigrew.[1] [1]*Atlanta, GA;* [2]*Leeds, UK*

Purpose and Methods: The aim of this study was to determine the potential of magnetic resonance phase velocity mapping (PVM) to diagnose aortic and mitral regurgitation (AR and MR) by measuring the aortic and mitral regurgitant volumes (ARV and MRV). The accuracy of measuring the ARV from single-slice PVM measurements in the ascending aorta during diastole was tested experimentally. A compliant aortic model with a porcine valve and coronary arteries was studied under steady and pulsatile flow conditions (AR flow rate, 0.1–5.5 l/min; ARV, 8–75 ml/beat) in a 1.5-T Philips MRI scanner. Gradient echo velocity-encoding acquisitions (TR/TE/α = 30 6/35) provided the velocity profiles across the aorta. To eliminate the effects of aortic compliance and coronary flow, the slice was placed between the valve and the coronary ostia. In vivo, 19 AR patients were studied with the slice placed as close to the aortic valve as possible, just above a signal loss region (due to flow acceleration) located proximal to the valve. Because of the interaction between the regurgitant flow field and the aortic outflow field in the left ventricle (LV), the single-slice method is not reliable in MR. The great advantage of PVM to measure all three velocity components in a slice is a control volume (CV) approach. By placing a number of slices at the mitral valve and measuring all three velocity components of blood flow, a CV can be selected encompassing the valve. Becuase of mass conservation, all net inflow through the faces of the CV during systole should be equal to the regurgitant flow. This method was studied experimentally using a Plexiglas LV model and mitral regurgitant orifices under steady and pulsatile flow conditions (MR flow rate, 1–7 l/min; MRV, 10–55 ml/beat). Five contiguous slices using gradient echo sequences were acquired with velocity encoding in all three directions in space. In AR, integration of the velocity over the aortic cross-sectional area and over diastole provided the ARV. In MR, the size of the CV was selected and integration of the velocity over the area of all faces of the CV and over systole provided the MRV.

Results and Discussion: In AR, the PVM-measured and the actual regurgitant flow rates agreed very well ($r^2 = 0.99$). The same accuracy was found in the pulsatile flow results (error of 2 ± 3%). In vivo, the measured ARV correlated well with clinical AR grading data. There was a general distinction between grades even in mild cases ($p < 0.05$). In MR, results showed that the CV method has the potential to accurately quantify the MRV without effects from the aortic outflow ($p > 0.2$) or the regurgitant orifice shape ($p > 0.4$). The CV should be large enough for its boundaries to exclude the distorted signal region too close to the valve. The single-slice method provides accurate results in AR, whereas the CV method appears promising in MR, particularly when there are multiple regurgitant or shunt lesions so that a biventricular stroke volume comparison is inaccurate. This study shows that the PVM CV method has some major advantages over another recent CV method, the Doppler ultrasound proximal isovelocity surface area (PISA) method. The PVM CV method is not affected by the presence of aortic outflow in contrast to PISA. In addition, the accuracy of PISA depends on the assumption made for the shape of the CV, whereas PVM, allowing all three velocity components to be measured, does not require such assumptions.

Conclusion: This study shows that PVM can accurately quantify the regurgitant volume in AR with the slice close to the valve. Because of the complex perimitral flow field, a CV approach may be needed for MR in multivalvular lesions where biventricular stroke volume differences cannot be used.

Effect of Revascularization on Left Ventricular Geometry as Assessed by MRI in Advanced Coronary Artery Disease

F. Roder,[1] S. Nekolla,[1] J. Neverve,[1] J. Stollfuß,[1] F. Haas,[2] H. Meissner,[2] M. Schwaiger.[1] [1]*Nuklearmedizinische Klinik, Klinikum Rechts der Isar, TU München, München, Germany;* [2]*Deutsches Herzzentrum, München, Germany*

Introduction: Revascularization has been shown to improve regional wall motion and ejection fraction (EF) in patients with coronary artery disease (CAD). The purpose of this study was to evaluate left ventricular function before and after revascularisation with cine-MRI.

Methods: Eighteen patients (17 male, 60 ± 10 yr) with advanced CAD and impaired left ventricular function were investigated before and after (4.5 ± 0.8 month) revascularization by coronary bypass grafts. Gradient-echo-cine images in 12 heart phases and 10–12 slices were acquired at 1.5 T (Philips ACS2). Images were acquired in short axes view with slice thickness of approximately 10 mm (depending on heart size). TE was 9.4 ms (flow compensated), two averages, matrix size 128. MR data were transferred to UNIX workstations. Endo- and epicardial contours were semiautomatically traced using MASS software (University Leiden) (1,2). Based on these contours, left ventricular mass (M), end-diastolic (ED) and end-systolic (ES) left ventricular volumes (EDV, ESV), wall thickness (WT), wall thickening (WTg), and wall motion (WMo) are calculated. To account for different numbers of usable slices, a volume index is calculated (EDV index). The wall parameters (WT, WTg, WMo) are stored with 100 values (chords) per slice. For a regional analysis, the wall parameters are averaged for standard-vessel territories (LAD, LCX, RCA) for each patient.

Results: Patients were divided into two groups based on preoperative EDV index. Group I consisted of seven patients with enlarged LV (EDV index > 90), whereas group II included 11 patients with normal EDV index (c. 90). Group I shows significantly greater reduction in volume than group II (see table). Regions with ED wall thickness of more than 11 mm show significantly greater improvement of wall motion (ΔWMo = 1.78 ± 2.33 mm) than those with less than 1 mm ED-WT (ΔWMo = −0.78 ± 2.03 mm, $p = 0.0001$).

Change of parameters pre- and postrevascularization for groups I and II

	n	EDV-pre (ml)	ΔEF (%)	ΔED V-i	ΔESV-i	ΔM (g)
I	7	135	5.1	−31.1	−26.3	−8.3
II	11	70	3.4	5.0	−1.1	18.4
p			0.72	0.002	0.007	0.05

p denotes significance between groups (Student *t*-test).

Conclusion: Revascularization in patients with advanced CAD and dilated LV lead to significant decreases of EDV, ESV, and LV-Mass, suggesting beneficial hemodynamic effects independent of changes in

LV ejection fraction. Regional preoperative WT was associated with functional recovery. MRI provides quantitative means to monitor LV remodeling after revascularization in ischemic heart disease.

References
1. Buller VGM, van der Geest RJ, Kool MD, Reiber JHC. Comp. Cardiol., 1995; 245–248.
2. van der Geest RJ, Jansen E, Buller VGM, Reiber JHC. Comp. Cardiol., 1994; 33–36.

Simultaneous MRI Tagging and Through-Plane Velocity Quantification: A Three-Dimensional Myocardial Motion Tracking Algorithm

J.P.A. Kuijer, J.T. Marcus, M.J.W. Götte, A.C. van Rossum, R.M. Heethaar. *Vrije Universiteit, Amsterdam, The Netherlands*

A tracking algorithm was developed for calculation of three-dimensional point-specific myocardial motion. The algorithm was designed for MRI images acquired with simultaneous grid tagging and through-plane velocity quantification (1). The tagging grid was used to provide the in-plane motion, whereas the velocity quantification measured the through-plane motion. The in vivo performance was tested using data sets of four healthy subjects.

A stack of four or five short-axis (SA) cines was acquired with simultaneous tagging and through-plane velocity quantification. The LV contours and tagging-grid intersections (tag points) were traced using "snakes" (2). Next, an estimate of the velocity at a tag point's location was needed. However, the SNR of the measured velocity in pixels in the tag lines was low because of the saturation of the magnetization. Those pixels were removed from the velocity maps by setting a threshold in the magnitude images, and the local velocity was interpolated using 2-D finite elements. The in-plane coordinates x,y and through-plane velocity v_z of the material point were estimated by linear interpolation between two tag points in adjacent SA image planes. Finally, the differential equation describing the motion of a material point "sliding" along the intersecting line of two orthogonal presaturated tissue slices, $dz/dt = v_z(t,z)$, was solved.

The in vivo performance was tested by comparing the z-displacement of a set material point with tag points in three long-axis (LA) image planes. Figure 1 shows they are in good agreement. A scatter plot of the z-displacement of all four volunteers is shown in Fig. 2. The correlation coefficient was 0.93 ($p < 0.001$, $n = 183$). A t-test for paired samples revealed a small underestimation of the through-plane displacement by 0.04 ± 0.09 cm (mean ± SD, $p < 0.001$) on an average displacement of 0.77 ± 0.23 cm toward the apex. We conclude that three-dimensional (3-D) point-specific motion tracking based on simultaneous tagging and velocity quantification is competitive to other methods such as tagging in mutually orthogonal image planes or quantification of three orthogonal velocity components.

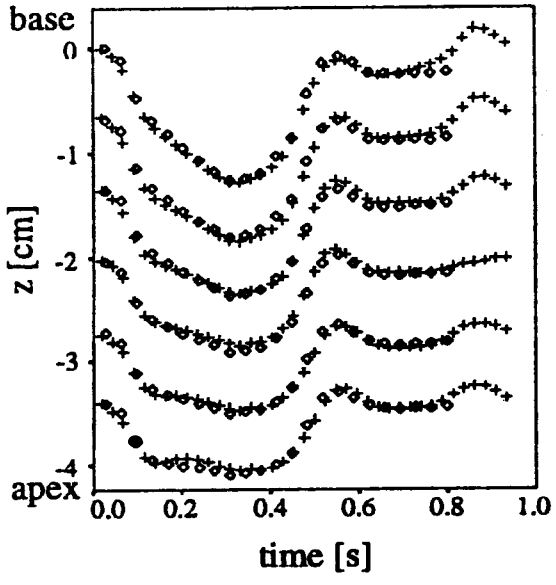

Figure 1. Example of motion along z axis of 3-D tracked material points in the lateral LV heart wall of a healthy volunteer (×) and corresponding LA tag points (diamonds).

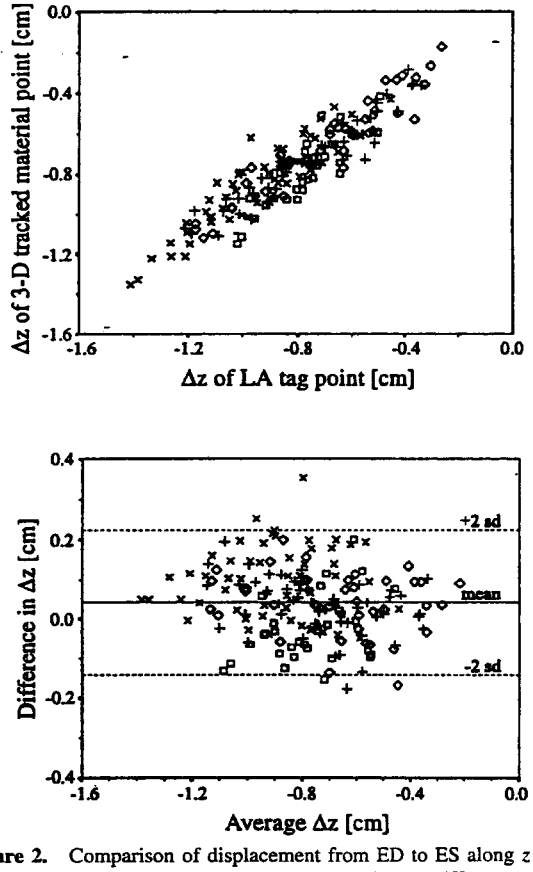

Figure 2. Comparison of displacement from ED to ES along z axis of material points and corresponding LA tag points. A different marker is used for each of the four volunteers.

References
1. Perman WH, Cresswell LL, Wyers SG, Moulton MJ, Pasque MK. JMRI, 1995; 5:101.
2. Young AA, Kraitchman DL, Dougherty L, Axel L. IEEE Trans. Med. Imag., 1995; 14:413.

Image Artifact Correction in Real-Time Interactive MRI

J.M. Pauly,[1] A.B. Kerr,[1] W.F. Block,[1] C.H. Meyer,[1] B.S. Hu,[2] Phil Yang,[2] D.G. Nishimura,[1] A. Macovsky.[1] *Departments of [1]Electrical Engineering and [2]Cardiovascular Medicine, Stanford University, Stanford, CA*

Real-time interactive magnetic resonance imaging (RTI-MRI) will be an important component of cardiac MRI systems. Efficient k-space trajectories are required to image the heart continuously without gating. Two acquisition methods are spirals and EPI. Each has well-known characteristics with respect to flow and off-resonance. Spiral has better flow response but produces image blurring off-resonance. EPI is more tolerant to off-resonance but produces more flow artifacts. Here we consider another aspect of these sequences, implementation in an RTI-MRI system. The major issue is the reconstruction of high-fidelity images in the presence of eddy currents and gradient delays, which can differ on different axes. Correction must be performed continuously, following the interactive positioning of the scan plane. For EPI, gradient delays and eddy currents both produce image ghosts. Typically, these effects are corrected using a calibration scan. This takes time and can be unreliable when a large part of the signal in the image is flowing blood. We take the approach of modeling these effects and then predicting and correcting them in acquisition and reconstruction. The corrections result in non-Cartesian EPI data, so we use a gridding reconstruction as we do for spirals. For spirals, most of these effects are relatively benign. Gradient delays primarily produce an image rotation. B0 eddy currents produce an image shift. These effects can also be corrected in reconstruction, but the correction is much less critical. We use a spectral-spatial pulse for lipid suppression in both EPI and spirals. This uses an EPI k-space trajectory, so the concerns are similar to EPI acquisitions. The delay must be accurate, particularly when offsetting the slice. In addition, B0 eddy currents can significantly degrade lipid suppression for some types of spectral-spatial pulses. The corrections are the same as for EPI acquisition but are applied to the RF waveform. By applying these approaches, high-fidelity images can be continuously acquired and reconstructed at any scan plane orientation. This will be important for responsive RTI-MRI for cardiac applications.

Vectorcardiographic-QRS Detection Improves Gating Accuracy in Magnetic Resonance Imaging

S.E. Fischer, S.A. Wickline, C.H. Lorenz. *St. Louis, MO*

Accurate electrocardiogram (ECG) gating is essential in cardiac magnetic resonance imaging. The magnetohydrodynamic effect and noise by switching high-performance gradient systems reduce the accuracy of R wave detection, resulting either in poor image quality or low scan efficiency. The purpose of this study was to compare different QRS detection algorithms using both standard surface-lead ECG and vectorcardiograms (VCGs). VCGs (1) in 12 healthy volunteers (33 ± 7 yr, 71 ± 8 kg, 179 ± 7 cm, heart rate 56 ± 9 bpm) outside an MR scanner and exposed to a 1.5-T magnetic field (Gyroscan ACS-NT, Philips Medical Systems, Best, NL) were digitized and used as a reference data set, including manually corrected onsets of R waves. From the VCG, a standard surface-lead ECG was derived and selected real-time R wave detection algorithms (2) (i.e., based on the first derivative) were applied. A novel "target-distance" algorithm, which uses the VCG directly, is based on the observation that the QRS loop and the loop generated by the magnetohydrodynamic effect differ spatially (3). In the figure, ECG/VCG signals of one heart beat in a healthy volunteer used to detect the R wave are compared. The "Projection," comparable with a single surface-lead ECG, shows the magnetohydrodynamic artifact higher in amplitude than the R wave. In the "First Derivative" gradient, switching causes signal amplitude in the same magnitude as the slopes of the QRS complex (arrows). The "Target-Distance" algorithm clearly enhances the R peak, damps the blood flow artifact, and is insensitive to gradient switching. In the magnet, the ratio of the amplitude of the blood flow-related artifact to the actual R wave was 0.87 ± 0.75 and greater than 1.0 in 28% of the 818 analyzed RR intervals. The target-distance R wave detection algorithm yielded a score of 100% for detection with 1% false positive, a delay between onset of R wave and time of detection of 0.5 ± 1.7 ms, and was superior to all other selected methods (i.e., algorithm based on first derivative applied to lead I: 83% detected, 9% false positive). Thus, the VCG of subjects exposed to a strong magnetic field can be used to separate the magnetohydrodynamic artifact and the actual R wave and markedly improves the trigger accuracy in gated MR scans.

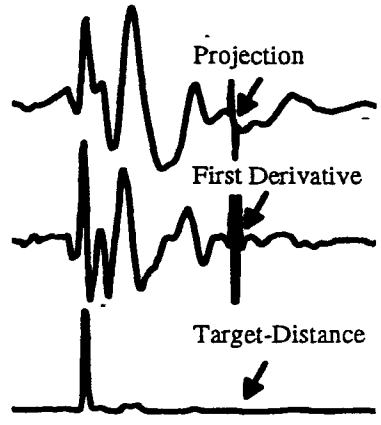

References
1. Frank E. An accurate, clinically practical system for spatial vectorcardiography. Circulation, 1956; 13:737–749.
2. Friesen GM, Jaqnnett TC, Jadallah MA, Yates SL, Quint SR, Nagle HT. Comparison of the noise sensitivity of nine QRS detection algorithms. IEEE Trans. Biomed. Eng., 1990; 37:85–98.
3. Dimick RN, Hedlund LW, Herfkens RJ, Fram EK, Utz J. Optimizing electrocardiograph electrode placement for cardiac-gated magnetic resonance imaging. Invest. Radiol., 1987; 22:17–22.

Fast Cine-Magnetic Resonance Imaging Measurements of Cardiac Performance Under Bicycle-Induced Exercise Stress

G.P. Chatzimavroudis,[1] J.N. Oshinski,[1] W.T. Dixon,[1] J.A. Doyle,[1] J. Stewart,[1] R. de Boer,[2] R.I. Pettigrew.[1] *[1]Atlanta, GA; [2]Best, The Netherlands*

Purpose: The aim of this study was to determine whether fast cine-MRI techniques can provide reliable information about cardiac performance under exercise stress.

Methods: We studied nine healthy volunteers with a 1.5-T Gyroscan NT Philips MRI scanner. An MRI-compatible cycle ergometer was used to induce exercise stress. The bicycle allowed the subjects to recline and pedal with the heart positioned near the isocenter of the magnet. The pedaling resistance of the cycle ergometer was controlled by a workload programmer (Lode, Groningen, the Netherlands). In five subjects (group A), a set of three breathhold turbo field echo (TFE) left ventricular (LV) short-axis images (TR/TE/α = 11/6/35) were obtained to determine the ejection fraction (EF) at rest with seven to nine phases per beat collected, depending on heart rate. In the remaining four subjects (group B), a set of three slices were obtained in the LV short axis using a multishot segmented k-space breathhold echo planar (EPI) sequence (TE/α 14/20) with 9–11 k-space lines per excitation to determine the EF at rest. The temporal resolution per slice in this case was 16–20 phases/beat. Subjects began pedaling at a negligible resistance, and the workload was increased by 25 W every 3 min. The target stress heart rate was 65% of the maximum heart rate (defined as 220 minus age) in group A and 65–85% of the maximum heart rate in group B. When the target heart rate was met, the subjects were asked to stop pedaling and hold their breath, during which a 4- to 6-s TFE acquisition (TR/TE/α = 11/6/35) with 5–7 phases/beat was obtained for group A and a 3- to 4-sec EPI acquisition (TE/α 14/20) with 11–20 phases/beat was obtained for group B to determine the EF at stress. The subjects resumed pedaling and repeated the breathhold scan two more times at the target heart rate for two more slice acquisitions.

Results and Discussion: The EF increased between rest and stress in both groups, from 54.5 to 61.8% in group A and from 58.8 to 71.1% in group B. The higher increase in EF observed in group B (EPI) compared with group A (TFE) is due to the fact that group B included cases with higher target heart rate (85% of the maximum heart rate) than group A. The quality of the EPI acquisitions was generally better than that of the TFE. Although TFE provided adequate image quality for EF calculations, it did not permit distinct visualization of regional wall motion abnormalities. On the other hand, EPI acquisitions were of better quality and permitted wall thickening calculations. Mean normal thickening range was 75–100% in the septum, 76–150% in the anterior wall, 120–198% in the lateral wall, and 106–197% in the inferior wall.

Conclusion: Fast cine-MRI acquisitions can provide reliable information for evaluation of cardiac function under exercise stress. EPI seems preferable because of better image quality and higher temporal resolution.

Cardiac Magnetic Resonance with a Pacemaker In Situ: Can It Be Done?

D.J. Pennell. *London, UK*

There are five cases of pacemaker-related death during MRI, and they are considered an absolute contraindication. However, some cases have been reported with successful outcomes (1). We report here our experience of five scans with the pacemaker programmed for noncapture. Patient 1 suffered five VF arrests despite polytherapy. A diagnosis of sarcoidosis was suggested by MR and proved by a Kveim test, after insertion of a cardioverter-defibrillator. Patient 2 underwent a piggyback heart transplant and now had dyspnea. Native heart function was poor by echo, but the donor heart could not be visualized. For MRI, gating was only possible to the native heart, which showed near absent function. A second MRI using EPI showed excellent donor heart function but limited cardiac output because the heart was from a 5-year-old donor. Invasive tests for possible rejection were subsequently deferred. Patient 3 had complex congenital heart disease with an urgent clinical need to visualize the pulmonary valve, which had failed with echo. MRI was requested but was abandoned because the pacemaker switched into fixed-rate pacing at full voltage in the magnet. Patient 4 had marked exertional dyspnea and a prosthetic aortic valve with clinical regurgitation, but none found on echo. MR showed a regurgitant fraction of 58% and poor valve opening requiring surgery. Therefore, a pacemaker is not an absolute contraindication to cardiac MRI but should only be performed in experienced centers with pacing facilities. Cardiac monitoring during the scan is mandatory. Preparation of the patient should clearly include an overriding clinical need for more information, a positive risk–benefit assessment, nonpacemaker dependency, informed written consent with witnesses, full resuscitation facilities at the scanner, experienced cardiology assistance during scanning, slow introduction into the magnet with monitoring, and graded scanning sequences starting with single-slice, low-resolution and progressing. The following pacing variables should be considered: 000 mode if available, or V00, with minimum voltage and pulse width settings, bipolar lead configuration, and testing with a magnet to ensure that the pacemaker does not revert to full output mode during MR. Considerably more work needs to be performed in this area, but successful MR is possible in selected clinical circumstances where important diagnostic information is required.

Reference

1. Gimbel JR, Johnson D, Levine PA, Wilkoff BL. Safe performance of magnetic resonance imaging on five patients with permanent cardiac pacemakers. PACE, 1996; 19:913–919.

Improvements in the Spatial and Temporal Resolution of Cardiac MRI Using the SMASH Imaging Technique

D.K. Sodickson, P.M. Jakob, M.A. Griswold, R.R. Edelman, W.J. Manning. *Boston, MA*

Background: A number of important applications of cardiac MRI are often hindered by competing constraints of spatial and temporal resolution. To resolve small structures such as the coronary arteries, high spatial resolutions are required, but the long acquisition times associated with high-resolution scans can lead to blurring from cardiac and respiratory motion. Although motion compensation schemes such as cardiac gating, breathholding, and navigator gating can adjust to some extent for the effects of physiologic motion, a technique that allowed simultaneous improvements in spatial and temporal resolution would be of substantial benefit for both the efficiency and the quality of cardiac MRI studies.

Purpose: We present preliminary results of cardiac studies using the newly introduced SMASH imaging technique (1). SMASH (SiMultaneous Acquisition of Spatial Harmonics) uses a partially parallel acquisition strategy in which multiple lines of *k*-space are effectively acquired at once, using combinations of signals from an RF coil array. This approach may be used to multiply the speed of conventional imaging sequences without sacrificing spatial resolution.

Methods: SMASH was implemented in conjunction with standard cardiac imaging protocols in healthy adult volunteers, using prototype coil arrays on two commercial imaging systems. The SMASH acquisitions were used to reduce the acquisition windows of segmented *k*-space images and therefore to improve temporal resolution while maintaining constant spatial resolution and total imaging time; to increase spatial resolution at constant temporal resolution in a fixed acquisition time; and to reduce breathhold times for constant spatial and temporal resolution.

Results: Image quality was preserved in the accelerated SMASH images compared with conventional reference images. Increased spatial and/or temporal resolution in the SMASH images allowed improved visualization of coronary arteries and other cardiac structures.

Conclusions: SMASH imaging may be used to increase the achievable spatial and/or temporal resolution in cardiac MR images. Although

two- and threefold improvements were demonstrated in these studies, the maximum achievable accelerations are expected to scale up with the number of array elements, and work is underway to develop the hardware necessary for substantially greater improvements in cardiac imaging.

Reference

1. Sodickson DK, Manning WJ. Simultaneous acquisition of spatial harmonics (SMASH): fast imaging with radiofrequency coil arrays. Magn. Reson. Med., 1997; 38:591–603.

Breathhold Duration: Navigator Echo Assessment of Supplemental Oxygen and Hyperventilation

P.G. Danias, K.V. Kissinger, M. Stuber, M.L. Chuang, R.M. Botnar, W.J. Manning. *Boston, MA*

Cardiac magnetic resonance (MR) imaging frequently requires breathholding (BH). We used navigator (nav.) assessment of right diaphragmatic (RHD) position to measure BH duration with hyperventilation (HV) and supplemental oxygen (O_2).

Methods: Testing was performed on 10 adults (6 men, 4 women, age 31 ± 7 yr) in a 1.5-T whole body scanner (Gyroscan ACS/NT, Philips Medical Systems, Best, The Netherlands). Room air (RA) or O_2 were administered via nasal prongs (2 l/min), with the subjects unaware of which gas they were receiving. For HV, six rapid inhalations and exhalations were used. The average of duplicate measurements was determined for all BHs. Four end-expiratory BHs were assessed in random sequence: RA, continuous O_2, RA + HV, and O_2 plus HV, with O_2 starting immediately before HV (O_2 + HV). A nav. (1) was positioned vertically at the dome of the RHD. Nav. position was determined in real time every 500 ms. BH duration was determined from the RHD position and its relative craniocaudal displacement. A repeated-measures ANOVA was used for group comparisons of BH duration. Post-hoc analysis was performed with a two-tailed paired *t*-test.

Results: The BH duration differed significantly among the four techniques ($p < 0.001$): RA, 35 ± 12 s; RA + HV, 48 ± 26 s (*); O_2, 43 ± 15 s (*); O_2 + HV, 55 ± 24 s (*,†,‡,); $p < 0.001$ for comparisons against RA (*), RA + HV (†), and O_2 (‡). The longest BH duration was achieved with O_2 + HV. Relative to RA, O_2 + HV resulted in a 59% prolongation of the BH duration ($p < 0.001$). Both continuous O_2 and RA + HV resulted in smaller (24–37%) prolongation of the BH duration compared with RA. Individual subject data are presented:

Conclusions: HV in combination with brief periods of O_2 supplementation HV significantly prolongs BH duration, as measured by RHD MR nav. These data have potential significance for clinical imaging of the cardiovascular system and other applications in which sustained BH is required.

Reference

1. Danias PG, et al. Radiology, 1997; 203:733–736.

Pediatric Aortic Pathology: Magnetic Resonance and Radiographic Imaging

K. Ahrar, M.S. McLeary. *Loma Linda, CA*

Purpose: We present a pictorial review of pediatric aortic pathology diagnosed by magnetic resonance imaging (MRI) and provide radiographic and conventional angiographic correlation.

Methods: We retrospectively reviewed MRI of the thoracic aorta in 24 children. Clinical data, including patients' age, symptoms, and findings at surgery, were collected from the medical records. Plain radiographs and conventional angiograms were reviewed. MRI findings were correlated with other imaging and surgical findings.

Results: Congenital abnormalities of the thoracic aorta were optimally depicted by MRI. These included coarctation of the aorta (hypoplastic arch, periductal, and long segment), double aortic arch (with atresia and with aneurysms), cervical arch, circumflex aortic arch, aortic arch branch anomalies, transposition of the great vessels (D and L), situs abnormalities (asplenia and polysplenia), and aortic root abnormalities (tetralogy of Fallot, double outlet right ventricle). Acquired diseases of the thoracic aorta, such as aneurysms (Marfan, mycotic, and anastomotic), dissection, and postoperative changes (Mustard, Arterial swith, and Glenn), were also optimally evaluated.

Conclusion: MRI provided complete and optimal depiction of the anatomy, including thoracic aortic configuration and caliber, aortic wall characterization, arch vessel origin, aortic root, and the mediastinal and periaortic structures.

References

1. Flamm SD, VanDyke CW, White R. MR imaging of the thoracic aorta. Magn. Reson. Imaging Clin. North Am., 1996; 4:217–235.
2. Bank ER. Magnetic resonance of congenital cardiovascular disease: an update. *Radiol. Clin. North Am.*, 1993; 31:553–572.

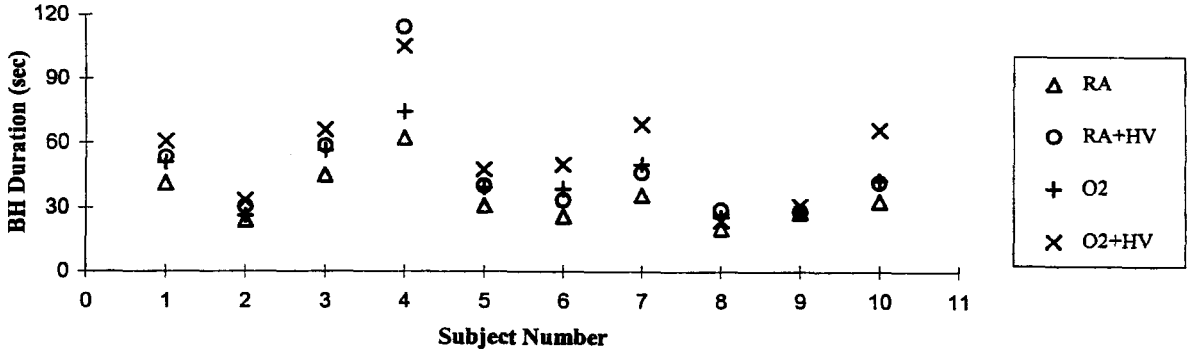

Assessment of Coronary Bypass Graft Patency by Conventional Magnetic Resonance Imaging Techniques

F. Carreras, G. Pons-Lladó, X. Borrás, J. Llauger, J. Palmer, A. Bayés de Luna. *Barcelona, Spain*

The purpose of the present study was to assess the usefulness of conventional widely available magnetic resonance imaging (MRI) sequences in the detection of patency of coronary bypass grafts. A series of 25 consecutive patients were studied accounting for a total of 64 grafts: 19 of the left internal mammary artery (IMA) and 45 of saphenous vein, 13 to the left anterior descending (LAD) coronary artery or one of its branches, 14 to the left circumflex (LCx) or one of its branches, and 18 to the right coronary artery (RCA). All patients were submitted to diagnostic invasive angiography, MRI studies being performed within 1 week of the catheterization. ECG-gated T1 spin-echo and gradient-echo techniques were practiced on axial and sagittal thoracic planes. The number and type of grafts were known by the observer performing MRI studies, the diagnosis of patency being made when a flow signal was detected at a location where a graft was known to be present and at least on two contiguous imaging slices in any of the studied planes. Results showed that 63 of 64 grafts could be successfully catheterized, 48 (76%) being patent, although 10 of them (20%) had a significant obstructive lesion (>70% stenosis). MRI studies were deemed as technically adequate in all cases to establish graft patency or occlusion in at least one of the imaging planes. The global diagnostic accuracy of MRI for the assessment of graft patency was 90%, the figures corresponding to particular grafts as follows: IMA 90%, LAD 92%, LCx 93%, RCA 89%. The predictive value of MRI for graft patency was 98% and for graft occlusion, 74%. The presence of graft stenosis was not detected by MRI, a signal of graft patency being observed in all but one of the stenosed vessels. Axial spin-echo was the sequence that more frequently allowed the visualization of IMA and RCA grafts; for grafts to the LAD and LCx, both sagittal spin-echo and gradient-echo were equally useful. Artifacts due to surgical clips were particularly apparent in gradient-echo sequences, not infrequently preventing an adequate visualization of the flow signal of the vessel. In conclusion, conventional MRI spin-echo sequences on axial and sagittal thoracic planes are adequate to establish patency of IMA and venous coronary artery bypass grafts with a high degree of accuracy, although the presence of obstructive vessel lesions is not detected by this technique.

Early MRI Evaluation of Marfan Syndrome: Study of Thoracic Aorta and Dural Ectasia

R. Fattor, E. Negrini, F. Celletti, P. Ambrosetto, G. Pepe,[1] G. Gensini, B. Descovich, G. Gavelli, *Institute of Radiology and Neurology, University of Bologna, Italy; [1]Institute of Internal Medicine, University of Florence, Italy*

The diagnosis of Marfan syndrome is codified on the basis of clinical criteria, first presented in 1986. Over time, weakness has emerged in these criteria because of the wide phenotypic expression of the disease and of some overlaps with other connective tissue disorders. Dural ectasia (DE) constitutes one of five major criteria (1,2), but few studies analyzed its real incidence and time of appearance in Marfan patients (MP). The purpose of this study was to estimate the incidence of DE in MP. Furthermore, in an attempt to individualize the precocity of this sign, the presence of DE has been correlated to aortic dilation.

Methods: MRI of the thoracic aorta and neural canal was performed in 31 MP who fulfilled the diagnostic criteria (18 males and 13 females, 6–44 yr old). Thirty patients (17 males and 13 females, 25–39 yr old) underwent MRI study of the lumbar spine as the control group.

Results: Among MP, 9 were already undergoing ascending aorta and/or aortic arch replacement, 10 presented severe ascending aorta dilation, 6 moderate ascending aorta dilation, and 3 mild ascending aorta dilation. Three patients presented normal aortic diameter. All patients presented DE; the most severe alterations (meningocele) were observed in the 2 oldest patients.

Conclusions: An incidence of 100% of DE and of 90.3% of aortic dilation was found in MP, suggesting that in the previous study, the incidence of DE might have been underestimated. Furthermore, DE might appear before aortic dilation, and no correlation has been found between the severity of these two diagnostic criteria.

References

1. Stern WE. Dural ectasia and the Marfan syndrome. J. Neurosurg., 1988; 69:221–227.
2. Pyeritz RE. Dural ectasia is a common feature of the Marfan syndrome. Am. J. Hum. Genet., 1988; 43:726–732.

MRI Monitoring of Traumatic Aortic Rupture: Evolution of the Aortic Lesion in the Subacute Phase

R. Fattori, F. Celletti, B. Descovich, G. Napoli, P. Bertaccini, A. Pierangeli, G. Gavelli, *Institute of Radiology and Cardiac Surgery, University of Bologna, Italy.*

Objectives: Recent surgical series documented that in traumatic aortic rupture, a surgical repair postponed until after treatment of associated lesions reduces operative and overall mortality (1). Nevertheless, some isolated cases may evolve to free rupture (2). The aim of this study was to analyze the behavior of traumatic aortic ruptures in the subacute phase to detect the morphological characteristics of unstable posttraumatic aneurysms.

Methods: Twenty-seven consecutive patients affected by traumatic aortic rupture (1 intimal hemorrhage, 21 partial lesions, and 5 circumferential lesions) were admitted to the department of Cardiac Surgery. MRI was the imaging modality used to confirm the diagnosis (3). No one was operated in the acute phase. Delayed surgery was carried out in 20 patients at 243 ± 127 days, after the resolution of associated lesions. A scheduled MRI follow-up was performed at 7, 15, and 30 days and immediately before the operation. The parameters examined were increase of posttraumatic aneurysm, increase of periaortic hematoma, and modification of the thoracic-associated lesions.

Results: At 30 days, a 3.0 ± 3.7-mm median increase of the aneurysm was observed, whereas in the subsequent period the lesion was substantially stable, resulting in a 4.4 ± 3.6-mm increment at the end of the follow-up. The circumferential lesions presented a higher increment with respect to the partial lesions. In three cases, an augmentation of 6, 7, and 12 mm was detected, and surgical repair was anticipated. In 13 cases, a periadventitial hematoma surrounding the aortic aneurysm decreased through the time. One case of intimal hemorrhage healed spontaneously, with no aneurysm formation.

Conclusions: Despite the common knowledge considering traumatic aortic rupture highly evolutive in the acute and subacute phase (4), this study demonstrated that this pathological entity is relatively stable if a proper pharmacological treatment is administrated. MRI follow-up is recommended to detect isolated cases of unstable aneurysm.

References

1. Stulz P, Reimond MA, Bertschmann W, Graedel E. Decision-making aspects in the timing of surgical intervention in aortic rupture. Eur. J. Cardiothorac. Surg., 1991; 5:623–627.
2. Pate JW, Fabian·TC, Walker W. Traumatic rupture of the aortic isthmus: an emergency? World J. Surg., 1995; 19:119–126.
3. Fattori R, Celletti F, Bertaccini P, Galli R, Pacini D, Pierangeli A, Gavelli G. Delayed surgery of traumatic aortic rupture: role of magnetic resonance imaging. Circulation, 1996; 94:2865–2870.
4. Duhaylongsod FG, Glower DD, Wolfe WW. Acute traumatic aortic aneurysm: the Duke experience from 1970 to 1990. J. Vasc. Surg., 1992; 15:331–343.

Assessment of Patency of Aortocoronary Grafts by Magnetic Resonance in Cabrol's Operation of Aorta

L.J. Jiménez-Borreguero, I. Maté, J. Pereira, M. Mateos, J. Dago, J. Sánchez. *Madrid, Spain*

Cabrol's operation entails implantation of a valved prosthetic tube in the ascending aorta and the reconnection of coronary arteries via synthetic grafts in which occlusion is a serious complication. The purpose of this study was to evaluate the use of MRI for noninvasive diagnosis of occlusion of coronary grafts. Eight male patients were studied 45.2 ± 35.5 months after Cabrol's operation, with a total of 16 coronary grafts, for aortic dilatation without previous coronary disease. MRI was performed on a 0.5-T system using a spin-echo sequence (TE 40 ms, NEX 2, FOV 40 cm) with multiple 5-mm-thick contiguous cuts, parallel to the aortic prosthesis' plane and obtained in diastole. The MRI studies were evaluated by two observers who were unaware of the patients' clinical or investigative status. In four patients with clinical suspicion of graft occlusion, catheterization had already been performed, three of them 1.5 ± 3.0 months previously and the other 45 months previously. The remaining four patients, without symptoms or findings suggestive of ischemic cardiopathy, were not studied invasively. The branches of the coronary grafts were considered to be patent when, in the expected position, an image signal void was identified in at least three successive tomographic cuts below the origin of the graft. They were interpreted as occluded when these criteria were not fulfilled.

Results: The mechanical aortic prosthesis did not prevent interpretation of the MRI images. MRI studies indicated occlusion of four grafts (three right and one left) and patency of the remaining eight grafts (four patients). These MRI findings coincided with those of catheterization for all eight grafts. In the remaining four patients, who showed no clinical evidence of myocardial ischemia, all grafts were found to be patent by MRI.

Conclusion: Initial experience indicates that MRI is a useful technique for assessment of the patency of coronary artery grafts of Cabrol's operation.

How Does T1 Reduction in Blood Affect Contrast-Enhanced Magnetic Resonance Coronary Angiography?

L.O. Johansson, M.B.M. Hofman, S.E. Fischer, S.A. Wickline, C.H. Lorenz. *St. Louis, MO*

Contrast agents have proven to improve magnetic resonance (MR) angiography of the abdominal and peripheral arteries. The imaging techniques for these anatomies usually use a steady-state acquisition, and the relationship between T1 in blood and the MR signal is well known. However, in ECG triggered angiography with limited acquisition windows, this relationship is more complex. Therefore, the purpose of this work was to study the relationship between the T1 in blood and the MR signal in 3D-magnetic resonance coronary angiography (3D-MRCA). In steady-state imaging, the maximum signal is achieved at the Ernst angle. The signal can be written as $S = \sin\alpha(1 - e^{-TR/T1})/[1 - \cos\alpha(e^{-TR/T1})]$. In a triggered situation, as in 3D-MRCA, relaxation will occur between the excitation windows. To use the additional magnetization, a flip-angle sweep is applied to maintain a constant maximal signal. The MR signal can be written as $S(n) = [Mz(n - 1)](e^{-TR/T1})[\cos\alpha(n - 1)] + (1 - e^{-TR/T1})(M_0)[\sin\alpha\alpha(n)]$, where n = the number of excitations. $Mz(n = 1)$ will depend on the heart rate because this determines the time for relaxation between the acquisition windows. In 3D-MRCA with targeted 3D volumes we can assume, however, that $Mz(1) = M_0$ because fresh blood has entered the volume between the acquisition windows. This means that the Mz is larger for blood than for static tissues. The MR signal for steady-state and triggered acquisition with and without flow was calculated as a function of T1.

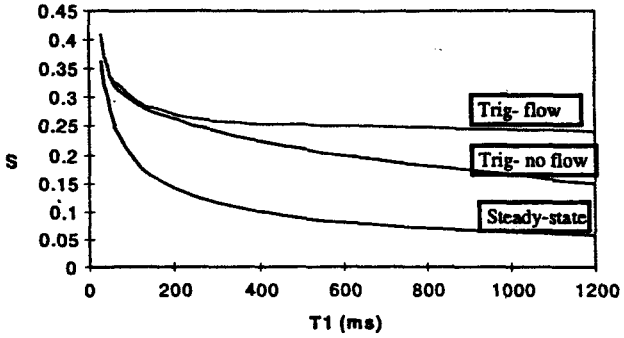

Figure. Relative MR signal as a function of different T1's for steady-state and triggered acquisitions without flow and with flow.

These simulations indicate that to use a contrast agent for 3D-MRCA, T1 should be below 200 ms to have any visible effect on the MR signal in a triggered acquisition with flow, whereas the same change in steady-state acquisition would increase the MR signal from blood by approximately 260%. To increase the MR signal by 50% in a triggered acquisition with flow, the T1 should change from 1,200 ms to approximately 50 ms. In conclusion, the effect of T1 shortening in contrast-enhanced 3D-MRCA differs substantially from conventional contrast-enhanced MR angiography, because the triggered acquisition allows unsaturated blood to enter the volume between the acquisitions, thereby giving a much higher signal at long T1's than steady-state acquisition.

An Algorithm for Automatic Tracking and Measurement of Coronary Arteries in 3D MR Datasets

T.P. Kerwin, M.B.M. Hofman, S.E. Fischer, L.O.M. Johansson, C.H. Lorenz. *St. Louis, MO*

An algorithm is described that automatically tracks the coronary arteries and measures their cross-sectional area as a function of distance along the vessel. The algorithm proceeds by iteratively reformatting the volume at different angles and finding the view that points in the direction of the vessel's path through the volume. Once the user has defined a view where a vessel of interest is roughly centered, the x and y axis rotation angles are passed as parameters to a genetic optimization routine (PGAPack, David Levine, Argonne National Laboratory), which finds the optimal cross-section, perpendicular to the vessel's path through the volume. The fitness function used for optimization is the distance traversed in the positive and negative z direction without leaving the vessel. Reformatted images are created in the local x–y, z–y, and x–z planes, and a simple segmentation algorithm determines the cross-sectional area. Then a step is taken in the local z direction (perpendicular to the cross-sectional view), and the optimization procedure is repeated. This continues until the end of the vessel is reached or the view steps out of the volume. The output of the algorithm is a graph of cross-sectional area versus distance along the path of the vessel and a series of reformatted images from three perpendicular views at each step along the vessel, which can be concatenated into a movie. The algorithm requires less than a minute of user time (to find the vessels in the volume), after which its operation is completely automatic. Optimization of the cross-sectional view at each step takes about 30 s on a 200-MHz Pentium-running Linux.

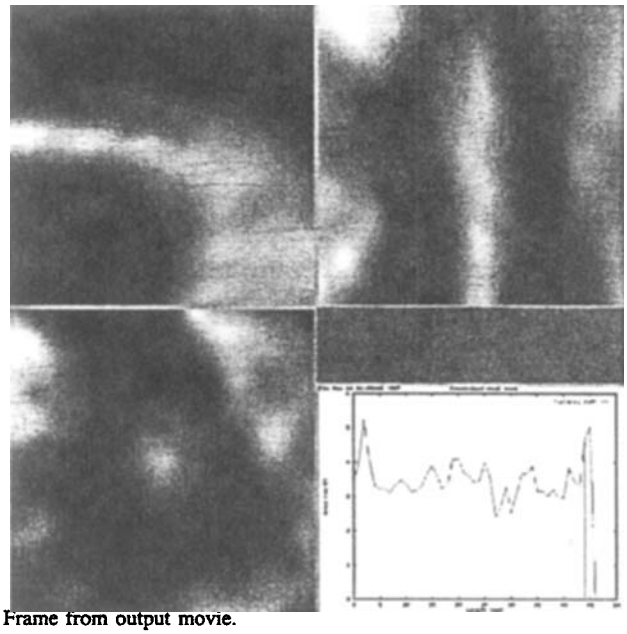

Frame from output movie.

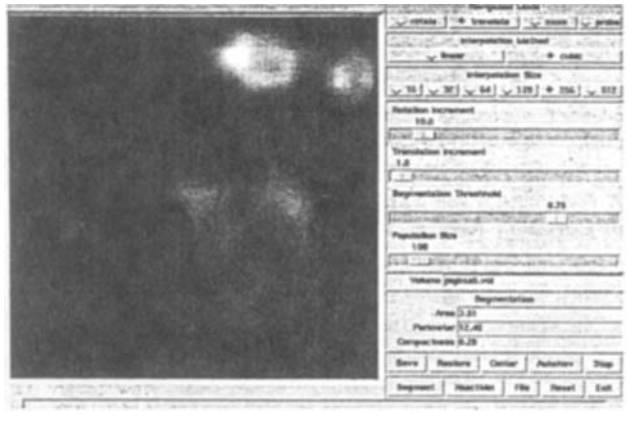

User interface.

Contrast-Enhanced Magnetic Resonance Angiography of the Internal Mammarian Arteries: Preoperative Assessment Before Minimally Invasive Coronary Artery Bypass Grafting (MICABG)

M.G. Lentschig, P. Reimer, A. Hoffmeier, R. Soeparwata, E. Rummeny, H. Scheld. *Muenster, Germany*

Purpose: The purpose of our study was to evaluate the value of 3D CE MRA in the preoperative assessment of the internal mammarian arteries before MICABG.

Methods: Twenty-five patients underwent breathhold 3D CE MRA at 1.5 T (Magnetom Vision, Siemens AG, Germany). To evaluate the individual contrast transit time, a test bolus of 1 ml Gd (Magnevist, Schering AG, Berlin, Germany) was injected intravenously and a Turbo-FLASH sequence (TR 8.5 ms, TE 4.0 ms, TI 100 ms, TD 84 ms, α 10°) was used. A 3D FISP sequence (TR 7.3 ms, TE 2.8 ms, α 20°, coronal slab 30–45 mm, 20–30 partitions) was used for the MRA study. Contrast injection was performed by means of automatic bolus injections with a MR-compatible power injector. Qualitative image analysis was performed by consensus of two blinded radiologists. Source images and maximum intensity projections were assessed together for image quality.

Results: Of the 25 patients examined, 10 examinations were graded excellent, 9 were rated as good, 4 as moderate and diagnostically sufficient, and 2 as nondiagnostic. All patients underwent minimally invasive coronary artery bypass grafting within 3 days, and the left internal mammarian artery could be used for bypass grafting in all cases.

Conclusion: 3D CE MRA can sufficiently depict the left internal mammarian artery and is a very useful noninvasive technique for preoperative and possibly postoperative workup of patients with coronary disease of the LAD scheduled for MICABG and could be also useful in conventional bypass surgery.

Two-Dimensional Breathhold Coronary Magnetic Resonance Angiography

M.G. Lentschig, A. Brinkmann, P. Reimer, S. Kerber, B. Tombach, E. Rummeny. *Muenster, Germany*

Purpose: We assessed image quality and diagnostic value of breathhold 2D MRA in normal volunteers and patients with coronary vessel disease.

Methods: Ten healthy volunteers and 20 patients with suspected ischemic heart disease and elective cardiac catheterization underwent breathhold 2D coronary MRA. Coronary MRA was performed with a fat-suppressed electrocardiographically gated breathhold gradient echo sequence (TR 800 ms, TE 7.4 ms, TD 300 ms, slice thickness 5 mm, FOV 280 6/8, matrix 154 × 256) with k-space segmentation at 1.0 T (Magnetom Expert, Siemens AG, Erlangen, Germany). Three independent readers evaluated the coronary MRAs. Visible vessel length and presence of stenoses were evaluated. Image quality was classified as good, medium, or poor.

Results: The length of the visible coronary artery segments was variable: good quality, RCA 3.55 cm ± 1.75, LCA 1.35 cm ± 0.82, LAD 2.82 cm ± 1.48, LCX 1.10 cm ± 0.65; medium quality, RCA 5.07 ± 1.61 cm, LCA 1.73 ± 0.53 cm, LAD 3.92 ± 1.15 cm, LCX 1.97 ± 0.90 cm. The sensitivity of coronary MRA for detection of coronary stenoses varied between 76% for the RCA and 30% for the LCX. Insufficient breathholding was the main reason for poor image quality (up to 45%).

Conclusion: Breathhold 2D coronary MRA can depict up to 76% of hemodynamically significant stenoses in the proximal parts of the coronary arterial tree. Best image quality was found for the RCA and the LAD, whereas the LCX had the worst quality. Image quality was disturbed by insufficient breathholding, ghost artifacts, and incomplete fat suppression. Diagnostic problems were caused by incomplete differentiation of the coronary arteries from veins and from the pericardial sac.

Magnetic Resonance Coronary Angiography Using Prospective Navigator Echo-Based Slice Following

J.N. Oshinski,[1] W.T. Dixon,[1] P. Salverda,[2] L. Hofland,[2] R.I. Pettigrew.[1] [1]*Atlanta, GA;* [2]*Best, The Netherlands*

Purpose and Methods: Navigator echo-gated MR coronary angiography allows a subject to breathe freely during image acquisition by obtaining data during only a portion of the respiratory cycle. The gate window determines the amount of the respiratory cycle used for imaging. Use

of a large gating window causes residual motion artifacts, and use of a small gating window prolongs scan times. We implemented a prospective slice-following technique that uses the navigator echo-derived respiratory position of the heart to update the slice excitation position in real time. The effect is to excite the same anatomical location of the heart despite respiratory movement of the coronary artery. To assess the effectiveness and potential clinical utility of the technique, we conducted studies on a coronary artery model, on volunteers, and on patients with coronary artery disease.

Results: The slice-following technique was compared with simple navigator echo-gating using gating windows from 1 to 6 mm in a model of a 70% coronary artery stenosis that was undergoing 10 mm of respiratory motion. The slice-following technique reduced blurring and improved visualization of the stenosis geometry as assessed by accurate depiction of stenosis severity. The model studies indicated that a gating window of 4–5 mm with slice following produced image quality equivalent to a simple gating window of 2 mm. Applying the prospective slice-following technique using a 5-mm window in 10 volunteers increased the gating efficiency (the percent of cardiac cycle accepted) from 29% to 63% as compared with a simple gating window of 2 mm. MR imaging was successful in 9 of 10 patients with coronary artery disease who had also undergone cardiac catheterization and x-ray angiography. In three patients with significnat lesions, MR correctly identified an abnormality.

Conclusion: Prospective navigator echo-based slice following improves scan efficiency while preserving image quality. Preliminary results suggest this technique should enhance the clinical utility of MR coronary angiography.

Correlation of Atherosclerotic Plaque by Magnetic Resonance Imaging and Clinical Presentation of Patients With Obstruction of the Carotid Artery

Ibraim Pinto, Ricardo Pavanello, Rodrigo Barretto, Simone Barretto, Maria H. Abib, Enilton Egito, Amanda Sousa, J. Eduardo Sousa, Luiz C.B. Souza. *Hospital do Coração, ASS, São Paulo, SP, Brazil*

Magnetic resonance imaging (MRI) has high spatial and contrast resolution. Some studies suggested that it might identify the main components of atherosclerotic plaques (AP), but there is little information regarding a possible correlation of such findings at MRI and the clinical presentation of patients with carotid artery obstruction. The goal of this study was to evaluate the actual value of MRI in the analysis of AP. For such purpose, we selected 50 patients with carotid artery stenosis undertaken to MRI. Spin-echo series with high resolution, acquired with a surface coil, identified AP components according to the signal intensity so that lipids were light gray, calcium was very dark, fresh thrombus was bright, and fibrotic tissue was dark gray. Through the same acquisitions, we defined the artery reference diameter (RD), minimum lumen diameter (MLD), percent stenosis, and maximum wall thickness. We included 50 patients in this study, 38 male, all with a Doppler ultrasound study indicating the presence of a severe carotid stenosis. The mean RD was 8.4 ± 3.9 mm, the mean MLD 1.7 ± 0.7 mm, and the percent stenosis 78 ± 9% and measured the maximum wall thickness as 7.2 ± 3.5 mm. MRI identified lipids as the main component of AP in 24 patients, fibrotic tissue in 19, and calcified plaques in 7. It also identified fresh thrombus in 12 patients. Of the 12 patients with signs of fresh thrombus in the carotid lesion, 9 had a history of a recent cerebrovascular accident, whereas the 26 patients with either fibrosis or calcium as the main AP component had a history of carotid murmur but no history of recent cerebrovascular accidents. All patients underwent surgery. The AP was excised during surgery and undertaken to pathological study. The MRI results correlated well to the pathological evaluation, but MRI did notidentify calcium in four lesions where it was present. It correctly evaluated the existence of fresh thrombus. Quantitative analysis of the AP by pathology also confirmed the dimensions measured by MRI. We conclude that MRI may perform a detailed in-depth analysis of AP, estimating its composition, that correlates well to the clinical presentation of the patients and to the pathological findings.

References

1. Toussaint JF, Southern JF, Fuster V, et al. T2 Contrast for NMR characterization of human atherosclerosis. Arterioscler. Thromb. Vasc. Biol., 1995; 15:1533–1542.
2. Toussaint JF, Southern JF, Fuster V, et al. Diffusion properties of human atherosclerosis and thrombosis measured by pulse field gradient NMR. Arterioscler. Thromb. Vasc. Biol., 1997; 17:542–546.

Early Diagnostic of Rupture of the Descending Aorta by Magnetic Resonance Imaging

Rodrigo Barretto, Simone Barretto, Ricardo Pavanello, J. Eduardo Sousa, Amanda Sousa, Enilton Egito, Edson Romano, Leopoldo Piegas, Ibraim Pinto, Luiz C.B. Souza. *Hospital do Coração, ASS, São Paulo, SP, Brazil*

There is controversy regarding the optimal therapy for patients with type B aortic dissection (AoD). One factor that may precipitate surgery for this population is the presence of aortic rupture. Sometimes though, this may represent a serious diagnostic challenge. Magnetic resonance imaging (MRI) has potential to be used in this set, but its utility early after the clinical suspicion is controversial. The aim of this study was to evaluate the utility of MRI as a diagnostic tool for evaluating patients with type B AoD. From 02/92 to 05/97, 120 patients with suspected type B AoD underwent MRI in a 1.5-T superconducting magnet. The scan included spin-echo images to evaluate anatomy, cine-MRI, and angio-MRI to evaluate blood flow. Blood in the thoracic cavity and suggestion of aorta rupture by cine- and angio-MRI defined aortic rupture. The diagnosis was confirmed in 90 patients, 42 within the first 48 hr and 48 within the first 72 hr after symptoms onset. There were 63 men, and their mean age was 63 ± 38 yr. The mean aortic diameter was 56 ± 42 mm (range, 42–130 mm); there was flow to the false lumen in 58, whereas some degree of thrombosis was present in the false lumen of 32 patients. MRI revealed hemothorax in 38 patients. The point of aortic rupture was near the left subclavian artery in 12, in the middescending aorta in 9, and near the thoracic-abdominal transition in 17. All patients underwent computed tomography that did not suggest the location of the point of rupture in 18 of 38 patients. Surgery was done in 32 patients with suspected aortic rupture and confirmed the presence of hemothorax in all the cases and pointed out aortic rupture in the 32 patients in whom MRI suggested the diagnosis. Of the six not taken to surgery, four died 12–20 hours after MRI and two were kept under clinical treatment and were discharged alive. We conclude that MRI is capable of accomplishing a precise diagnosis of type B AoD and correctly identifying the presence of blood in the thoracic cavity and the point of rupture. This may prove to be a useful tool to evaluate and plan the treatment of patients with suspected AoD.

References

1. Neubauer CA, Spielmann RP, von Rodolish Y, et al. Diagnosis of thoracic aortic dissection: Magnetic resonance imaging versus transesophageal echocardiography. Circulation, 1992; 85:434–447.
2. Kouchoukos NT, Dougenis D. Surgery of the thoracic aorta. N. Engl. J. Med., 1997; 336(26):1876–1888.

Diagnosing and Evaluating the Complications of Thoracic Aorta Aneurysms by Magnetic Resonance Imaging

Ricardo Pavanello, Ibraim Pinto, Rodrigo Barreto, J. Eduardo Sousa, Leopoldo Piegas, Enilton Egito, Carlos Ferreiro, Maria H. Abib, Adib Jatene, Luiz C.B. Souza. *Hospital do Coração, ASS, São Paulo, SP, Brazil*

Different techniques may identify aneurysms of the thoracic (T) aorta (Ao), but few give any prognostic information. Magnetic resonance imaging (MRI) with high spatial and contrast resolution could explore more completely the details of the aneurysm and therefore identify patients at higher risk for adverse events in the follow-up. To evaluate the potential role of MRI in this set, we analyzed 200 patients with TAo aneurysms undertaken to MRI from 12/91 to 12/94. MRI included high-resolution spin-echo series that measured Ao diameter (D) and wall thickness (WT) and identified the presence of atherosclerotic plaques and calcium in the artery wall. Gradient-echo sequences evaluated blood flow, identified thrombus, and determined the presence of aortic rupture when present. Of the 200 patients, 90 had dilation of the ascending Ao, 72 of the descending Ao, and 38 of the entire TAo; D ranged from 42 to 176 mm (mean, 78.5 mm). The Ao had mural thrombus in 160 patients, severe atherosclerosis in 153, and strong evidence of artery wall calcium in 138; the WT was 3.2 ± 5.6 mm. Four patients presented findings suggesting rupture and were taken to immediate surgical treatment. In the follow-up (mean, 3.2 yr), 28 patients (14%) were in clinical treatment, 148 (74%) underwent elective surgery, 8 (4%) presented dissection, and 16 (8%) presented aortic rupture. At baseline, patients undertaken to surgical treatment had D > 45 mm (mean, 53.2 mm). Patients with dissection at baseline had a mean WT of 4.8 ± 22 mm, less evidence of wall calcium, and no signs of mural thrombus. Patients with Ao rupture had, at baseline, larger D (65 ± 23 mm), thinner WT (1.2 ± 0.8 mm), and lower signal intensity in the spin-echo images (16 ± 8) than the rest of the patients ($p < 0.05$). We conclude that MRI allows a detailed evaluation of patients with TAo aneurysms, revealing details about Ao anatomy, size, and wall that may identify patients at higher risk for presenting complications at mid- and long-term follow-up.

References

1. Kouchoukos NT, Duogenis D. Surgery of the thoracic aorta. N. Engl. J. Med., 1997; 336(26):1876–1888.
2. Neubauer CA, Spielmann RP, von Rodolish Y, et al. Diagnosis of thoracic aortic dissection: Magnetic resonance imaging versus transesophageal echocardiography. Circulation, 1992; 85:434–447.
3. Cigarroa JE, Isselbach EM, De Sanctis RW, et al. Diagnostic imaging in the evaluation of suspected aortic dissection. Old standards and new directions. N. Engl. J. Med., 1993; 328:35–43.

Preliminary Findings with an Intravascular Contrast Agent, NC100150 Injection, for MR Coronary Angiography

A.M. Taylor,[1] J.R. Panting,[1] J. Keegan,[1] P.D. Gatehouse,[1] P. Jhooti,[1] G.Z. Yang,[1] J.M. Francis,[1] E.D. Burman,[1] S. McGill,[2] D.N. Firmin,[1] D.J. Pennell.[1] [1]*London, UK;* [2]*Oslo, Norway*

In this study we present our initial experience with the iron oxide particle contrast agent NC100150 injection (Nycomed Imaging AS, Oslo, Norway, a part of Nycomed Amersham) when performing 2D Turbo-FLASH MR coronary angiography in humans. Nine healthy male subjects were studied at 1.5 T. Transaxial 2D Turbo-FLASH (TE 2.6 ms, TR −6 ms, flip angle 30°) images of the right coronary artery were acquired during a single breathhold before and after the administration of NC100150. For all images the signal was measured within the artery, the adjacent fat surrounding the artery, and the septal myocardium. A value for noise was recorded as the signal standard deviation outside the image. Contrast-to-noise ratios were calculated for coronary minus fat signal (CNR [fat]) and coronary minus myocardium signal (CNR [myc]) before and after the administration of NC100150. There was no significant change in the coronary artery signal-to-noise ratio (SNR) ($p = 0.43$). However, there was significant improvement in the CNR (fat) ($p = 0.02$) and the CNR (myc) ($p = 0.02$) in the transaxial images. There was no significant change in the coronary artery diameter ($p = 0.22$) (Table 1).

Table 1. Data from a transaxial image

	SNR	CNR (fat)	CNR (myc)	Diameter (mm)
Pre	33.8	16.3	9.7	3.2
Post	31.7	23.2*	18.0*	3.1

* Represents significant increase in parameters between pre- and post-NC100150 ($p < 0.05$).

This was a phase I study of NC100150, which allowed a preliminary assessment of MR coronary imaging. NC100150 was well tolerated both systemically and locally.

At 1.5 T, there was a significant improvement in both the SNR between the coronary artery and fat and the coronary artery and myocardium, using a standard 2D Turbo-FLASH sequence. Further investigation of NC100150 dose and acquisition sequences (2D and 3D) is required for MR coronary angiography.

In Vitro Validation of the Breathhold MR Measurement in Quantifying the Pattern of Coronary Bypass Flow

T. Voigtländer,[1] K.-F. Kreitner,[2] W. Ludolph,[1] T. Wittlinger,[1] M. Thelen,[2] J. Meyer,[1] W. Landschütz,[3] W. Nitz.[3] [1]*2nd Medical Clinic and* [2]*Clinic for Radiology, University of Mainz, Germany;* [3]*Siemens, Erlangen, Germany*

MR flow measurements of coronary bypass grafts provide functional data (1,2) that overcome the inherent limitations of morphological assessment alone. The aim of the study was to evaluate in vitro the reliability of MR breathhold measurements when applied to the coronary bypass flow pattern.

Method: We measured in vivo intraoperatively blood flow in coronary bypass grafts (venous grafts $n = 10$; internal mammarial [IMA] graft $n = 12$) using the transit-time flowmeter (TTF) method. A typical flow pattern of both graft types was applied to a programmable pump-(UHDC flow system, Canada) tube (diameter 3 mm) system. MR measurement ($n = 20$; Siemens Vision 1.5 T, PC, VENC 75, breathhold, TR 125 ms) and FFT were performed to compare the results for mean flow/min and maximum flow.

Results: MR measurement using breathhold sequences resulted in flow profiles comparable with FFT results, and measurement of mean and maximum flow could be performed. The table contains the mean and standard deviation and error of the MR measurement compared with FFT:

	Mean Flow (ml/min)		Maximum Flow (ml/min)	
	Venous Graft	IMA	Venous Graft	IMA
MR	63.72 ± 0.18	73.38 ± 0.22	106.2 ± 0.42	107.4 ± 0.53
TTF	65.21 ± 1.15	78.64 ± 1.81	108.19 ± 3.43	94.82 ± 5.49
Error (%)	2.28	6.69	1.84	13.27

Conclusion: Mean flow for both graft types was slightly underestimated by MR breathhold measurement, but the error was acceptable. For the venous-type flow pattern, MR measurement of the maximum flow was very similar to the FFT measurement, whereas the maximum flow of the IMA-type flow pattern was less reliably measured by MR.

References

1. Debatin JF. MR characterization of blood flow in native and grafted internal mammary arteries. JMRI, 1993; 3:443–450.
2. Galjee MA. Value of MRI in assessing patency and function of coronary artery grafts. Circulation, 1996; 93:660–666.

Three-Dimensional Zonal Echo-Planar Coronary Imaging

G.Z. Yang, P.D. Gatehouse, J. Keegan, R.H. Mohiaddin, D.N. Firmin. *Magnetic Resonance Unit, Royal Brompton Hospital, London, UK*

Despite the advances in magnetic resonance (MR) coronary imaging achieved in recent years, reliable and consistent imaging of the coronary arteries remains difficult because physiological motion coupled with the small size and tortuous nature of the coronary vessels present unusual challenges. The goal of this study was to develop a routine and clinically viable technique for acquiring 3D coronary images in a reasonably short imaging time by using a new zonal echo-planar imaging technique. The method carries the robustness of gradient-echo sequences while maintaining the efficiency of echo-planar techniques. The reliability of the described approach originates from the relatively short forward echo-only interleaves used for the segmented 3D *k*-space coverage. A reduction in imaging time was made possible by using 2D spatially selective radiofrequency (RF) excitation and a locally focused encoding scheme that minimizes the required phase-encoding steps. The sequence was implemented on a mobile 0.5-T whole body scanner with actively shielded magnetic field gradient coils delivering 20 mT/m peak strength and 60 mT/m/ms maximum slew rate. Sixteen asymptomatic volunteers (11 men and 6 women, aged 24–42 yr) underwent MR imaging with the proposed technique after they provided informed consent. The technique was evaluated using the right coronary artery (RCA) images of the volunteers, and the results were compared with those acquired from the conventional 2D segmented FLASH sequence with navigator echoes. The image assessment reuslts for all 16 volunteers are listed in the table, in which the length and diameter of the RCA were measured by two independent observers. The visibility of the origin of the RCA and the confidence of vessel following were scored using a grading system of 1 (poor) to 5 (excellent). Advantages of the technique include an improved signal-to-noise ratio, clearer depiction of tortuous coronary vessels due to decreased partial volume effects, and reduced motion blurring by the use of a short echo-planar readout. The technique holds the potential for performing spatially selected motion-adaptive excitation and imaging and thus allows the development of a robust and clinically viable 3D MR coronary imaging method without breathholding.

Coronary Artery Imaging with the Intravascular Contrast Agent MS-325

M. Stuber, R.M. Botnar, M.V. McConnell, P.G. Danias, K.V. Kissinger, R.R. Edelman, W.J. Manning. *Boston, MA*

Changes in heart rate primarily affect the duration of the diastolic portion of the cardiac cycle. Therefore, signal sampling at end systole is a promising approach to reduce heart motion-induced blurring of the coronary arteries in the images (1). However, a limitation of imaging at end systole is the relatively slow flow in the coronary arteries that reduces the inflow contrast in the images. The application of an intravascular contrast agent that lowers the T1 of blood together with an inversion prepulse (2) might help to overcome this problem and might lead to a considerable improvement of blood–muscle contrast in the images. In the present abstract, a method for end-systolic imaging of the coronary arteries with an intravascular contrast agent is presented. It is based on navigator gating and real-time navigator tracking.

Methods: In four patients, the Gd-based intravascular contrast agent MS-325 (EPIX Medical Inc., Cambridge, MA) was applied in a single-dose injection of 0.05 mmol/kg. Five minutes after the IV injection of the agent, imaging of the coronary arteries was started. Image acquisition was performed using an ECG gated 3D TFE sequence on a 1.5-T Philips Gyroscan ACS/NT whole body system (Philips Medical Systems, Best, NL). A five-element cardiac synergy coil was used for signal acquisition. A nonselective 180° prepulse preceded the 2D selective navigator. For excitation pulse, the navigator was used for gating and real-time tracking of the imaged volume. The imaging sequence was performed at end systole and the inversion delay of the prepulse was optimized for maximum blood–muscle contrast. The acquisition window was 60 ms for maximum efficiency of the prepulse. Total imaging time was approximately 15 min.

Results: In general, the coronary vessels are enhanced even though the images were acquired at end systole where coronary flow is markedly reduced. The efficiency of the real-time navigator did not seem to be affected by the nonselective prepulse. By the application of the 180° inversion, muscle signal is reduced by the factor of 6 when compared with the signal of blood. The signals of the thoracic muscle and fat are suppressed in the images. The acquisition of the 3D dataset was finished 20 min after the injection of the contrast agent. Despite the relatively long acquisition time, the coronaries are enhanced, consistent with the intravascular localization of the agent.

Conclusions: Because MS-325 remains intravascular for long periods, it is well suited for navigator-based techniques with high-resolution imaging and an increased overall measurement time. Dose optimization and optimal T1 remain to be defined; however, the concept of end-systolic image acquisition and signal enhancement due to the application of an intravascular contrast agent opens a wide field for cardiac applications in the future.

References

1. Sodickson D, et al. Proc. ISMRM, 1997; 2:910.
2. Hofmann M, et al. Proc. ISMRM, 1997; 1:442.

	Segmented Flash				3D Zonal EPI			
	Length (mm)	Midsegment Diameter (mm)	RCA Origin Visibility	Confidence of Vessel Following	Length (mm)	Midsegment Diameter (mm)	RCA Origin Visibility	Confidence of Vessel Following
Range (min–max)	20.5–74.5	2.5–5.0	0–4	1–4	38.1–83.5	3.5–5.4	2–5	3–5
Mean ± SD	47.4 ± 13.9	4.0 ± .65	1.5 ± 1.5	2.4 ± 1.2	61.4 ± 13.8	4.4 ± .44	4.2 ± 0.9	4.1 ± 0.7
			1 (9)	1 (5)			1 (0)	1 (0)
Score (distribution)	—	—	2 (1), 3 (5)	2 (3), 3 (4)	—	—	2 (1), 3 (2)	2 (0), 3 (3)
			4 (1), 5 (0)	4 (4), 5 (0)			4 (6), 5 (7)	4 (8), 5 (5)

Quantification of "No-Reflow" Zone with Gadomer-17–Enhanced MR Imaging During ATP-Induced Hyperemia

K. Chung, T. Chung, H. Weinmann, T. Lim, B. Choi. *Department of Radiology, Ajou University, Sumon, Korea*

Quantification of myocardial ischemia in MR imaging has been limited by inadequate steady-state signal intensity (SI) differences. As in recent successful identification of viable myocardium using first-pass MR imaging, implementation of the higher-molecular-weight intravascular contrast media combined with hyperemic agent may intensify SI differentiation, leading to expedient quantification of the "no-reflow" zone throughout the steady-state transit of the contrast media.

Methods: The left anterior descending coronary artery in seven cats was occluded for 3 hr followed by 30 min of reperfusion. Gadomer-17 (0.1 mmol/kg) was injected in bolus during ATP infusion. Series of postcontrast MR images were acquired on a 1.5-T unit using SE sequence (TR/TE 400/15 ms, matrix 256 × 128, field of view 120 mm, collimation 5 mm, and two excitations). The third transaxial image from the apex was selected to measure area of the no-reflow zone relative to the sectional myocardium, and the time course of the area and SI changes were monitored.

Results: Maximal SI for normal, periinfarct, and no-reflow zones were 1.65 ± 0.09, 2.26 ± 0.2, and 1.57 ± 0.16, occurring, respectively, at postcontrast 5, 10, and 15 min. Maximal SI difference between the ischemic zones was 0.88 ± 0.08 attained at postcontrast 10 min. However, maximal area of no-reflow zone was 7.23 ± 1.65% attained within the first 5 min, and the initial steep rise was followed by a sharp drop to 3.36 ± 0.59% for 10 min followed by steady decrease to 0.64 ± 0.29% for 45 min. The no-reflow zone was sharply defined as central low SI distinct from surrounding high SI periinfarct zone. The time course of the area change was highly related ($r = 0.805$, $p < 0.05$) with the time course of the SI difference, whereas maximal size of the area showed reverse correlation ($r = 0.805$, $p < 0.05$) with the time course of the SI difference, whereas maximal size of the area showed reverse correlation ($r = -0.7$, $p < 0.05$) with the initial periinfarct SI at postcontrast 5 min.

Conclusion: Gadomer-17–enhanced steady-state MR imaging during ATP-induced hyperemia displayed the no-reflow zone as a distinct low SI, leading to expedient quantification of the area that was closely related to time-dependent SI changes.

Value of Combining Rest and Stress Data in a MR Perfusion Analysis in the WISE Study

M. Doyle, A. Fuisz, E. Kortright, E. Walsh, E. Martin, W. Rogers, G. Pohost, for the WISE investigators. *Birmingham, AL*

It has been established that in first-pass MRI perfusion studies, a stress agent enhances differences between normally perfused and underperfused territories. However, the diagnostic value of the nonstress MRI perfusion images has not been established. As part of the NHLBI WISE study, 53 women were examined with MR first-pass perfusion imaging and cardiac catheterization. Two to three short-axis slices were obtained every or alternate heart beats during bolus injection of a gadolinium by peripheral IV. Rest and "stress" images were obtained (stress induced by administration of dipyridamole). Two groups emerged from a retrospective unblinded analysis: those with evidence of significantly increased rate of signal change with time postdipyridamole (53% of patients) and those without this finding. Sensitivity and specificity for the detection of the presence of a >70 stenosis by coronary angiography of the stress images were better in the group with increased response (IR) (75% and 81%, respectively) than in the remaining patients without the response (WR) (67% and 40%, respectively). The rest analysis yielded similar results (IR sensitivity and specificity of 67% and 75% versus WR, 47% and 50%). Using the rest images along with the stress images in a combined analysis, the sensitivity and specificity for the IR group improved to 86% and 91%, respectively (18 patients, 34% of total). In the WR group, no improvement was seen. It appears that by combining rest and stress analysis, the diagnostic accuracy of MRI perfusion imaging is improved in a substantial subgroup of patients. Interestingly, in patients in the IR group, resting differences in myocardial perfusion could be identified. The enhanced accuracy of the IR group's rest images may represent a fundamental difference between the two groups rather than merely reflecting the adequacy of stress.

Gadophrin-2, a Necrosis-Avid Magnetic Resonance Imaging Contrast Agent for Noninvasive Quantification of Myocardial Infarct Size

S. Dymarkowski,[1] Y. Ni,[1] J. Bogaert,[1] C. Pislaru,[1] H. Bosmans,[1] Y. Miao,[1] F. Van de Werf,[1] W. Semmler,[2] G. Marchal.[1] [1]*Leuven, Belgium;* [2]*Berlin, Germany*

Background and Purpose: Paramagnetic metalloporphyrins can be used as necrosis-avid contrast agents for MRI. The present study was designed to evaluate whether a small dose of gadophrin-2 (*bis*-gadolinium mesoporphyrin) can serve as a diagnostic adjuvant to PTCA for assessment of myocardial viability.

Methods and Results: Twelve closed-chest dogs underwent balloon occlusion of coronary artery for 20 or 180 min to induce reversible myocardial ischemia or irreversible acute myocardial infarction (AMI). Thirty minutes after reperfusion, 20 ml of diluted gadophrin-2 at 5 μmol/kg was infused in the coronary artery for 10 min. In vivo ECG-gated T1-weighted turbo-FLASH and T2-weighted HASTE MRI and T1- and T2-weighted spin-echo MRI of excised heart were performed 2–4 hr after infusion. Findings of MRI and TTC staining were planimetrically correlated. In dogs with 20-min occlusion, part of the myocardium appeared hyperintense on T2-weighted images, but no contrast enhancement was detectable on the T1-weighted images. In dogs with 180-min occlusion, a strong (200–300%) and persistent enhancement was observed in T1-weighted images. The infarcts enhanced by gadophrin-2 correlated closely to TTC-negative areas ($R^2 = 0.994$, slope = 1.004), whereas T2-weighted MRI overestimated the infarct size by 130%.

Conclusion: Besides intravenous administration, a small dose of gadophrin-2 can also be administered directly in the coronary artery during PTCA for postprocedure assessment of myocardial viability.

Intravascular Contrast Agent Improves 3D Magnetic Resonance Coronary Angiography in Humans

L.O. Johansson,[1] M.B.M. Hofman,[1] S.E. Fischer,[1] S.A. Wickline,[1] C.H. Lorenz,[1] S. Witte.[2] [1]*St. Louis, MO;* [2]*Cambridge, MA*

Extracellular contrast agents have limited applicability for magnetic resonance coronary angiography (MRCA) due to the short intravascular half-life, which limits the resolution and possibilities for repeated scans. The purpose of this study was to evaluate the effect of a new intravascular contrast agent, MS-325 (EPIX Medical Inc.), with a long intravascular half-life for 3D-MRCA. Six patients with known coronary artery disease were scanned using a Gyroscan ACS-NT (Philips Medical Systems) 1.5-T scanner. The protocol was a navigator-based respiratory-gated and ECG-triggered 3D gradient echo sequence with a resolution of 1 × 1 × 1.9 mm^3 with TR/TE 7.8/3.0 ms with a flip angle sweep maintaining constant magnetization over the acquisition. Spectral fat suppression was applied. A transverse scan for the left coronary system and an oblique scan for the right coronary system were performed both precontrast and 5–30 min postcontrast. MS-325 was injected over 75 s using a dose of 0.05 mmol/kg. The SNR and CNR were measured

in the source images. CNR were defined as the contrast between blood and myocardium. Curved reformats were performed on the data sets, and the length of the visible segments of the RCA, LM, LCX, and LAD were measured using an EasyVision workstation (Philips Medical Systems). The SNR of the RCA increased by 43–98% from pre- to postcontrast injection, whereas the CNR increased by 28–51%. On average, the RCA was visible for 7.5 cm and the LM + LAD were visible for 6.3 cm postinjection. The LCX was poorly visualized due to the limited slab thickness.

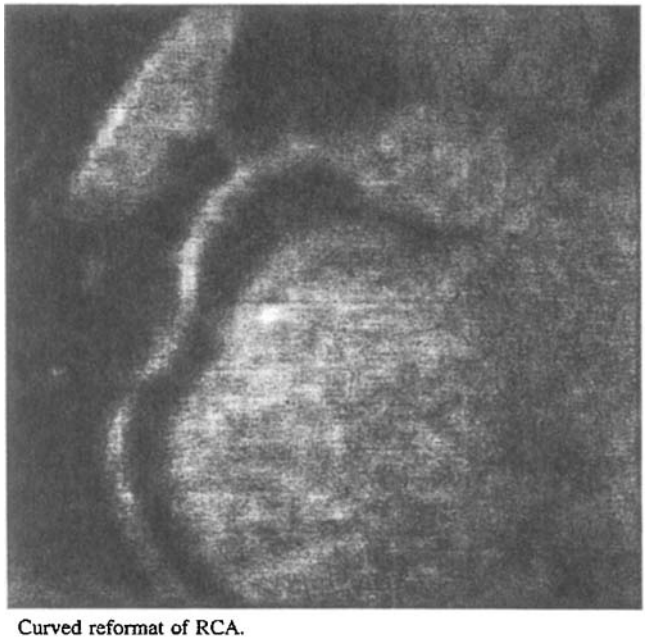

Curved reformat of RCA.

Curved reformat of RCA and LAD.

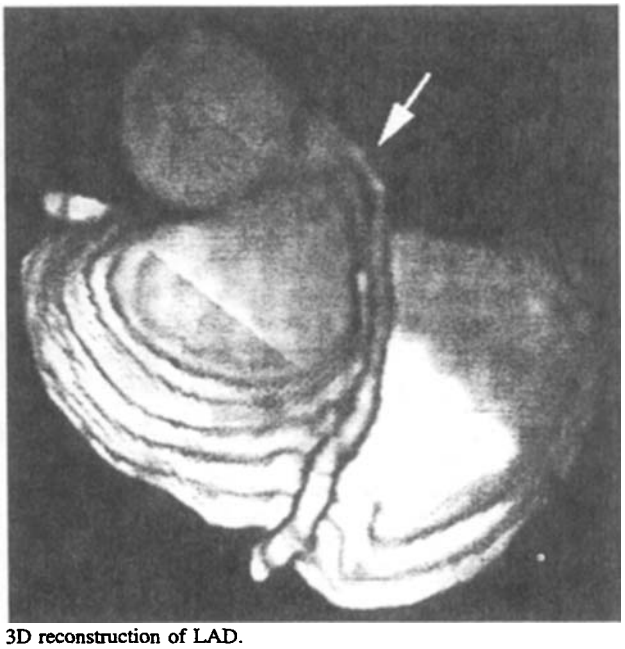

3D reconstruction of LAD.

We showed that MS-325 improves 3D-MRCA. The improvement, however, is less for ECG-triggered coronary MRA than for conventional nontriggered contrast-enhanced MRA because the gating allows more relaxation to occur between the acquisitions. Therefore, a shorter T1 in blood would be helpful to increase the utility of intravascular contrast agents for 3D-MRCA. Further studies are needed to assess the potential for diagnosis of CAD using this contrast agent.

Respiratory Motion Correction for Rapid Cardiac Perfusion Imaging Without Navigator Echoes

E. Kortright, M. Doyle, E. Walsh, G. Pohost. *Birmingham, AL*

In the presence of respiratory motion, first-pass cardiac perfusion images require registration to track a region of interest through time. For rapid cardiac imaging, we use a distributed k-space sampling scheme to acquire data from multiple slices at every heartbeat. This scheme leaves segments of k-space unsampled at certain frames, requiring interpolation of the missing information. Because each frame is synthesized from k-space segments acquired at different points in the respiratory cycle, shape distortions and misregistrations result. To track respiratory motion, navigator echoes are potentially problematic: targeting a secondary feature such as the diaphragm may not correspond with cardiac motion, targeting the organ of interest may interfere with signal detection, and navigators require time that could be spent acquiring image data. Thus, instead of navigators, we sought to use the image data itself to track cardiac motion, register the images, and eliminate distortion. Because the central k-space line represents a projection of the entire field of view, we sought to use it for motion tracking. However, features at the same level as the heart (e.g., the diaphragm) obscure the heart's motion, requiring central-line enhancement. Our protocol acquires up to five lines from the center of k-space for every frame, which are then placed in a zero-filled matrix and transformed, giving a very low resolution image of the heart. The areas to either side of the heart are set to zero, and the resulting images are inverse transformed. The central k-space line thus formed yields a much cleaner estimate of cardiac motion. Once the extent of respiratory motion is determined, the raw data can be corrected. A linear gradient multiplied by the motion estimate

for each frame is added to the phase of each acquired line of k-space. The missing lines are then synthesized to obtain registered images with significantly reduced distortion.

Very-Low-Dose Gadolinium-P760–Enhanced First-Pass Perfusion and Spin-Echo MR Imaging of Infarcted Myocardium in Pigs

L.J.M. Kroft, J. Doornbos, R.J. van der Geest, E. Haselhoff, A. van der Laarse, A. de Roos. *Leiden, The Netherlands*

Purpose: We assessed the potential value of very-low-dose gadolinium-P760 for the detection of acute myocardial infarction by magnetic resonance (MR) imaging.

Methods: T1-weighted fast gradient-echo first-pass MR imaging was used during administration of 0.09 ml/kg of 0.072 mol Gd/l (0.0065 mmol Gd/kg) P760 (Guerbet, Aulnay-s-Bois, France) in seven pigs with surgically induced myocardial infarction. P760 is a newly designed, low-dose, gadolinium-based, low diffusion, extracellular contrast agent with high relaxivity. Spin-echo imaging was performed before and after P760 administration. First-pass measurements in the myocardium were performed in pigs with necrotic areas covering 50–90% of the regional wall thickness in which regions of interest could be drawn containing >15 pixels ($n = 4$). The first-pass difference in enhancement of normal and infarcted myocardium was measured, as well as the contrast ratio (CR) of normal and infarcted myocardium on spin-echo imaging ($n = 7$).

Results: Values are expressed as mean ± SEM. There was a significant difference between the enhancement of the normal myocardium (37 ± 6%) and infarcted myocardium (5 ± 3%; $p = 0.03$). Spin-echo imaging showed a significant CR enhancement of 131% at 15 min and 129% at 25 min after contrast agent administration (precontrast CR 0.21 + 0.03, at 2–5 min 0.67 ± 0.30 [p = ns], at 15 min 0.48 ± 0.05 [$p = 0.002$], at 25 min 0.47 + 0.07 [$p = 0.003$]).

Conclusions: Low-dose gadolinium-P760 perfusion imaging is useful to identify enhancement differences between normal and infarcted myocardium at rest. P760 contrast-enhanced MRI improves the detection of acute myocardial infarction on spin-echo imaging.

First-Pass Myocardial Perfusion Imaging and Equilibrium Signal Changes Using the Intravascular Contrast Agent NC100150 Injection

J.R. Panting,[1] A.M. Taylor,[1] P.D. Gatehouse,[1] J. Keegan,[1] P. Jhooti,[1] G.Z. Yang,[1] S. McGill,[2] J.M. Francis,[1] E.D. Burman,[1] D.N. Firmin,[1] D.J. Pennell. [1]*London, UK;* [2]*Oslo, Norway*

The use of intravascular contrast agents for assessment of MR myocardial perfusion has been validated in animals (1). We studied the intravascular contrast agent NC100150 (Nycomed Imaging AS, Oslo, Norway) for first-pass myocardial perfusion imaging and equilibrium signal changes in the myocardium as a marker of myocardial blood volume. These studies were performed as part of a phase I trial of the contrast agent. Eighteen healthy male subjects were studied, 9 each at 0.5 T and 1.5 T. At each field strength, three subjects were studied for each dose of NC100150 (2, 3, and 4 mg/kg). Each dose was administered as two boluses, 4 min apart. First-pass studies were weighted for T1 using gradient-echo FLASH (TE 2.7) at 1.5 T and spin-echo EPI (TE 6.7) at 0.5 T. T1-weighted FLASH sequences at both 0.5 T and 1.5 T and T2* images using gradient-echo EPI at 1.5 T were used for equilibrium imaging. At both field strengths, mixed T1 and T2* effects were seen during first pass. At 0.5 T, this occurred in the myocardium with all but the lowest dose. At 1.5 T, the mixed effect was most marked in the blood pool, not occurring in the myocardium with the first bolus.

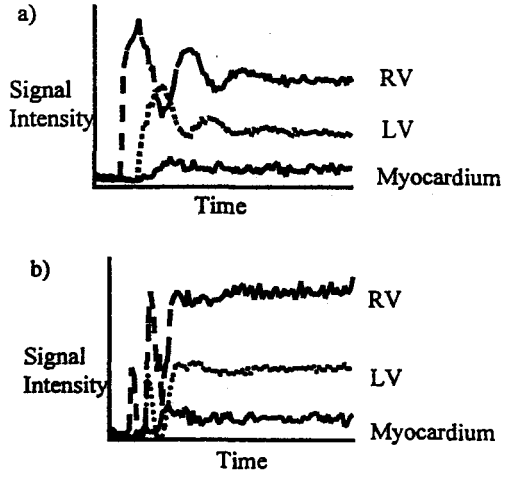

Figure 1. First pass imaging, FLASH at 1.5 T: signal intensity vs time curves. (a) 0.5 mg/kg NC100150; (b) 3 mg/kg NC100150. Note the mixed T1 and T2* effects in the blood pool in b.

With equilibrium imaging, signal changes were noted with all doses. The T1 images showed no difference between the different doses. Using T2*, however, the 3- and 4-mg/kg doses resulted in significantly lower myocardial signal than 2 mg/kg. There was no difference between these doses. In conclusion, first-pass imaging with NC100150 requires the use of small doses to avoid T2* effects in the myocardium with long TE SE-EPI at 0.5 T and in the LV blood pool with short TE FLASH at 1.5 T, the latter affecting the input function for quantification. Significant myocardial signal changes at equilibrium can be produced; however, it needs to be determined whether this method would lead to useful information under rest and stress conditions in ischemic heart disease.

Reference

1. Wilke N. Regional myocardial blood volume and flow: First pass MR imaging with polylysine-Gd-DTPA. JMRI, 1995; 5(2):227–237.

Gradient-Echo Cine and Spin-Echo Imaging of the Heart, Using the Intravascular Contrast Agent NC100150 Injection

A.M. Taylor,[1] J.R. Panting,[1] J. Keegan,[1] P.D. Gatehouse,[1] P. Jhooti,[1] G.Z. Yang,[1] J.M. Francis,[1] E.D. Burman,[1] S. McGill,[2] D.N. Firmin,[1] D.J. Pennell.[1] [1]*London, UK;* [2]*Oslo, Norway*

We studied the intravascular iron oxide particle contrast agent, NC100150 injection (Nycomed Imaging AS, Oslo, Norway, a part of Nycomed Amersham) for MR imaging of the human heart. Eighteen healthy male volunteers were studied at both 0.5 and 1.5 T before and after the administration of NC100150. Conventional gradient-echo cines were acquired at 0.5 T, and breathhold Turbo-FLASH cines were acquired at 1.5 T. A contrast- (global LV blood pool signal minus myocardial signal) to-noise ratio (CNR) was calculated for the diastolic and systolic frames. Noise was measured as the standard deviation of the signal in a region of interest outside the phase-encoded artifact. Spin-echo images were acquired on both scanners. Blood pool noise was measured (signal standard deviation) in these images. At 0.5 T, there

was a significant increase in the CNR in the diastolic (56%, $p = 0.01$) and systolic (141%, $p < 0.001$) cine frames. There was also a significant increase in the signal intensity (SI) gradient at the LV blood pool/myocardial border in the diastolic and systolic frames (both $p < 0.001$). At 1.5 T, there was a significant increase in the CNR in the diastolic (221%, $p < 0.001$) and systolic (916%, $p < 0.001$) cine frames. Again, there was also a significant increase in the SI gradient at the LV blood pool/myocardial border in the diastolic and systolic frames (both $p < 0.001$). Spin-echo images showed a significant improvement in image quality, secondary to a reduction in the flow artifact at both field strengths ($p = 0.01$ at 0.5 and 1.5 T). In conclusion, NC100150 showed no adverse effects in 18 subjects, and image quality and LV blood pool/myocardial definition were improved. These improvements enable better spin-echo anatomical definition, better definition of myocardial wall motion, and should improve automated edge detection algorithms.

Multislice First-Pass Magnetic Resonance Perfusion Imaging in Comparison with Regional Myocardial Wall Thickening in Chronic Myocardial Ischemia

B.J. Wintersperger, H. Penzkofer, A. Knez, M. Reiser. *University of Munich, Germany*

Purpose: The purpose of our study was to compare findings of first-pass MR perfusion imaging and cine MRI in patients with chronic myocardial infarction.

Methods: Twelve patients with chronic myocardial infarction underwent MR perfusion imaging and cine MRI on a 1.5-T Magnetom Vision. Perfusion was assessed using a triple-slice saturation recovery Turbo-FLASH sequence (2.5 ms/1.2 ms/8°) and automated injection of gadopentetate dimeglumine (1). Myocardial thickening was assessed using a segmented breathhold 2D FLASH sequence (80 ms/4.8 ms/10°). Perfusion and wall thickening were determined for corresponding slice positions. Systolic myocardial wall thickening was evaluated after semiautomated segmentation of myocardial contours, and results were compared with mean values obtained from six healthy volunteers. Myocardial wall thickening percentage more than two standard deviations below the mean values of the control group was considered abnormal. Anterior, lateral, posterior, and septal myocardial regions (ROIs) were classified for comparison with perfusion MRI. Multisection first-pass perfusion imaging was analyzed with a user-developed software tool, calculating color-coded parameter maps for signal intensity upslope.

Results: Mean wall thickening percentage in our control group rose from the base (40.0 ± 12.4%) to the apex (71.7 ± 19.6%). In the patient group in 11 of 48 ROIs, first-pass MR perfusion imaging showed hyperperfusion correlating well to ^{99m}Tc-Sestamibi SPECT. Cine MRI showed abnormal myocardial wall thickening percentage in 13 of 48 ROIs. One ROI with abnormal myocardial perfusion did not show reduced myocardial wall thickening. Additionally to perfusion MRI, three ROIs with reduced wall thickening could be identified.

Conclusion: Myocardial wall thickening analyzes and myocardial perfusion in MRI provides complementary informations in patients with CHD. In patients with chronic myocardial infarction, wall thickening is significantly reduced in hypoperfused areas than in normal perfused areas. Hypoperfusion and restricted myocardial thickening correlate well.

Reference

1. Wilke N. Myocardial perfusion reserve: Assessment with multisection, quantitative first-pass MR imaging. Radiology, 1997; 204:273–384.

Interobserver Reproducibility of MRI Tagged Data in Patients with Hypertensive Left Ventricular Hypertrophy

R.W.W. Biederman,[1] M. Doyle,[1] A. Young,[2] S. Thrupp,[2] E. Kortright,[1] S. Oparil,[1] G. Pohost,[1] L. Dell'Italia,[1] for LIFE study investigators. [1]*Birmingham, AL;* [2]*Auckland, New Zealand*

In this study we sought to compare the reproducibility of MRI tagging by spatial amplitude modulation (SPAMM). We evaluated 14 patients with left ventricular hypertrophy by ECG criteria in the LIFE study (9 m and 5 f, 56–78 yr). As prescribed by the LIFE study, the site of the 2D MRI acquisitions were based on American Society of Echocardiography standards and positioned just above the level where the papillary muscles attach to the myocardium. Data were acquired on a 1.5-T system. In the 2D analysis, the intersection of tagged regions were semiautomatically detected and tracked from systole to diastole. From this analysis, intramyocardial strain (ε) can be calculated for specific myocardial regions. Strain between diastole and systole was calculated for two regions—the intraventricular septal wall (IVS) and the posterior wall (PW)—to correspond with parallel echocardiography measurements. The strain was resolved into radial (εR) and circumferential (εC) components. Two separate readers using the same software package analyzed the data (the software makes an attempt to automatically track the vertices, but due to low signal-to-noise ratio, substantial manual intervention is required to override obvious errors). The correlation coefficient (r) was calculated for each variable, summarized below:

Variable	r value
εR(IVS)	0.85
εC(IVS)	0.80
εR(PW)	0.86
εC(PW)	0.34

All r values are in an excellent level with the exception of the circumferential strain in the posterior wall, which is due to a single outlier. Correcting for this outlier, the r value becomes 0.84. To obtain such a high level of correlation in a difficult patient population is promising for clinical utility of this new technology.

Regional Analysis of Left Ventricular Wall Thickness and Motion Myocardial Infarction

B.R. Cowan,[1] A.A. Young,[1] L.J. Dell'Italia.[2] [1]*Auckland, New Zealand;* [2]*Birmingham, AL*

The assessment of cardiac function after myocardial infarction is generally based on the measurement of global parameters such as end-systolic volume, end-diastolic volume, ejection fraction, and left ventricular mass. The process of infarction and the response of uninvolved myocardium is, however, a highly regionalized phenomenon, with reduced wall thickening occurring in the ischemic areas and compensatory increases in those supplied by unaffected vascular territories. Standard global indices therefore tend to average out these effects. The aim of this investigation was to develop a methodology whereby multislice long- and short-axis MRI data could be analyzed on a regional basis. Initially, the endocardial and epicardial contours were defined on all images, and fiducial markers were inserted to locate the position of the right ventricle and base plane. These results were then transferred to a customized finite-element software package that fitted a moving three-dimensional surface to the epicardium and endocardium, resulting in a

beating model of the raw data. Throughout this process, great care was taken to ensure that the smoothing applied to the data both spatially and temporally was sufficient to eliminate noise in the data but did not compromise regional variations in wall motion. Once these surfaces had been determined, 16 separate regions of the ventricle were defined using standard echocardiographic criteria (although any other scheme is also possible) for numerical sampling of 4,000 points, averaging and reporting of results.

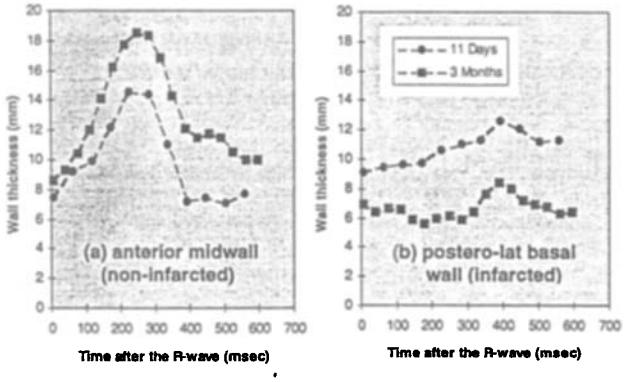

A 61-year-old postinfarct patient is presented. He suffered an inferoposterior myocardial infarction (peak CPK 2,768), with a catheter study demonstrating a right dominant circulation with total occlusion of the right coronary artery. MRI was performed at 11 days and 3 months. Results in the figures show the compensatory increase in anterior midwall function and the poor wall thickening in the area of infarction. Of note is the loss of muscle seen in this region between 11 days and 3 months. In addition, a beating model of the left ventricle was color-coded according to wall thickening to allow direct visualization of regional ventricular performance, and standard global indices were calculated, which showed global dilatation and an increase in left ventricular mass. These results show that careful smoothing by four-dimensional finite-element modeling of MRI data, and subsequent numerical sampling of wall thickness, is a promising way of analyzing regional wall motion postmyocardial infarction.

Rapid-Phase Velocity Mapping

M. Doyle, A. Anayiotos, E. Kortright, A. Fuisz, E. Walsh, G. Pohost. *Birmingham, AL*

Rapid-phase velocity mapping can be accomplished by use of segmented (or "turbo") scans. However, in typical in vivo applications, compromises in both spatial and temporal resolution have to be made to accommodate breathhold requirements. We sought to reduce the acquisition time by incorporating BRISK (block regional interpolation scheme for k-space) imaging. BRISK distributes data sampling over k-space and time in a sparse manner and interpolates data not directly acquired. The accuracy with which turbo-BRISK represents phase-velocity data was tested in a flow phantom. Pulsatile flow, simulating cardiac output, was generated by a Harvard pump with a solution of water and copper sulfate. The phantom was constructed of a rigid pipe of 19 mm diameter surrounded by static water. All data were acquired on a 1.5-T system in a triggered manner. Scan parameters were FOV 300 mm, matrix 256 × 256, TE/TR/flip 8.4/16/40. Phase-velocity data were acquired in both in-plane and through plane manners, with BRISK turbo factors ranging from 2 to 5. For analysis, velocity data in the flow section were integrated for each frame and tabulated over the cycle. A correlation analysis was performed comparing the full scanned data with the various BRISK runs. Results are summarized below:

Technique	Scan Time (Min:Sec)	In-Plane Flow *r* Value	Through-Plane Flow *r* Value
Conventional	8:32	1	1
BRISK	2:49	0.99	0.99
BRISK turbo 2	1:24	0.99	0.99
BRISK turbo 3	0:56	0.99	0.99
BRISK turbo 4	0:42	0.98	0.98
BRISK turbo 5	0:34	0.97	0.96

Turbo-BRISK is capable of accurately imaging pulsatile flow with high resolution and in short scan times. Excellent-quality in vivo results have been obtained using turbo-BRISK in breathholds of 20 s. BRISK images did not suffer motion artifacts, as did full acquisitions, and accurately reproduced the quantitative information.

Real-Time Cardiac Function Assessment with Segmented EPI Using Asymmetrical k-Space Acquisition

S.E. Fischer,[1] S.A. Wickline,[1] C.H. Lorenz,[1] R. de Boer,[2] J.P. Groen,[2] G. Mens.[2] [1]*St. Louis, MO;* [2]*Best, The Netherlands*

The purpose of this study was to investigate the feasibility of real-time imaging methods for the assessment of cardiac function. Cardiac function can be assessed very accurately with MRI (i.e., by the use of breathhold) ECG-triggered cine acquisitions but is less successful than echocardiography in noncooperative patients or in patients with arrhythmias. Because spiral MRI makes optimal use of the gradient system, the feasibility for fluoroscopy has been demonstrated (1). However, asymmetrical k-space acquisition schemes (2) to further reduce scan time are difficult to apply in spiral imaging as compared with echo planar imaging (EPI). To reduce scan time while limiting echo time, an interleaved EPI sequence (3) was combined with an acquisition scheme covering 67% of k-space starting with a phase encoding close to the center of k-space. The sequence was implemented on a 1.5-T whole body system (Gyroscan ACS-NT/Powertrak 6000, Philips Medical Systems, Best, The Netherlands) with a gradient slew rate of 105 T/m/s and tested in seven volunteers. Scan time of a complete image (no profile sharing) with a 300 × 225 mm field of view and a scan matrix of 128 × 75 was 70 ms, yielding a frame rate of 14 images per second. For each image, five to six RF pulses were applied followed by a short, echo-shifted EPI read-out with an echo time of 5 ms. The figure shows the manually segmented short-axis area (% of end-diastolic area) of a healthy volunteer with a heart rate of 72–80 bpm. The scan was applied in a free run, without ECG triggering. The application of a hybrid turbo gradient echo/echo planar imaging sequence to assess real-time cardiac function is demonstrated. Because no gating or patient cooperation (i.e., breathhold or remaining still) is required, this method overcomes some of the current problems in MRI assessment of cardiac function.

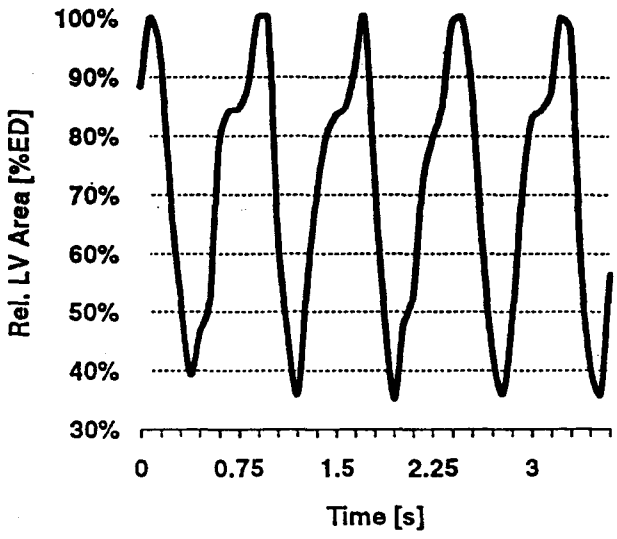

References

1. Spielman DM, Pauly JM, Meyer CH. Magnetic resonance fluoroscopy using spirals with variable sampling densities. Magn. Reson. Med., 1995; 34(3):388–394.
2. McKinnon GC. Ultrafast interleaved gradient-echo-planar imaging on a standard scanner. Magn. Reson. Med., 1993; 30(5):609–616.
3. Feinberg DA, Hale JD, Watts JC, Kaufman L, Mark A. Halving MR imaging time by conjugation: Demonstration at 3.5 kG. Radiology, 1986; 161(2):527–531.

Flow Quantification with Magnetic Resonance Using the Isovelocity Area Method Close to an Orifice: An In Vitro Study

L.J. Jiménez-Borreguero, P.J. Kilner, S.R. Underwood, D.N. Firmin. *London, UK*

The proximal isovelocity surface area (PISA) method for flow calculation has been amply studied using color Doppler but very little using magnetic resonance. The purpose of this study was to evaluate, in vitro, the precision of MRI for quantification of flow through an orifice using the PISA method. Five continuous flows between 49 and 349 ml/s were applied (time and volume being precisely measured) for each of eight flat orifices (areas between 0.24 and 1.92 cm^2) interposed in a 3.85-cm diameter tube. Flow was measured by two-directional phase contrast gradient echo velocity mapping in a plane aligned with the axis of orifice flow using a 0.5-T system and surface coil (TE 14 ms, FOV 25 cm, 1 × 1 × 6-mm resolution). Four concentric PISA levels were selected for each flow and orifice. The maximum and minimum radius was used for the calculation of the area by two formulas, hemisphere and hemielipse. The flow was obtained by multiplying each isovelocity value by its PISA.

Results: Flows calculated by the hemielipse formula for all orifices and PISA levels correlated well with the reference (r = 0.95), and the regression line was close to identical (slope = 1.01); however, the hemisphere formula gave less satisfactory results (r = 0.79, slope = 0.45). The mean and standard deviation of the difference between the flow calculated by PISA and that of the reference were excellent for the hemielipse formula (−10.5 ± 20 ml/s) but were not satisfactory for the hemisphere (108 ± 89 ml/s).

Conclusion: Magnetic resonance phase-contrast velocity mapping offers an alternative method for flow quantification, at least in vitro. Proximal isovelocity surface forms were closer to a hemielipse than a hemisphere, although there may be more variation of form in vivo.

Precision of Magnetic Resonance Velocity Mapping to Calculate Flow: An In Vitro Study

L.J. Jiménez-Borreguero, P. Kilner, D. Firmin. *London, UK*

The purpose of this study was to evaluate the precision of magnetic resonance (MRI) velocity mapping to quantify flow in a tubular model. A system of 3.85-cm diameter plastic pipes was built, through which a solution of copper sulfate and water was pumped continuously at rates between 49 and 349 ml/s. Fifty-four different flow rates were studied. Phase-contrast gradient-echo velocity mapping through planes transecting the axis of flow was performed on a 0.5-T system (TE 14 ms, NEX 2, FOV 25 cm). Flows by MRI (QMRI) were measured by multiplying the transverse surface area of the column of liquid by the mean velocity through plane. Results were compared with flow calculated by the liquid collected (QR) in a basin during 30 s, averaging three samples.

Results: QMRI correlated closely with QR (r^2 = 0.99, slope = 1.02). The differences between the QMRI and the QR were small (mean = 2.41 ± 4.11 ml/s and % differences = 1.54 ± 2.67%) and did not vary significantly with rates of flow measured.

Conclusion: Phase-contrast velocity mapping gave accurate measurements of a range of continuous tube flow rates in vitro.

Assessment of Right Ventricular Regional Wall Motion Using Three-Dimensional Phase Contrast Magnetic Resonance Velocity Mapping

H.W.M. Kayser, R.J. van der Geest, E.E. van der Wall, J.H.C. Reiber, A. de Roos. *Leiden, The Netherlands*

Purpose: We assessed right ventricular (RV) regional function using three-dimensional phase-contrast MR velocity mapping.

Methods: 3D PC velocity mapping in three orthogonal directions was performed in 10 healthy volunteers in a single midventricular short-axis slice (VENC 30 cm/s), obtaining one modulus and three phase images per phase of the cardiac cycle. RV endo- and epicardial contours were manually traced in 29 phases of the cardiac cycle. Using the Centerline method, chords were constructed at 75 evenly spaced intervals along the circumference of the RV myocardium. The RV myocardial wall was divided in six different segments, from the posterior septal to the anterior septal insertion (Fig. 1).

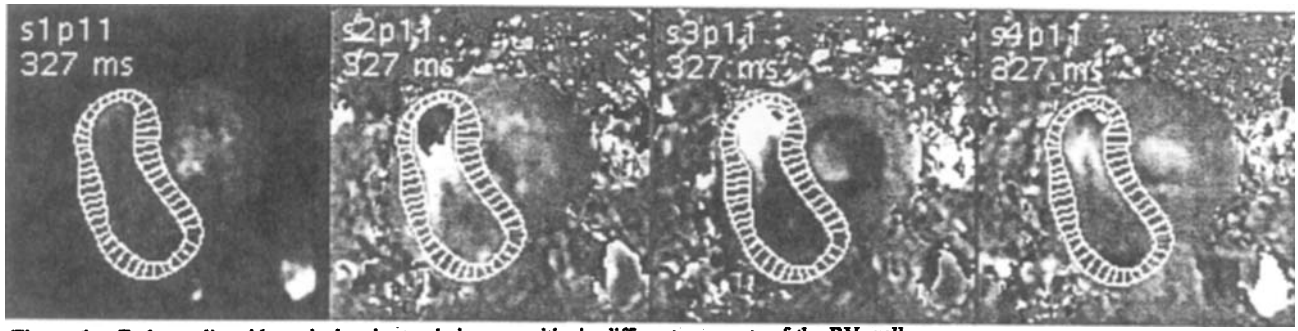

Figure 1. End-systolic midventricular short-axis images with six different segments of the RV wall.

Results: Figure 2 shows the myocardial velocity in radial (toward the RV lumen) direction at peak ejection. The motion of the RV free wall (segments 2–5) is much higher than the velocity measured at the insertion points of the RV with the septum (segments 1 and 6): radial shortening of the RV free wall was 14.8 mm, shortening at the insertion points was 2.7 mm. Figure 3 shows the radial RV velocity as a function of time for every segment of the RV. The myocardial motion shows a monophasic movement during systole and an opposite biphasic movement during diastole. Velocities are highest in the RV free wall. RV velocity in the through-plane direction showed the same pattern.

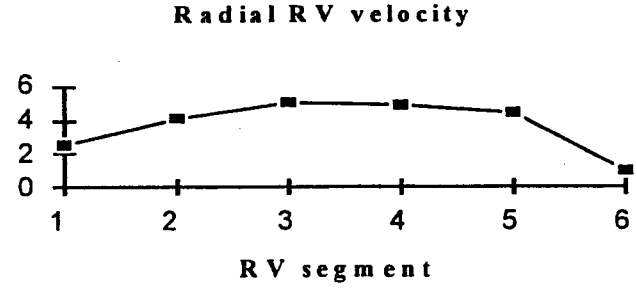

Figure 2. RV myocardial velocity in radial direction at peak ejection.

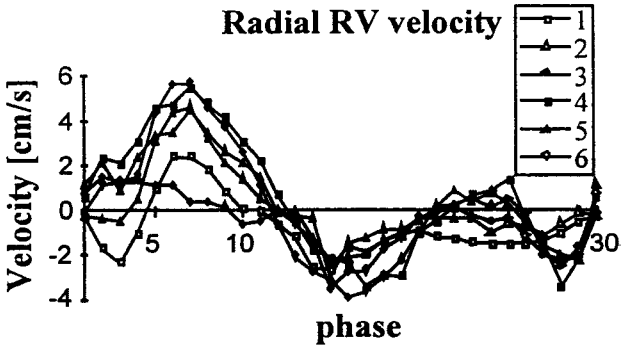

Figure 3. RV myocardial velocity in radial direction as a function of time.

Conclusions: Assessment of RV myocardial motion with a high temporal and spatial resolution can be done using 3D PC MR velocity mapping. The measured complex pattern of RV contraction and relaxation corresponds well with RV movement assessed with myocardial tagging or radionuclide studies. The short acquisition times (3–4 min) and the relatively easy postprocessing makes it a very promising tool for the evaluation of RV regional function.

Interleaved Spiral and Segmented FLASH Coronary Artery Imaging and Velocity Mapping in a Mobile 0.5-T Scanner

J. Keegan, P.D. Gatehouse, A.M. Taylor, G.Z. Yang, P. Jhooti, D.N. Firmin. *London, UK*

The ability to perform MR coronary angiography at low field strengths would improve the availability of the technique and promote its widespread usage.

Methods: We implemented real-time navigator-echo controlled segmented FLASH and interleaved spiral sequences for coronary imaging on a mobile 0.5-T system, overcoming low signal-to-noise levels by averaging data acquired over multiple reproducible breathholds. The segmented FLASH sequence (TE 6 ms) acquires data over 32 segments (eight views/segment, 105-ms duration) and the spiral sequence over 20 interleaves (readout duration 18.6 ms). Early diastolic in-plane and through-plane images were acquired in 10 normal subjects with a 6-mm slice thickness and 1 × 1mm in-plane resolution. In a further six subjects, early diastolic through-plane and in-plane segmented FLASH (TE 8 ms) and interleaved spiral (TE 14 ms) velocity maps (sensitivity ± 25 cm/s) were generated by phase map subtracting data acquired with equal and opposite velocity sensitivities on alternate cardiac cycles.

Results: Good quality through-plane and in-plane segmented FLASH and interleaved spiral images were obtained in all 10 subjects with mean acquisition times of 123 ± 22 s and 71 ± 14 s, respectively. Unlike the segmented FLASH images, the interleaved spiral acquisitions were sensitive to local field inhomogeneities and to the off-resonance effects of residual epicardial fat, generally requiring a degree of postprocessing. Whereas good quality through-plane velocity maps were acquired in six subjects using both techniques, in-plane velocity maps were achieved in only four. In the problematic studies, the velocity maps looked "moth-eaten," with the poor quality also extending to the magnitude images in those subjects with poor fat suppression.

Discussion: Segmented FLASH and interleaved spiral images were acquired in a mobile 0.5-T scanner. The segmented FLASH sequence is very robust and, unlike the interleaved spiral sequence, images do not require postprocessing. This, to some extent, compensates for its lower signal-to-noise ratio, poorer temporal resolution, and longer imaging time. Through-plane velocity maps have also been acquired successfully, but partial volume effects make in-plane velocity mapping difficult, a problem exacerbated by difficulties in achieving good and uniform fat suppression in the nonfixed and poorly controllable surroundings of the mobile unit.

Magnetic Resonance Imaging for Assessment of Myocardial Remodeling in an Experimental Pig Model

W.Y. Kim, K. Terp, V. Koudal, M. Veien, T. Silkjær, F.T. Jensen. *Aarhus, Denmark*

Background: In IHD, left ventricular function is affected by either diffuse or segmental loss of myocardium. These two types of injury frequently coexist, clouding the functional significance of diffuse ischemic lesions. In this animal experimental study, we evaluated the the hemodynamic impact of the diffuse myocardial fibrosis present in patients with IHD with no prior history of transmural ischemia.

Methods: In 20 domestic pigs, diffuse myocardial fibrosis was induced by repeated intracoronary microembolizations. Magnetic resonance imaging (MRI) was performed for assessment of LV volumes, mass, and end-systolic wall stress. Six pigs underwent serial MRI and hemodynamic examination at baseline, immediately after embolization, and after 129 days mean follow-up.

Results: Repeated microembolizations induced a diffuse pattern of perivascular fibrosis covering 12 ± 3% of the LV wall. Acute ischemic myocardial injury induced infarct expansion and increased LV wall stress preceeding chronic LV remodeling. End-systolic and end-diastolic volumes increased from 15.12 ± 2.75 to 41.37 ± 11.56 cm^3 ($p < 0.002$) and from 52.07 ± 6.74 to 81.15 ± 9.24 cm^3 ($p < 0.0007$), respectively. End-systolic wall stress increased from 17.55 ± 2.78 to 29.78 ± 6.27 N/m^2 ($p < 0.001$). Compared with baseline, $+dP/dt$ increased from 856 ± 263 to 1,682 ± 665 mm Hg/s ($p < 0.05$) and $-dP/dt$ from 1,120 ± 360 to 1,705 ± 417 mm Hg/s ($p < 0.05$). LV filling pressures and cardiac index did not change significantly.

Conclusion: This study demonstrates that repeated ischemic episodes different from confined regional myocardial infarctions induce acute infarct expansion preceding chronic LV remodeling. In compensated LV dysfunction secondary to diffuse myocardial fibrosis estimates of LV volumes, pre- and afterload are important in early detection of irreversible LV deterioration.

Detection of Early-Stage Diabetes-Induced Changes in Ventricular Function in the Rat with MRI

C.H. Lorenz, M. Janif, J.S. Allen, M.J. Scott, S.A. Wickline. *St. Louis, MO*

Successful early detection of abnormal myocardial function in diabetics may help in the development of therapeutic strategies to prevent or delay progression to overt cardiac disease. Therefore, the purpose of this study was to assess the sensitivity of MRI for detecting early changes in ventricular function in diabetes. Type 2 diabetes was produced in 10 Sprague-Dawley rats by injection of streptozotocin 50 mg/kg wt at 4 weeks of age (1). The HbA1c was kept between 8 and 10%, which corresponds to blood glucose > 350 mg%. Six months later, the animals and nine age-matched control rats were imaged to determine left ventricular (LV) volume and mass. Imaging was performed on a clinical 1.5-T whole body scanner (Philips Gyroscan ACS-NT, Best, the Netherlands) using a custom-designed 3.8-cm surface coil. Cine imaging was then performed in short-axis contiguous slices using a turbo-field echo sequence with the following parameters: TE/TR 7.2/17 ms, trigger delay 16 ms, 126 × 256 acquisition matrix, 4 NSA, slice thickness 1.4–2 mm. Temporal resolution was 17 ms. The resulting in-plane image resolution was 352 × 476 μm. Mean heart rate was 300–350 bpm, and triggering efficiency was 30–50%. The endocardial and epicardial borders were outlined manually using methods described previously (2) to determine mass and volume.

Despite no significant difference in systolic function as measured by ejection fraction and preservation of cardiac output, reductions in both emptying and filling dynamics could be detected with MRI. LV hypertrophy was present consistent with findings of other studies. The increase in LVEDV in these animals may reflect compensation to maintain cardiac output due to the chronotropic effects of anesthesia, requiring further study. MRI may prove to be a sensitive method for detecting ventricular performance changes in early-stage diabetic cardiomyopathy.

References

1. Norton GR, Candy G, Woodiwiss AJ. Circulation, 1996; 93(10): 1905–1912.
2. Lorenz CH, Walker ES, Graham TP, Powers TA. Circulation, 1995; 92[suppl II]:II-233–239.

Influence of Papillary Muscles and Through-Plane Motion on Left Ventricular Volume and Mass Measurements

J.T. Marcus,[1] M.J.W. Götte,[1] L.K. de Waal,[1] M.R. Stam,[1] R.J. van der Geest,[2] A.C. van Rossum.[1] [1]*Vrije Universiteit, Amsterdam;* [2]*Leiden University Hospital, The Netherlands*

For the assessment of left ventricular (LV) function in patients, it is necessary to obtain correct LV volume and mass measurements (1). When measuring LV mass and volumes, papillary muscles (PM) and through-plane motion of the heart are usually neglected, even though they can introduce a large bias. Sixty-three healthy volunteers (37 male), and 19–69 years, body mass index 17.4–31.5 kg/m^2, were examined using a 1.0-T (49 subjects) or a 1.5-T (14 subjects) Siemens whole body system. Segmented k-space breathhold cine imaging was used for acquiring a stack of short-axis images covering the LV from base to apex. Slice thickness was 8 mm and slice gap was 2 mm. End-diastolic volume (EDV), end-diastolic mass (EDM), end-systolic mass (ESM), and PM mass (PMM) were calculated by slice summation. An additional long-axis cine acquisition was performed in 15 volunteers to measure the LV long-axis systolic shortening. In the table below, the PM are considered as part of the EDV:

EDM (g/m^2)	PMM (g/m^2)	PMM/EDM (%)	EDV (ml/m^2)	Vol. PM (ml/m^2)	Vol. PM/EDV (%)
58.9 ± 10.7	4.4 ± 1.1	7.7 ± 2.0	70.8 ± 11.2	4.2 ± 1.1	6.0 ± 1.7

The mean longitudinal shortening was 11.4 ± 8 mm (in earlier reports, 12 mm [2]). Because one cine is made every 10 mm, one basal image plane more is needed at end diastole (ED) than at end systole (ES) to cover the entire LV. This most basal plane shows the LV wall at ED but not at ES. If this most basal image plane was included, EDM and ESM were more alike (difference 11.1 ± 9.2 g) than when neglecting this plane (difference 29.5 ± 15.8 g). The ratios shown in the table are the relative underestimation of the EDM and overestimation of the EDV, if the PM are considered as a part of the EDV. The contribution of the PM should thus be quantified when measuring LV volumes and mass. In these measurements, because of through-plane motion of the

	LV Mass (g/kg)	LVEDV (cc/kg)	LVM/LVEDV (g/cc)	Peak Ejection Rate (EDV/s)	Peak Filling Rate (EDV/s)
Control	1.87 ± 0.07	1.39 ± 0.07	1.36 ± 0.08	9.74 ± 0.55	10.3 ± 0.81
Diabetic	2.35 ± 0.06*	2.35 ± 0.10*	1.01 ± 0.04*	7.48 ± 0.44*	8.4 ± 0.55*

* $p < 0.05$

heart, one image plane more is needed at ED than at ES. Neglecting this first slice results in a considerable underestimation of the EDV and EDM.

References

1. Higgins CB, Sakuma H. Heart disease: Functional evaluation with MR imaging. Radiology, 1996; 199:307–315.
2. Rogers WJ, Shapiro EP, Weiss JL, et al. Quantification of and correction for left ventricular long axis shortening by magnetic resonance tissue tagging and slice isolation. Circulation, 1991; 84:721–731.

Improved Differentiation Between Infarcted and Noninfarcted Myocardial Regions by Magnetic Resonance Tagging and Strain Analysis

J.T. Marcus,[1] M.J.W. Götte,[1] A.C. Van Rossum,[1] J.P.A. Kuijer,[1] L. Axel,[2] R.M. Heethaar,[1] C.A. Visser.[1] *[1]Vrije Universiteit, Amsterdam, The Netherlands; [2]University of Pennsylvania, Philadelphia, PA*

Purpose: The motion of the heart wall is usually qualified as hypo- or normokinetic. However, myocardial motion is a composite of active deformation (strain) and passive displacement. Our aim was to assess the relevance of separating strain from displacement after infarction.

Methods: Ten patients (age 52 ± 11 yr, males) had an anterior infarction due to an angiographically proven culprit lesion in the LAD coronary artery. Within 8 ± 3 days after infarction, magnetic resonance imaging with tagging (7-mm grid) was performed on the vertical long-axis image plane. The motion of triangular finite elements of myocardium was analyzed between end diastole and end systole (1). Results are the maximum principal strain λ1 (1 + greatest systolic stretch) and the rigid-body displacement D of the elements. The anterior and posterior left ventricular walls were subdivided in basal, mid, and apical levels. Mean values of λ1 and D were obtained for each region. The anterior wall at midlevel was an infarcted region and the posterior wall at basal level a noninfarcted region. Patients were compared with healthy controls (n = 8, age 53 ± 10 yr, males).

Results: D was equally decreased in the infarcted and noninfarcted regions. λ1, however, was decreased (less stretching) in the infarcted region but not decreased (rather increased) in the noninfarcted region (2).

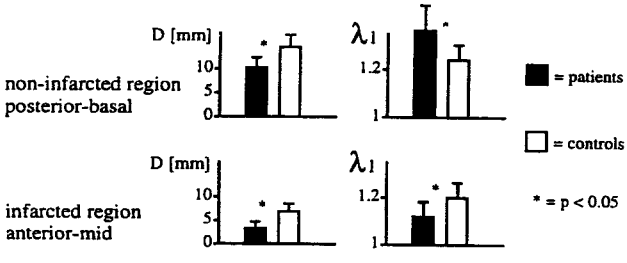

Conclusion: The maximum principal strain of myocardium better differentiates between infarcted and noninfarcted regions than displacement.

References

1. Axel L, Concalves RC, Bloomgarden D. Regional heart wall motion: Two-dimensional analysis and functional imaging with MR imaging. Radiology, 1992; 183:745–750.
2. Marcus JT, Götte MJW, Van Rossum AC, et al. Myocardial function in infarcted and remote regions early after infarction in man: Assessment by magnetic resonance tagging and strain 1 analysis. Magn. Res. Med., 1997; 38:803–810.

Burst Imaging of Heart

T. Matsuda, M. Motooka, M. Komori, S. Sasayama, T. Takahashi. *Kyoto, Japan*

Burst imaging can obtain a MR image in a short acquisition time compared with EPI (1). A poor SNR, however, limits its application only to brain imaging. As an important target of the ultrafast imaging method, we applied a phase-optimized Burst imaging with half Fourier acquisition to the human heart (2,3). The purposes of this study are to evaluate the applicability of this method to cardiac imaging and to clarify its limitations. A Burst imaging with spin-echo acquisition was performed with Siemens Magnetom (1.0 T). Excitation pulse train consisted of 40 RF pulses with phases of 0° and 180°. Forty echoes acquired with Helmholtz surface coil were reconstructed to a 64 × 128 matrix image for 200 × 400 mm² FOV. The effective echo time was reduced from 53 to 16 ms using half Fourier acquisition, and the resulting acquisition time was 68 ms. Cardiac images of 10-mm-thick transverse slices were obtained in three healthy volunteers. The delay time from ECG trigger was changed at 100-ms intervals to obtain images at several cardiac phases. Left ventricular wall showed distorted Burst images obtained at systole and early diastole. However, its configuration in the middiastolic image was equivalent to that in the conventional cine MR image. Although SNR was still inferior to EPI, susceptibility artifact was not significant in the middiastolic image. Because slice selection was performed only by the selective refocus pulse in Burst imaging, spins in flowing blood potentially produce echo signals. The practical application to human heart, however, yielded a black blood image. This result suggests Burst imaging has remarkable sensitivity to flow despite its short acquisition time. Motion may also be responsible to the distortion of left ventricular configuration in the images at the phases other than middiastole. Consequently, careful choice of cardiac phase is important to Burst imaging when applied to cardiac imaging.

References

1. Hennig J, Hodapp M. Burst imaging. MAGMA, 1993; 1:39–48.
2. Zha L, Lowe IJ. Optimized ultra-fast imaging sequence (OUFIS). Magn. Reson. Med., 1995; 33:377–395.
3. Jakob PM, et al. Half-Fourier burst imaging on a clinical scanner. Magn. Reson. Med., 1997; 38:534–540.

Quantification of Left Ventricular Flow Propagation Speed by Magnetic Resonance Phase Velocity Mapping

S. Milet, A. Yoganathan. *Petit Institute of Bioengineering and Bioscience, Georgia Institute of Technology, Atlanta, GA*

Diastolic dysfunction is an important early indicator of cardiovascular diseases. The quantification of diastolic function is usually based on transmitral flow indices such as E wave, A wave, and E/A ratio. However, these indices can be misleading. To improve the test of diastolic function, we suggest using magnetic resonance phase velocity mapping (MRPVM) to quantify the propagation speed of the early diastolic inflow in the left ventricle. MR measurements were performed on a Philips Gyroscan 1.5-T full-body scanner. The MR parameters were the following: shortest echo time, slice thickness 10 mm, resolution 128 × 128, field of view 400 × 400 mm, up to 32 images per cardiac cycle, ECG-gated. Postprocessing was performed off-line after correcting the velocity images for eddy currents. The flow patterns were studied from the series of vector plots of the in-plane flow velocity components superimposed on the anatomical images of the heart. We extracted the temporal flow velocity amplitude profiles along the diastolic inflow path. The time-dependent averaged velocities along the inflow path were visualized as a function of time and space (figure). These plots

show the velocity amplitude along the diastolic inflow path into the left ventricle during the entire cardiac cycle. For each plot the inflow propagation speed (PS) is computed as the slope of the diastolic inflow area. Diastolic filling propagation speed can be computed in vivo using MRPVM of the left ventricular inflow. PS is a direct measurement of ventricular filling and has the potential to adequately quantify ventricular chamber properties. The propagation speed index can be used in diseases where relaxation and filling patterns are affected, such as ischemic heart disease or LV hypertrophy. This method provides a potentially powerful technique for the diagnosis of patients with diastolic dysfunction.

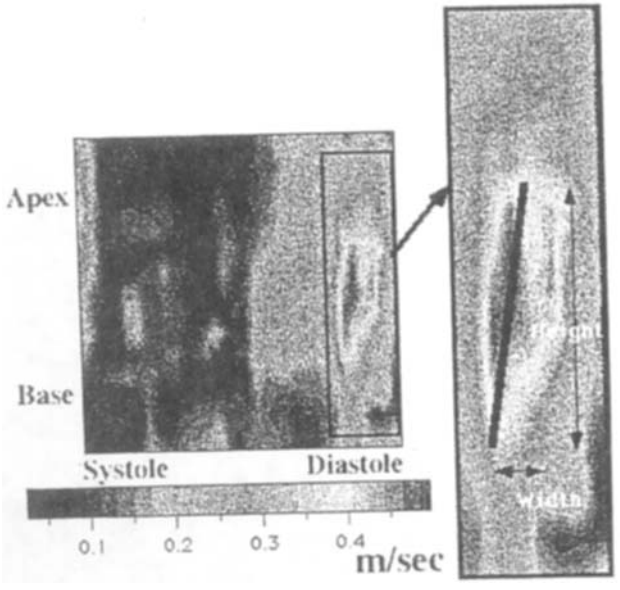

LV inflow velocity amplitudes as a function of time amd location.

Vortex Flow Demonstrated in the Healthy and the Dilated Left Ventricle by MR Velocity Mapping and an Automated Flow Pattern Recognition Method

R.H. Mohiaddin, G.Z. Yang, D.N. Firmin, D.J. Pennell. *Royal Brompton Hospital, London, UK*

Purpose: We describe an automated method for flow pattern recognition and demonstrate its application for studying vortical flow in the normal and the dilated ischemic left ventricles (LV) using multidirectional MR velocity mapping. This is important because in left ventricular disease, the disturbance of blood flow patterns within the ventricle may be important in maintaining or disrupting the blood flow in and out of the left ventricle.

Methods: Eight patients with dilated LV resulting from coronary artery disease and eight healthy subjects were studied. All patients were in sinus rhythm and had mild-to-moderate functional mitral valve regurgitation. Cine gradient-echo images were acquired in the LV vertical and horizontal long axes (HLA) to measure LV volumes and ejection fractions using the biplane area–length method. Vertical and horizontal velocity components in the HLA plane of the LV were encoded simultaneously by interleaving. Maps of velocity components acquired in the HLA plane of the LV were processed into multiple computer-generated streaks whose orientation, length, and movement corresponded to velocity vectors. Vortex flow is characterized by its circular or swirling motion and is recognized using ordinary differential equations to provide local linearization to the acquired multidirectional MR velocity data. The size and the travel distance of each vortex are automatically tracked through the entire plane during the entire cardiac cycle.

Results: In normal subjects the predominant direction of diastolic flow through the mitral valve was toward the apex, with short-lived vortices curling back behind each mitral leaflet at early and late phases of LV filling. In patients with dilated LV, the inflow was directed not toward the apex but toward the free wall, giving rise to a well-developed circular flow pattern turning back toward the septum and outflow tract and persisting through diastole. The following parameters (mean ± SD) differed significantly between the two groups: heart rate (patients 70 ± 11 beat/min, controls 57 ± 8, $p < 0.001$), end-diastolic volume (patients 264 ± 83 ml, controls 143 ± 25 ml, $p < 0.001$), ejection fraction (patients 31% ± 7, controls 61% ± 5, $p < 0.001$), the maximum diastolic size and the travel distance of the vortex below the septal leaflet of the mitral valve (patients 12.7 ± 2.0 cm^2, 3.4 ± 0.8 cm^2, controls 8.5 ± 2.5 cm^2, 2.6 ± 0.5 cm, $p < 0.003$, $p < 0.02$).

Conclusion: The ability of an automated method for measuring the topological features of vortical flow in the normal and dilated LV was demonstrated in healthy volunteers and in patients with dilated ischemic LV. The diastolic size and the travel distance of the vortex below the septal mitral valve leaflet are significantly larger in the patients than in the healthy volunteers. This technique may prove invaluable in understanding the fluid mechanics in the normal and dilated LVs.

Alignment and Visualization of Quantitative and Qualitative Data from Cardiac Studies in MRI, SPECT and PET

S. Nekolla, U. Schricke, F. Roder, M. Schwaiger. *Nuklearmedizinische Klinik rechts der Isar der TU, München, Germany*

Purpose: We demonstrated the feasibility of a semiautomated coregistration and fusion tool for inter- and intramodal PET, SPECT, and MRI image and polar map data.

Methods: Within the cardiac software environment "MunichHeart" developed in our department, several modules allow for the delineation of cardiac contours and calculation of regional parameters. For gated MRI studies, the manual definition of endo- and epicardial borders in ED and ES is supported. Using PET or SPECT studies, after manual definition of the long axis, automatically maximum count surfaces or endo- and epicardial surfaces through the cardiac cycle are delineated, encompassing the left ventricle. Subsequently, surface data from any two studies are used to align them initially using geometric properties. Because the high rotational symmetry along the heart's long axis, a user interaction is allowed to adjust the posterior junctions of left and right ventricle as defined during the calculation of the polar maps. Finally, the surfaces are matched automatically. After accepting the optimal coregistration, the quantitative information (i.e., the data represented in polar map or "bullseye" format) are projected onto the reference data set to provide an exact spatial alignment. During all steps advanced visualization features are supplied: display of orthogonal slices of original and overlay images in 2D and fully interactive 3D together with the cardiac surfaces with the various quantitative information mapped onto them.

Results: Depending on the selected surface, multimodality coregistration (e.g., endocardial surface MIBI-SPECT and MRI in ED) yielded minimal mean distances of less than 2.5 mm. Using single modality multitracer studies of the same patient (e.g., FDG/NH_3 PET viability), a minimal mean distance between the two surfaces of less than 1.5 mm could be achieved.

Conclusion: For both clinical purposes, like the precise alignment in rest/stress and follow-up studies, and scientific issues, such as the

comparison of the assessment of MRI and PET wall motion, the presented tool offers improved means of coregistering cardiac studies with limited yet necessary manual interaction.

Regurgitant Volume Index: Use of Cardiac MRI for the Assessment of Aortic Insufficiency

M.R. Newton,[1] K.V. Kissinger,[1] M.L. Chuang,[1] W.J. Manning,[1] J.N. Oshinski,[2] R.I. Pettigrew.[2] [1]*Boston, MA;* [2]*Atlanta, GA*

It has been previously suggested that the regurgitant volume index (RVI)—the aortic regurgitant volume (RV) expressed as a proportion of the left ventricular end-diastolic volume (LVEDV)—may better estimate the severity of aortic insufficiency (AI) and predict LV response to surgical intervention (1). Previous investigations have been hampered by the lack of a noninvasive technique for its measurement. We hypothesized that the unique ability of cardiac MRI to assess LVEDV and aortic flow could provide data for this index.

Methods: Thirteen subjects, 4 healthy adult volunteers (nl) and 9 patients with stable mild ($n = 3$), moderate ($n = 3$), and severe ($n = 3$) AI by echo, underwent cardiac MR study. Contiguous breathhold short-axis cine MR images were used to determine LV volumes; velocity-encoded images at the aortic sinotubular ridge were used to determine RV. LVEDV, RV, and RVI were compared using ANOVA.

Results: Highly significant differences between all groups was seen for RV and RVI. LVEDV was different only between the severe and the normal–mild groups.

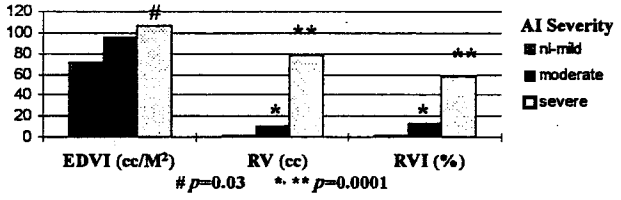

Conclusions: Cardiac MRI allows the noninvasive determination of the RVI. Further study is needed to determine the added value of this novel index for guiding the management of patients with chronic AI.

Reference

1. Levine H, Gaasch W. Am. J. Cardiol., 1983; 52:406–410.

User-Independent MRI Determination of Circumferential Subpixel Blood Vessel Wall Position and Wall Shear Stress by the Automatic Multiple Sectored Three-Dimensional Paraboloid Method

S. Oyre, W.P. Paaske, E.M. Pedersen. *Aarhus University Hospital, Skejby Sygehus, Denmark*

Methods are lacking for accurate, observer-independent, noninvasive (1), and invasive determination of the luminal vessel area and wall shear stress (WSS). The present study introduces a new user-independent method for determination of the above variables in peak systole based on detecting local maxima of data set obtained from the multiple-sectored three-dimensional paraboloid (3DP) method presented previously (2,3). The method has 0.9% error in area estimation and 2.0% WSS error as determined from computer simulations and in vitro studies (3).

Method: The method is based on simple hemodynamic assumptions (2) and is independent of user input apart from identification of the vessel of interest. Given that the velocity distribution is only parabolic in a thin boundary layer at the vessel wall, a 3DP fit (2,3) will only find the true vessel wall position and WSS if the data ("sector") used for the fit is situated in the middle of the boundary layer and the fit layer is made sufficiently thin to avoid both partial volume pixels at the vessel wall (known to overestimate the velocity) and pixels that are partially in the boundary layer and partially in the flat center part of the vessel. If the sector is moved in either radial direction, the mean WSS values (mean of all 24 sectors) will decrease and the luminal area increase. We hypothesize that mean WSS cannot be overestimated (has a local maximum) and that the luminal area cannot be underestimated (has a local minimum) when using the multiple sectored 3DP method. Therefore, we propose a new index that reaches a local maximum when the true edge is detected: $3DP_{index} = 3DP_{mean\_WSS}/3DP_{area}$. We changed the initial edge detection radius in steps of 100 μm until a distance of 0.5 mm (in both radial directions) from the initial automatically determined radius. We used 24 sectors evenly distributed around the circumference of the vessel with a 1-mm fit layer and 90° fit angle (2,3). The $3DP_{index}$ was calculated for each step, and the maximum was used as "correct" value. The mean of the paired values (mean WSS and luminal area) ± 100, ± 200, and ± 300 μm from this "true" value were calculated. Measurements were performed in six young volunteers where through-plane blood velocity data in the common carotid artery 2 cm upstream of the carotid bifurcation were acquired using a 1.5-T Philips NT scanner with a standard phase contrast sequence and in-plane resolution of 0.5 mm.

Results: The mean percent area change was +1.3, 3.5, and 5.9% higher for ±100, 200, and 300 μm distance from the "true" minimum area (43.1 mm²), whereas the corresponding mean WSS values for all subjects were −1.9, −5.2, and −9.9% reduced from the true maximum value of 2.44 N/m². The mean adjusted R^2 (coefficient of determination) was 0.96 and the mean RMSE was 0.023 m/s² for the correct values 3DP fit.

Conclusion: The new automatic and user-independent 3DP method, presented in this study, is unique by having a theoretical local maximum at the true vessel wall. This was proven to hold true for in vivo data acquired in the common carotid artery. In all subjects a local mean WSS maximum and a local minimum vessel area were found. With minor improvement, the method can be used in diastole as well and could potentially be applied throughout the cardiovascular system in peak systole. The method has experimental and clinical potential for studying intraindividual and temporal development of vascular disease and vascular responses to interventions. Future work includes more evaluation of the method through comparison with other noninvasive diameter/area estimations method.

References

1. Celermajer DS, et al. Lancet, 1992; 340:1111.
2. Oyre S, et al. ISMRM, 1997; 3:1879.
3. Oyre S, et al. Quantitation of circumferential subpixel vessel wall position and wall shear stress by multiple sectored three-dimensional paraboloid modeling of velocity encoded cine MRI. ISMRM, 1998.

Selected for Young Investigators' Awards (W.S. Moore) finalist proceeding & paper for MRM.

Myocardial Perfusion Imaging Using Spin-Echo EPI on a Mobile 0.5-T Scanner

J.R. Panting, P.D. Gatehouse, G.Z. Yang, D.N. Firmin, D.J. Pennell. *London, UK*

Most previous studies of MR myocardial perfusion have used fast gradient-echo sequences at 1.5 T. The main limitation has been the limited myocardial coverage, typically only three slices being acquired per

heartbeat due to long acquisition times (200–300 ms per slice). To obtain greater coverage, spin-echo EPI with acquisition times of between 50 and 100 ms have been suggested. We report our experience of using this type of sequence at 0.5 T. We studied 36 subjects. Of these, 26 were patients with coronary disease who underwent single-slice, one-shot, inversion-recovery, spin-echo EPI at rest and during stress with 140 μg/kg/min adenosine for maximal coronary hyperemia. The images were corrected for motion and assessed by visual analysis of the dynamic series, parametric mapping, and construction of signal intensity versus time curves. The results were compared with SPECT. Methods of achieving multislice acquisitions were then investigated. Studies were carried out on eight normal subjects, four using a single, nonslice-selective, 180° inversion pulse (SIP) 200 ms before imaging the slices in rapid succession and four using multiple, nonslice-selective, inversion pulses (MIP) of between 90° and 120° 100 ms before each slice acquisition. Comparative studies of patients with ischemic heart disease are now underway. The single-slice study showed good correlation with SPECT, achieving 80% concordance in the detection of perfusion defects. For the multislice technique, SIP resulted in varying baseline signal intensity depending on the length of time after the inversion pulse to slice acquisition. Despite this, the net signal change with contrast was similar, and all five slices were assessable. The MIP method gave uniform baseline intensity, but as a result of the inversion delay, the number of slices was typically limited to three. Initial experience of the SIP technique in five patients with CAD showed good ventricular coverage and good correlation with SPECT. With further development, this technique is a candidate rival for SPECT in clinical practice; however, large comparative studies are required.

Left Ventricular Mass by Echocardiography and Magnetic Resonance

G. Pons-Lladó, F. Carreras, X. Borrás, J. Llauger, J. Palmer, A. Bayés de Luna. *Barcelona, Spain*

The aim of the present study was to compare values of left ventricular mass (LVM) obtained by M-mode echocardiography (ECHO) with those from magnetic resonance imaging (MRI). Also, a simplified method of calculation of LVM by MRI was tested. Both ECHO and MRI studies were performed on an unselected series of 35 patients (28 males and 7 females aged 13–85; mean, 41 ± 18) with the following clinical diagnosis: 12 with symmetrical left ventricular hypertrophy due to hypertension (10) or aortic valve disease (2); 6 with hypertrophic cardiomyopathy of the asymmetrical type; 6 with ischemic heart disease, including a previous myocardial infarction; 6 with a structurally normal heart; and 5 patients with miscellaneous diseases. ECHO calculations were performed using two different formulas: Penn's convention method and American Society of Echocardiography (ASE) method. The MRI technique of summation of contiguous short-axis slices of the left ventricle on a spin-echo sequence was used as a reference against which ECHO measurements were compared. Also, a simplified MRI method of estimation of LVM based on Simpson's rule applied on a single long-axis left ventricular plane was also tested. Results showed that ECHO studies, which could not be applied due to technical limitations in 2 of 35 patients, systematically overestimated values of LVM by MRI, although results from the ASE method agreed more closely with MRI than those obtained by Penn's method (Figs. 1 and 2). Large overestimation persisted, however, in some cases, accounting for more than 50% of values calculated by MRI in five patients, all of them with either asymetrical septal hypertrophy or with a grossly distorted left ventricular shape due to a previous infarction. On the other hand, the simplified method of calculation of LVM by MRI using a single long-axis plane showed an excellent correlation with the method of summation of contiguous short axis slices (Fig. 3).

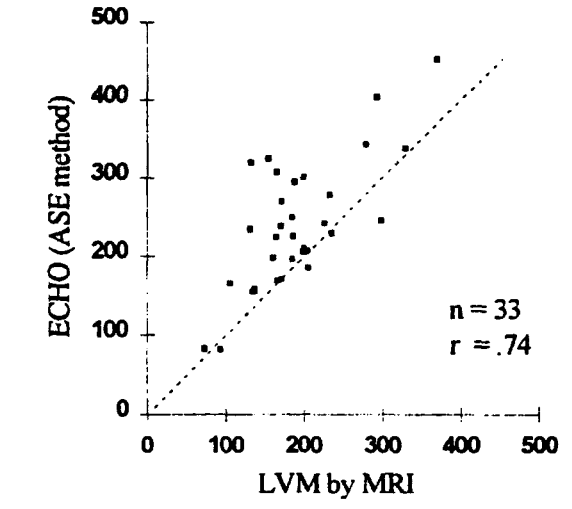

Figure 1

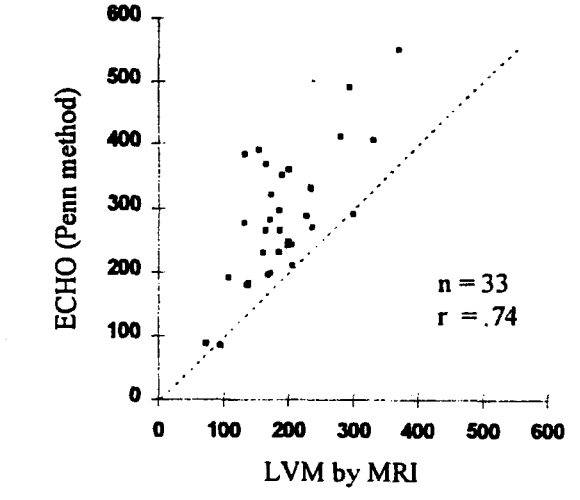

Figure 2

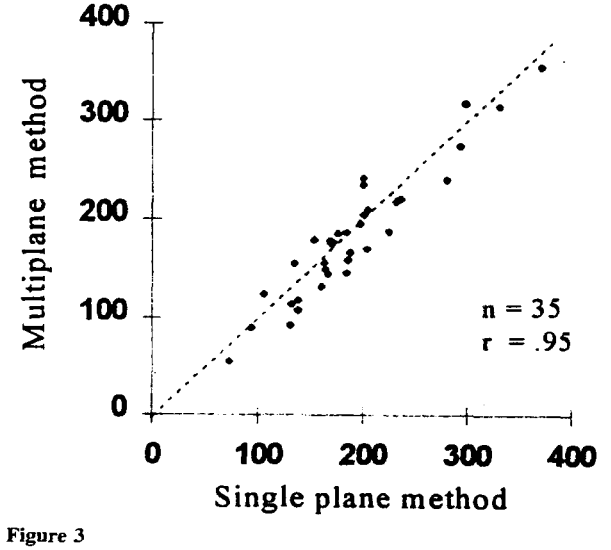

Figure 3

In conclusion, calculation of LVM by M-mode ECHO is not technically feasible in a small proportion of patients; values obtained by the ASE method, although more accurate that those resulting from Penn's convention equation, systematically overestimate LVM when an MRI anatomical method is used as a reference, and large unacceptable discrepancies occur in cases with distorted left ventricular cavity. MRI, on the other hand, allows the calculation of LVM in all cases by means of a true anatomical method, as is the summation of contiguous short-axis slices and also, alternatively, by using a single long-axis view of the left ventricle.

Assessment of Diastolic Abnormalities of Longitudinal Left Ventricular Function Using Cine Magnetic Resonance Imaging and M-Mode Echocardiography in Ischemic Heart Disease

M.A. Sakrana,[1] M.Y. Henein,[2] F.M. Eldemerdash,[1] S.R. Underwood.[2]
[1]*Internal Medicine Department, Mansoura Faculty of Medicine, Mansoura, Egypt;* [2]*Magnetic Resonance Unit, Royal Brompton, National Heart and Lung Hospital, London, UK*

Cine magnetic resonance imaging (MRI) is an established method for assessment of left ventricular (LV) function. We aim to assess longitudinal fibers of LV function by two noninvasive methods: cine MRI and M-mode echocardiography. We studied 13 patients (3 with single vessel disease and 10 with multivessel disease) and 20 normal volunteers using cine MRI in vertical and horizontal long axis. Endocardial and epicardial boundaries were defined manually in end-diastolic and end-systolic frames, and circumferential profiles of wall motion were generated in each plane. Categories for each variable were assigned according to the number of standard deviations from the mean of the normal group in each of three (lateral, septum, and inferior) segments. Longitudinal function abnormalities were assessed by M-mode echocardiography of the left, septal, posterior sites of the LV with simultaneous ECG and phonocardiography and classified according to overall longitudinal shortening, early diastolic excursion, and amplitude of the A wave. Areas were compared by the two techniques versus coronary angiograms.

Results: Thirty-nine segments were assessed. There was good agreement between quantitative wall motion abnormalities by MRI (hypo-, a- and dys-kinetic) and diastolic abnormalities of longitudinal LV function (mild, moderate, severe), differing by one category or less in 38 segments (97%, $K_w = 0.62$). The agreement between wall motion by cine MRI and longitudinal function by M-mode echocardiography versus coronary angiograms was 82% ($K_w = 0.31$) and 82% ($K_w = 0.4$), respectively. We conclude that objective method of assessing regional myocardial function agrees well with localized diastolic abnormalities of longitudinal LV function in coronary artery disease.

Determination of Left Ventricular Mass in Patients with Myocardial Infarction Using Breathhold Black Blood Prepared Turbo-FLASH Magnetic Resonance Imaging

S.L. Brinckman, M.J.W. Götte, J.T. Marcus, A.C. van Rossum.
Department of Cardiology, University Hospital, VU Amsterdam, The Netherlands

Measurement of left ventricular (LV) mass is an important prognostic indicator in patients with heart disease. Breathhold k-space segmented cine magnetic resonance (cine MR) imaging has been shown to be accurate for evaluation of cardiac function and anatomy (1). However, this technique is relatively time consuming. Using a black blood prepared turbo-FLASH (BB-TFL) technique for measurement of LV mass, the acquisition time can be reduced considerably. The purpose of the present study was to compare this rapid BB-TFL sequence with k-space segmented cine MR for the determination of LV mass.

Methods: Thirteen patients with a first myocardial infarction were evaluated. Images were acquired using a 1.0-T system with prospective cardiac triggering and a phased-array coil. Repetitive inspiration breathholds were required for acquisition of the short-axis cine MR images. Six to 11 slices were needed to encompass the LV from base to apex. Only one breathhold was required for obtaining the stack of BB-TFL images. Cine MR imaging required 15–20 min, whereas BB-TFL imaging required only 12–22 s.

Results: Table 1 summarizes the results and correlation of the LV mass obtained by cine MR at end diastole (ED), end systole (ES), and their mean, and mass obtained by BB-TFL. LV mass determined by cine MR (mean mass of ED and ES) and BB-TFL correlated well ($r = 0.96$), with a small standard error of the estimate (SEE = 12.0 g) (Fig. 1). The correlation between cine MR and BB-TFL LV mass determination, using a Bland and Altman analysis of the two estimates, is illustrated in Fig. 2.

Table 1

LV Mass Comparison	Cine MR (g)	BB-TFL (g)	Regression Equation	*r* Value	SEE
Cine ED vs. BB-TFL	163.3 + 44.3	171.4 ± 39.7	$y = 0.86x + 31.50$	0.96	12.2
Cine ES vs. BB-TFL	188.8 + 45.9	171.4 + 39.7	$y = 0.82x + 16.44$	0.95	13.0
Cine mean vs. BB-TFL	176.0 + 44.9	171.4 + 39.7	$y = 0.85x + 22.46$	0.96	12.0

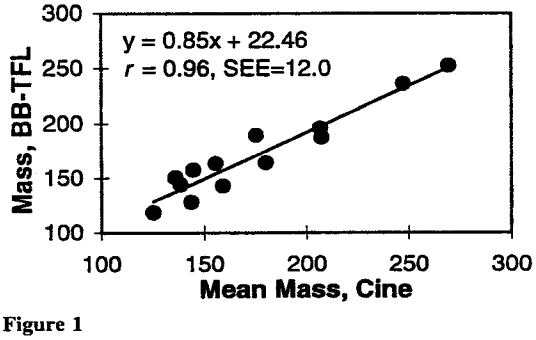

Figure 1

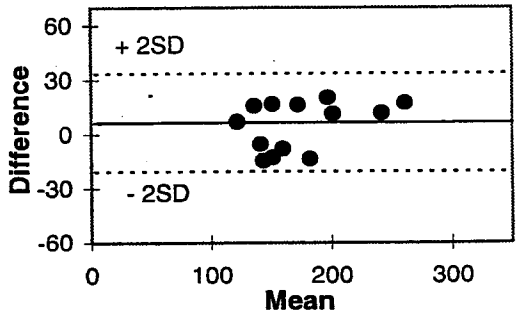

Figure 2

Conclusion: BB-TFL has a comparable accuracy to cine MR for determination of LV mass and reduces image acquisition time approximately by a factor of 10.

Reference

1. Sakuma H. Evaluation of left ventricular volume and mass with breath-hold cine MR imaging. Radiology, 1993; 188(2):377–380.

Effects of Maxwell Terms on Particle Traces Calculated from 3D Cine Phase-Contrast Images

L. Wigström,[1] T. Ebbers,[1] A. Fyrenius,[1] M. Karlsson,[1] J. Engvall,[1] B. Wranne,[1] A.F. Bolger.[2] [1]*Linköping University, Sweden;* [2]*University of California Riverside, CA*

The complex patterns of intracardiac flow can be visualized in an intuitive way using particle traces obtained from 3D phase-contrast data (1). Phase contrast has been shown to be sensitive to shading artifacts induced by eddy currents and Maxwell terms, however. The effects of eddy currents can be compensated for by subtraction of a linear function from the acquired velocity data (2). The Maxwell terms can be calculated, because the pulse sequence is known (3). We used a stationary phantom to determine the impact of Maxwell terms on particle traces derived from phase-contrast data. The study was performed using a Signa Horizon EchoSpeed scanner (GE Medical Systems, Milwaukee, WI) and a 3D cine phase contrast pulse sequence (256 × 96 × 16 matrix, FOV 30 × 30 × 12.8 cm, TR 18 ms, TE 6 ms, VENC 60 cm/s) (4). The correction for the Maxwell terms was performed by calculating the phase error from the gradient waveforms according to Bernstein et al. (3). Figures 1 and 2 show particle traces obtained by integrating the velocity field during 0.5 s, starting from a 16 × 16 grid through the center of the 3D phantom. Figure 1 shows the particle traces created without correction for Maxwell terms and Figure 2 the traces with correction performed before their calculation. In both cases, a 3D linear function was fitted and subtracted to compensate for eddy current effects. Without correction for Maxwell terms, some of the particle traces extended more than 3 cm from their starting points. Because the phase error due to the Maxwell terms is a nonlinear function of the distance from the center of the magnet, the effects on particle traces will be largest in the image periphery. When studying left ventricular flow patterns, these effects will be most severe at the apex and may cause some particle traces to drift outside the heart. Correction for eddy currents and Maxwell terms is therefore important when applying particle trace techniques to 3D phase-contrast data for the study of intracardiac flow.

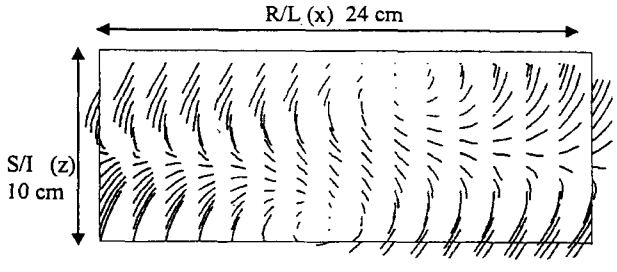

Figure 1. Without correction for Maxwell terms.

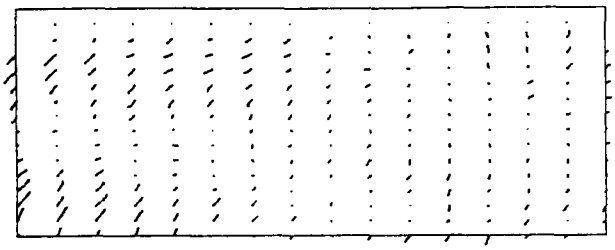

Figure 2. With correction for Maxwell terms.

References

1. Wigström L, Karlsson M, Bolger AF, Wranne B. *ESMRMB, Prague,* 1996; p. 158.
2. Pelc NJ, Herfkens RJ, Shimakawa A, Enzmann DR. Magn. Reson. Q., 1991; 7:229–254.
3. Bernstein MA, Zhou X, King KF, Ganin A, Pelc NJ, Glover GH. *SMR, Vancouver,* 1997; p. 110.
4. Wigström L, Sjöqvist L, Wranne B. MRM, 1996; 36:800–803.

Wavelet-Packet Denoising of Echoplanar and Fast-Card Images

John C. Wood, Kevin Johnson. *New Haven, CT*

High-spatial resolution is imperative for coronary artery imaging, but voxel size is limited by signal-to-noise ratio (SNR). Decreased bandwidth and increased NEXs improves SNR but at a "cost" of motional blurring and increased exam time. Consequently, postprocessing techniques to improve SNR are attractive. One such approach, wavelet-packet denoising, can produce striking improvements in magnetic resonance images, particularly in images with low SNR and modest spatial frequencies (1). Therefore, we sought to quantitate the tradeoff between noise suppression and edge preservation in a high contrast, sharply demarcated, "myocardial" phantom using a commercially available wavelet-packet program (2). Specifically, changes in SNR, signal-to-background ratio (SBR), "myocardial" wall full width-half maximum (FWHM), and edge width (EW, defined as the distance from 25% maximum to 75% maximum) were measured in 1, 2, 4, 8, 16, and 32 NEX single-shot echoplanar images images pre- and postdenoising. Median and Wiener filtering was performed for comparison (3). All three methods were also subjectively evaluated for blurring and artifact on Fast-Card and echoplanar cardiac images from normal volunteers.

Results: Denoising produced a 2:1 improvement in SBR and a 1.5:1 SNR improvement for 1, 2, and 4 NEX images (single-shot SNR 8.8). For higher NEXs, denoising yielded diminishing SNR returns; nevertheless, SNR improved 25% for a 32 NEX image without loss of detail. SBR improvement ranged between 1.7 and 2. Denoising did not increase the FWHM, in contrast to median filtering. Wiener filtering did not increase FWHM or EW, but SNR improvement was only 25% for 1 Nex and 2% for 32 Nex images, respectively. Most importantly, wavelet-denoised phantom and cardiac images were sharp and artifact free. Wavelet-packet denoising can improve SNR/SBR without sacrificing image clarity, even in images with high contrast and spatial frequencies, and may facilitate coronary artery imaging.

References

1. Woog L. Ph.D. Thesis, Department of Mathematics, Yale University.
2. Coifman RR, Wieckerhauser MV. Numerical Algorithms Research Group, Department of Mathematics, Yale University.
3. Matlab Image Processing Library. The Math Works Inc., 24 Prime Park Way, Natick, MA 01760.

Evaluation of Myocardial Venous Blood Oxygen Level Changes Using MRI: Correction for Blood Volume

W. Oellerich, D. Li, T.L. Sharp, R.J. Gropler. *Saint Louis, MO*

We previously developed a MRI technique to assess the myocardial venous blood oxygen saturation level by measuring the R_2* relaxation rate of the myocardium. These studies resulted in a good correlation between myocardial coronary sinus oxygen saturation (%$ScsO_2$) and ΔR_2* but with the suggestion that blood volume changes during the peak effect of hypoxia and dipyridamole administration may contribute to the measured R_2*, thus altering the theoretical linear relationship. To evaluate this blood volume effect, five dogs were anesthetized and intubated, with arterial, venous, left atrial, and coronary sinus catheters placed. Myocardial R_2* measurements were obtained at baseline and then during and after infusion of dipyridamole (0.14 mg/kg/min over 4 min), dobutamine (10 μg/kg/min), and when the dogs were ventilated with hypoxic air (10% oxygen and 90% nitrogen). Paired arterial and coronary sinus blood samples were withdrawn at different times of the study. Blood oxygen saturation levels were measured using a cooximeter. Technetium-99m labeled red blood cells were given at peak effect of one intervention per animal to measure the blood volume. The imaging technique was ECG and respiratory gated with nulling of the blood pool signal to reduce motion and flow artifacts, respectively. Eight echo times were used to estimate the myocardial R_2*. Blood volume (ml/100 g) was 6.33 ± 0.48 during peak hypoxia, 5.85 during peak dipyridamole effect, and 5.17 ± 0.29 during peak dobutamine effect. Resting myocardial blood volume, previously determined at our institution, was 3.19 ± 0.45. Mean values for Δ R_2* and % deoxyhemoglobin ± standard deviation were determined at peak Δ%$ScsO_2$ for each study and plotted with and without correction for blood volume (Fig. 1).

Correction of ΔR_2* for the change in blood volume resulted in a more linear plot consistent with the theoretical linear relationship between R_2* and deoxyhemoglobin concentration when the blood volume is constant. Thus, accurate assessment of myocardial oxygen saturation using BOLD MRI may need to correct for the change of blood volume.

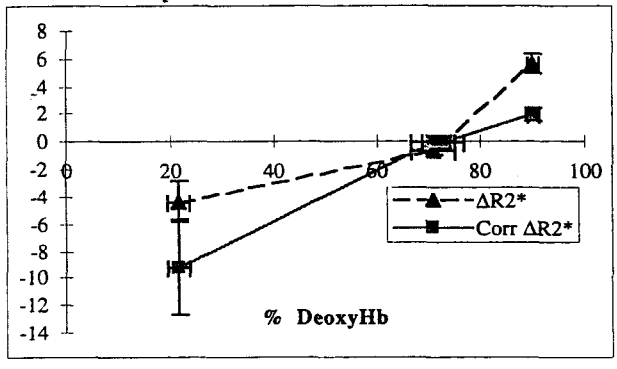

Figure 1. Relationship of ΔR_2* to % deoxyhemoglobin with and without blood volume correction.

Interleaved MRI/MRS Study of Perfusion, Oxygenation, and HEP Metabolism in Becker's Disease

J.F. Toussaint, C. Brillault-Salvat, P. Jehenson, G. Bloch, D. Duboc

Smooth muscle cells alterations have been described in myopathic patients, but their functional consequences are not known. We previously studied the interdependence between PCr recovery and flow (1,2). We use here a new interleaved NMRI/heteronuclear NMRS approach (3) to simultaneously quantify perfusion, 0_2 diffusion by myoglobin ^{1}H-NMRS, and 0_2 utilization by ^{31}P-NMRS in seven Becker's myopathic patients (Bk) and nine normal subjects (N). We studied the recovery phase of metabolism during reactive hyperemia (RH) and after two ischemic (Isc1 and Isc2) and one aerobic (Aero) exercise.

Methods: Upon reperfusion, two levels of counterpressure were used: diastolic blood pressure minus 10 mm Hg (DBP − 10) for RH, Aero, and Isc1, and systolic blood pressure minus 20 mm Hg for Isc2 (SBP − 20). Data were acquired at 3 T with homebuilt coils. The sequence interleaved 64 lines of a gradient-echo image, 64 ^{1}H FIDs, and one ^{31}P FID; TR 1,030 ms. Data were processed as previously described (3). The recovery time constant for PCr (PCrTC) was corrected for pH variation (4). Myoglobin resaturation was characterized by its resaturation time (MRT).

Results: Calf perfusion (Perf), PCrTC, and MRT results are shown below for normals and Becker patients (mean ± SD).

Discussion: These results suggest that myoglobin resaturation post-Isc1 is slowed as compared with RH rate, despite an absence of flow limitation (RH perfusion is similar to Isc1 [1]). In these conditions, it is likely that the larger O_2 conductance toward mitochondria (sites of higher metabolic demand) is responsible for myoglobin resaturation rate. Conditions of limited perfusion (Isc2 vs. Isc1 flow, −42%) demonstrate a highly significant effect on both myoglobin and phosphocreatine recovery. In Becker patients, leg perfusion does not seem to differ from N during RH. Isc2 reduces perfusion (−32%) and slows myoglobin resaturation (+82%) and PCr recovery (+86%). PCrTC during aerobic exercise recovery does not differ from controls, showing similar functional capacities once exercise has been terminated. Thus, the coupling between the measured perfusion and metabolism parameters does not seem to be affected by this myopathy. Such an approach might be of particular interest to study myocardial metabolism and function in Becker's disease.

References

1. Toussaint. J. Appl. Physiol., 1996; 81(5):2221.
2. Toussaint. Magn. Reson. Med., 1996; 35:62.
3. Brillault. Cell. Mol. Biol., 1997;4 3:751.
4. Iotti. NMR Biomed., 1993; 6:248.

	N Perf	N PCrTC	N MRT	Bk Perf	Bk PCrTC	Bk MRT
RH	22.4 ± 9.7		16.8 ± 3.1	25.4 ± 9.1*		11.1 ± 3.7†
Isc1	26.6 ± 9.2	35.3 ± 16.1	39.8 ± 13.0	21.2 ± 6.9*	31.4 ± 11.6*	19.7 ± 7.1†
Isc2	15.3 ± 8.9‡	78.4 ± 27.5‡	67.1 ± 20.8‡	14.5 ± 4.5*‡	58.3 ± 16.1*‡	35.9 ± 14.6†‡
Aero	24.2 ± 10.2	35.5 ± 14.6		19.9 ± 9.5	36.6 ± 15.8*	

*p = NS vs. N, †$p < 0.01$ vs. N, ‡$p < 0.01$ vs. Isc1.

^{1}H-MRS Demonstrates That Lipolysis in Diabetic Hearts Requires Neutral Lipase

P. Wolkowics, H. Shen, Z. Zhang. *Department of Medicine, Division of Cardiovascular Disease, University of Alabama at Birmingham*

Rats treated with 110 mg/kg streptozotocin (SZ) experience uncontrolled diabetes, their hearts becoming hypertriglyceridemic 36–48 hr after SZ treatment. Such hearts were isolated and then analyzed using ^{1}H-MRS. A linear relationship exists in these hearts between their chemical content of triglycerides (TG) and their content of ^{1}H-MRS-visible methylene protons (—$(CH_2)_n$—). The spin-lattice (T_1) and spin-spin (T_2) relaxation times for —$(CH_2)_n$— in these hearts are identical to those previously reported for heart TG. In the absence of alternate substrates, isolated perfused hearts use endogenous TG for energy production. This lipolysis causes a net decrease in heart TG. Time-dependent decreases occur in the —$(CH_2)_n$— content of hearts from SZ-treated rats when these hearts are perfused with glucose as exogenous substrate. Hearts perfused with glucose and acetate, an alternate substrate that inhibits TG lipolysis, have lower rates of —$(CH_2)_n$— decrease. Two pathways exist for cardiac lipolysis. The first requires an acid lipase, occurs in lysosomes, and is sensitive to methylamine. The second requires a neutral lipase, occurs on triglyceride droplets, and is sensitive to diethyl-nitro-phenylphosphate (DNPP). Rates of decrease in heart —$(CH_2)_n$— are similar in hearts perfused with glucose in the presence or absence of 5 mM methylamine. Treating glucose-perfused hearts with DNPP, however, greatly diminishes their rates of —$(CH_2)_n$— decrease. ^{1}H-MRS, therefore, can measure the content of heart TG in hearts isolated from SZ-treated rats. The (—$CH_2)_n$— protons of these TG have relaxation properties similar to those reported for heart TG. The TG in SZ-treated hearts are not only visible to ^{1}H-MRS, they also are metabolically active. Using ^{1}H-MRS, it is demonstrated that neutral lipase but not acid lipase is required for TG lipolysis in diabetic hearts.

Regulation of Oxidative Phosphorylation: Homeostasis of Intermediary Flux Rates from ^{13}C NMR

E. Douglas Lewandowski. *Massachusetts General Hospital and Harvard Medical School*

I. Metabolic flux in supporting the dynamic processes of cardiac function
  A. Fueling energy production from oxidative intermediary metabolism
    1) Energetic requirements in the myocyte contracting, ion homeostasis, chemical signaling, and cell maintenance
    2) ATP synthesis from progressive oxidation of substrates (harvesting electrons from carbon-based fuels)
    3) Reducing equivalents are currency for ATP synthesis
    4) Oxidative metabolism in the mitochondria
    5) Tricarboxylic acid (TCA) cycle flux and enzyme activity correspond to energy turnover
  B. Subcellular compartmentation of metabolic pathways
    1) Mitochondrial and cytosolic metabolism under aerobic conditions
    2) Malate-aspartate shuttle transfer reducing equivalents to the mitochondria and exchanges metabolic intermediates

II. Dynamic-mode ^{13}C-NMR of the intact functioning heart
  A. ^{13}C-NMR measurements of flux through oxidative metabolism
    1) Monitoring enrichment of key metabolites from ^{13}C-enriched fuels
    2) Labeling scheme for online measurement of metabolic flux
    3) Targeting key pathways with specific labeled precursors
    4) TCA cycle interactions with glutamate
    5) Enrichment rate (to steady state) is independent of fractional enrichment (^{13}C/[^{13}C + ^{13}C]) of precursor. This facilitates in vivo applications with competing bloodborne substrates.
  B. Analysis of ^{13}C enrichment kinetics
    1. Kinetic modeling
      a) formulation consistent with known biochemistry
      b) limiting unknown variables
      c) internal constraints to improve accuracy
      d) external constraints to improve accuracy (MVO_2) and reduce covariance in multiparameter fittings
    2. Utility and application of simple kinetic models
      a) fitting model to experimental data
      b) group fittings (standard deviation as error) versus individual fitting (noise level as error)
    3. Application to heart preparations—isolated hearts and in situ hearts

III. Mitochondrial transport processes: A new direction for spectroscopic measurements in normal and diseased hearts
  A. Subcellular exchange of metabolites and transport rates from ^{13}C-NMR
    1. Chemical interconversion between TCA cycle intermediates with glutamate
      a) 90% of detected, enriched glutamate is in the cytosol
      b) Catalysis of exchange between α-ketoglutarate and glutamate occurs via a rapid transaminase enzyme
    2. Delayed enrichment of glutamate due to transport as rate-determining step
      a) Discrepancy between rapid transaminase flux and observed interconversion rate between α-ketoglutarate and glutamate (10–20-fold)
      b) Responsiveness of malate-aspartate shuttle to cytosolic redox state (NADH/NAD$^+$)
      c) Net forward flux through malate-aspartate shuttle not required for ^{13}C enrichment of glutamate.
  B. Homeostasis of metabolic flux for energy production in normal and diseased myocardium
    1. Oxidation rate versus efflux rate of intermediate from mitochondria
    2. Response to rate-limiting dehydrogenase activity in the TCA cycle
    3. Studies previously limited to isolated mitochondria bathed in artificial "cytosol" without correlate of cardiac performance
    4. Stunned myocardium displays altered oxidation/efflux rates

Altered Myocardial Metabolism in Hypertensive Heart Disease Is Coupled with Diastolic Dysfunction

H.J. Lamb, H.P. Beyerbacht, A. van der Laarse, J. Doornbos, E.E. van der Wall, A. De Roos. *Leiden, The Netherlands*

Purpose: To study the myocardial high-energy phosphate (HEP) metabolism and left ventricular (LV) function in patients with hypertensive heart disease.

Methods: Eleven patients with hypertension and 13 age-matched healthy subjects were studied with MR imaging at rest and phosphorus-31 MR spectroscopy at rest and during atropine-dobutamine stress (1).

Results: Hypertensive patients showed higher LV mass (98 ± 28 g/m^2) than healthy controls (73 + 13 g/m^2, $p < 0.01$). LV filling was impaired in patients, reflected by a decreased peak rate of wall thinning (PRWThn), E/A ratio, early peak filling rate, and early deceleration peak (all $p < 0.05$), whereas systolic function was still normal. The

myocardial PCr/ATP ratio, a measure for cellular energy reserve, determined in patients at rest (1.20 ± 0.18) and during stress (0.95 ± 0.25) was lower than those values obtained from healthy controls at rest (1.39 ± 0.17, $p < 0.05$) and during stress (1.16 ± 0.18, $p < 0.05$). PCr/ATP determined at rest in patients was similar to values obtained in healthy subjects during stress ($p > 0.05$). PCr/ATP acquired at rest correlated statistically significantly with PRWThn and early deceleration peak ($r \geq 0.55$, $p < 0.01$).

Conclusions: Hypertensive heart disease is associated with altered myocardial HEP metabolism and diastolic dysfunction. The present study is the first to provide evidence of a direct relation between myocardial HEP metabolism and LV filling characteristics in humans. Myocardial HEP metabolism in hypertensive heart disease seems to be "stressed" to maintain global heart function at rest. The combination of functional and metabolic evaluation of the human heart seems to provide a sensitive tool for early detection of changes in myocardial performance and viability.

Reference

1. Lamb HJ, Beyerbacht HP, Ouwerkerk R, Doornbos J, Pluim BM, van der Wall EE, van der Laarse A, de Roos A. Metabolic response of normal human myocardium to high-dose atropine-dobutamine stress studied by ^{31}P-MRS. Circulation, 1997; 96:2969–2977.

Cardiac Transplant Patients Assessed by the P-31 MRS Stress Test

W.T. Evanochko, S. Buchthal, J. den Hollander, R. Bourge, R. Benza, G. Pohost. *Birmingham, AL*

Literature testifies that biopsies from cardiac transplant patients do not correlate with their bioenergetic profiles obtained by ^{31}P MRS. Yet these results indicate altered high-energy phosphate metabolism in certain patients. That certain resting myocardial PCr/ATP from heart transplant patients were significantly lower than in normal controls warrants further investigation (1). Vasculopathy is a competing mechanism of rejection and is associated with hemodynamic abnormalities in the microvasculature (2). Mildly stressing these patients using an isometric handgrip (IH) might allow detection of vasculopathy because they would demonstrate a PCr/ATP decrease consistent with ischemia. Therefore, IH exercise was used to induce mild stress and to observe transient changes in the PCr/ATP. A 10-cm ^{31}P surface coil was positioned over the apex of the heart (confirmed with scout images) with the patient in the supine position and secured with a Velcro strap to reduce respiratory artifacts. A voxel containing the anterior wall of the left ventricle was defined and shimmed. The IH exercise was performed similar to Weiss (3), at 30% maximum voluntary contraction during acquisition while blood pressure and heart rate were monitored. In all subjects studied, the handgrip exercise generated a small increase in the rate–pressure product (average ΔRPP, +12% ± 13). Although there was no significant difference in ΔRPP between controls and transplant, overall during exercise the normal subjects showed only an increase in heart rate, whereas the transplants, being denervated, showed only an increase in blood pressure. As expected, the normals showed no significant change in PCr/ATP during exercise (average, +2% ± 11). However, 7 of 28 transplants showed a significant decrease in PCr/ATP (>2 SD) compared with normals during exercise. The decrease in PCr/ATP in transplants may be the first signs of microvascular rejection, a contributing mechanism in the rejection process (2). The cause of this ischemia may be microvascular cardiac allograft vasculopathy.

References

1. Buchthal SD. Clinical cardiac rejection assessed by P-31 MRS: The final phase I analysis. ISMRM Proc., 1996; 2:1011.
2. Lones MA. Clinical-pathologic features of humoral rejection in cardiac allografts: A study in 81 consecutive patients. J. Heart Lung Transpl., 1995; 14:151–162.
3. Weiss RG. Regional myocardial metabolism of high-energy phosphates during isometric exercise in patients with coronary artery disease. N. Engl. J. Med., 1990; 323:1593–1600.

Transmural ^{23}Na and ^{31}P-NMR Measurements of Intracellular Na^+ and High-Energy Phosphates During and After Ischemia in the In Situ Dog Heart

J. Hai, H. Shen, J.A. Balschi. *Birmingham, AL*

The objective of this study was to define the relationship between the intracellular Na^+ (Na^+_i) and energetics during regional myocardial ischemia and reperfusion in the intact dog heart. A bilateral thoracotomy was performed on mongrel dogs ($n = 12$). A surface coil was attached to the anterior wall of the left ventricle (LV). An occluder was placed around the left anterior descending artery. The dog was placed in the magnet and a shift reagent for Na^+, $DyTTHA^{3-}$, infused until the shift of the extracellular Na^+ resonance was ≥2.5 ppm. Three 90-min periods followed: baseline, ischemia, and reperfusion. Nine animals entered this protocol, whereas an additional three entered a control protocol with no occlusion. ^{23}Na and ^{31}P-NMR one-dimensional chemical shift imaging (1DCSI) measured transmural Na^+_i and high-energy phosphate content. This 1DCSI technique generates four localized transmural spectra (slice thickness 0.25 cm). The sum of two 0.25-cm slices defined epicardial (Epi) and endocardial (Endo) regions (0.5 cm each). Four sets of interleaved ^{23}Na and ^{31}P 1DCSI (20 min) were acquired during each 90-min period. All data are mean ± SEM. Two-way repeated-measure ANOVA with Fisher's least protected significant difference test was used to compare any mean versus point A in the figures. Differences were declared statistically significant if $p < 0.05$. During ischemia, phosphocreatine (PCr) declines to a similar extent in Endo and Epi regions (Fig. 1). Na^+_i increases in the Endo region (Fig. 2) when PCr had decreased to 12% of baseline. The Epi Na^+_i does not significantly increase during ischemia (Fig. 2). This is consistent with a more rapid evolution of damage in the Endo region. Epi Na^+_i does increase during early reperfusion. These results are consistent with an inhibition of the Na^+/K^+_i ATPase in the Endo region during ischemia.

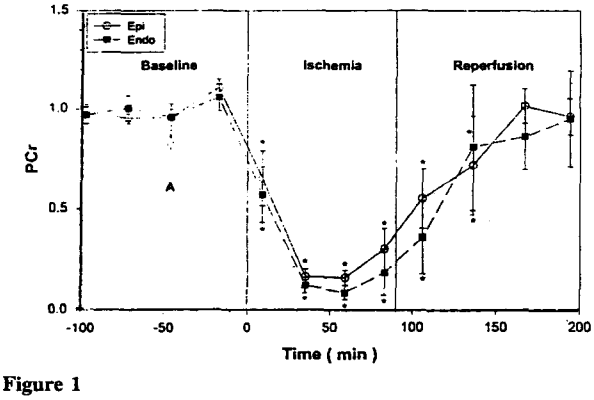

Figure 1

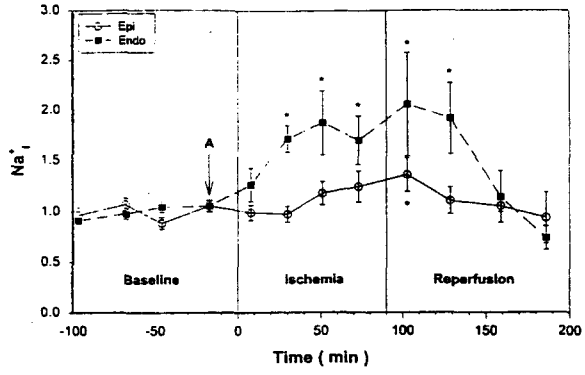

Figure 2

Magnetization Transfer Contrast in the Human Heart

S.D. Buchthal, G.M. Pohost, J.A. den Hollander. *Birmingham, AL*

Magnetization transfer contrast (MTC) depends on interactions between macromolecules and tissue water. Changes in myocardial tissue after an ischemic event may change these interactions and therefore cause a change in the MTC effect. MTC has been measured in isolated rat hearts, and in ischemic myocardial scar, MTC is reduced (1). Although MTC has been measured in human myocardium, little work has been done to characterize it in vivo (2,3). All studies were performed on a Philips ACS15 clinical imager using the standard body coil. A tygon tube filled with doped water was taped to the subject's chest as a control. Scout images were obtained fofllowed by two- and four-chamber views to prescribe the short-axis orientation. Gated gradient-echo images with TE 6 ms and flip angle 10–30° were obtained in cine loop format, tr 53 ms, from midventricle with and without an MTC prepulse. On resonance, MTC was generated using a 90-(−180)-90 composite pulse. A frequence selective pulse was used off-resonance. Images were obtained both with and without saturation slabs above and below the imaging plane to darken the blood pool. Signal intensity was measured in myocardial wall, background, and the water standard. The myocardial signal intensity was measured under four different conditions: with and without MTC and with and without the saturation slabs (M+S+, M+S−, M−S+, M−S−). Compared with the M−S− controls, the signal intensity dropped by 41 ± 8% with the MTC prepulse and increased at longer flip angles. When the saturation slabs were present, the signal intensity dropped 51 ± 11% compared with M−S− and by 33 ± 11% compared with M−S+. The off-resonance effects were studied to confirm that signal reduction was MTC related. The signal reduction was maximum on resonance and decreased in a sigmoid response out to 20 kHz. The signal from the water standard decreased asymptotically. In the rat heart, the MTC effect in myocardial scar is significantly less than in normal tissue (4). In preliminary studies, we observed the decrease in MTC signal reduction in established myocardial scar in two patients (average decrease in signal intensity, 23%). This suggests that tissue viability might be assessed noninvasively.

References

1. Wolff SD, Balaban RS. Magnetization transfer imaging: Practical aspects and clinical applications. Radiology, 1994; 192:593–599.
2. Balaban RD, Chesnick S, Hedges K, Samaha F, Heineman FW. Magnetization transfer contrast in MR imaging of the heart. Radiology, 1991; 180:671–675.
3. Mather R, Sinha U, Sinsha S. Magnetization transfer contrast in fast imaging of the LV myocardium. ISMRM, 1997; 5:1555.
4. Scholz TD, et al. Water-macromolecular proton magnetization transfer in infarcted myocardium: A method to enhance magnetic resonance image contrast. Magn. Reson. Med., 1995; 33:178–184.

Sodium Magnetic Resonance Imaging of Acute Myocardial Infarction at 1.5 T

Paul A. Bottomley, Ray F. Lee, Chris D. Constantinides, Robert G. Weiss. *Baltimore, MD*

Recent animal studies showing elevations in sodium (^{23}Na) magnetic resonance imaging (MRI) signals in acute reperfused rabbit and canine myocardial infarction, using 2.7- and 4.7-T systems (1,2) revised earlier interest (2) in human studies (3,4). Of interest is the possibility that the technique might be used to assess myocardial viability, which is critical for evaluating patient survival and therapeutic options after myocardial infarction. To investigate whether ^{23}Na-MRI can be used to assess myocardial viability on a clinical MRI scanner, instead of constructing a separate RF channel (4), we implemented ^{23}Na-MRI directly on a GE 1.5-T clinical scanner equipped with a standard broadbend spectroscopy package and a homebuilt 20-cm ^{23}Na transmit/receive surface coil. A gradient-refocused echo MRI pulse sequence was written to extend the limits of the conventional proton (^{1}H) MRI sequence by allowing smaller arrays (down to 32 × 32), coarser spatial resolution, smaller acquisition bandwidths, nuclei other than-protons, and access to the system's broadband spectroscopy excitation and acquisition hardware for MRI use. Excitation and reception parameters for ^{23}Na-MRI were adjusted with a manual prescan window that provided averaged sample projections. In addition, we implemented adiabatic excitation pulses (5) to provide a more uniform coverage 3D gradient echo human ^{23}Na-MRI and a novel image-enhancement method to incorporate a priori ^{1}H-MRI information into the ^{23}Na images, without compromising their heterogeneity, which is essential for detecting local abnormalities. We performed ^{23}Na-MRI on acute canine myocardial infarction induced by a 1-hr balloon occlusion of the left anterior descending coronary artery during x-ray fluoroscopy-guided coronary catheterization, followed by balloon deflation to allow reperfusion. MRI studies were performed within 6 hr, and ^{23}Na images were correlated with postmortem photographs of the myocardium stained for infarction. The results showed ^{23}Na-MRI signal elevations of approximately twofold in areas of infarction identified by staining. We extended this work to ^{23}Na-MRI of patients with acute myocardial infarction within 1 week postonset. In human studies, subjects are positioned prone on the ^{23}Na coil beneath the heart, ^{1}H-MRI done, followed by ^{23}Na-MRI with TR 33 ms, 0.5 × 0.5 × 2 or 1.5 cm (0.38–0.5 ml) resolution in scan times of 6–12 min.

References

1. Cannon PJ, Maudsley AA, Hilal AK, Simon HE, Cassidy F. JACC, 1986; 7:573–579.
2. Kim RJ, Lima JAC, Chen EL, et al. Circulation, 1997; 95:1877–1885.
3. Ra JB, Hilal SK, Oh CH, Mun IK. Magn. Reson. Med., 1988; 7: 11–22.
4. Parrish TB, Fieno DS, Fitzgerald SW, Judd RM. Magn. Reson. Med., 1997; 38:653–661.
5. Garwood M, Ke Y. J. Magn. Reson., 1991; 94:511.

Atherosclerotic Plaque Components Studied with Magnetization Transfer

M. Pachot-Clouard, F. Vaufrey, L. Darasse, J.F. Toussaint. *SHFJ, CEA, Orsay and CNRS URA 1458 Paris, France*

Background: Developing imaging technologies capable of identifying unstable atheromatous plaques in vivo is a major issue of present cardiovascular research (1). Plaque stability depends on plaque structure

and composition: lipid core and fibrous cap. T2 and diffusion contrasts allow the discrimination of these components (2,3). We test here a third contrast mechanism and hypothesize that magnetization transfer (MT) may occur between free water and restricted protons of macromolecules inside atherosclerotic components, where large exchange surfaces and numerous potential sites are present.

Methods: All experiments were performed at 3 and 7 T on Bruker magnets and at 37°C. We used optimized T2-selective binomial pulses and tested MT in four pools of microdissected components from 10 atherosclerotic plaques: lipid core (L), collagenous cap (C), media (M), and adventitia (A). Binomial pulses of the third order were used with incremented duration pulses (1*T*-3*T*-3*T*-1*T*) and an interval time (T_{int}), RF amplitude being left constant (4). We measured T1 and T2 for each component and simulated the effect of saturation without exchange using an analytical program to differentiate restricted and free protons; $\varpi 1$, T_r and T_{int} were adjusted to saturate almost completely the restricted protons with a given T2 (T_{2sel}). This prevents misinterpretation of a direct saturation effect (5).

Results: The effect of MT (reduction of signal expressed as a percentage of initial magnetization without MT) for L, C, M, and A are shown in the table at 3 and 7 T:

	L	C	M	A
3 T	15%	20%	28%	12%
7 T	40%	45%	50%	26%

Discussion: This is the first demonstration of a magnetization transfer effect in plaque components. The presence of numerous possible sites of exchange between layers of free water protons and macromolecules restricted protons in collagen proteins may explain the large MT effect we show in the fibrous cap. Similarly, the effect seen in the media probably relates to the extent of fibers present (collagen and elastin). In the lipid atheromatous cores, the MT effect demonstrated may be related to the presence of lipoproteins largely denaturated by oxidation processes. These results provide a basis to develop new imaging sequences aimed at discriminating the components of the vulnerable plaques.

References

1. The Vulnerable Plaque. Futura Publishing, Inc. AHA Symposium, May 10–11, 1997.
2. Toussaint JF, et al. Arterioscler. Thromb. Vasc. Biol., 1995; 15: 1533–1542.
3. Toussaint JF, et al. Arterioscler. Thromb. Vasc. Biol., 1997; 17:542–546.
4. Pachot-Clouard M, Darasse L. Magn. Reson. Med., 1995; 34:462–469.
5. Henkelman RM, et al. Magn. Reson. Med., 1993; 29:759–766.

Results of the Analysis of the Changes in Signal Intensity or of the Wall Motion by Magnetic Resonance Imaging to Identify Hibernating Myocardium

Ibraim Pinto, Rodrigo Barretto, Ricardo Pavanello, Simone Barretto, Enilton Egito, Maria H. Abib, Amanda Sousa, J. Eduardo Sousa, Luis C.B. Souza, Adib Jatene. *Hospital do Coração, ASS, São Paulo, Brazil*

Some investigators used magnetic resonance imaging (MRI) to detect hibernating myocardium (HM), reporting conflicting results. It is possible that these differences were due to the fact that some groups analyzed the myocardium signal changes after drug infusion, whereas others studied the changes in wall motion (WM) after pharmacological stimulus. To compare these approaches, we designed a protocol by which patients with suspected HM underwent MRI with a 5-μg/kg/min infusion of dobutamine (DO) for 5 min. Signal intensity in spin-echo images and WM by cine MRI were measured at baseline and after the DO infusion. To evaluate this protocol, we studied 60 patients, with CAD who would undergo CABG. There were 72 areas of suspected HM (1.2 area/patient). Target areas had a baseline WM by cine MRI of −0.3 ± 0.4 and a mean signal intensity of 28 ± 18. After DO the WM increased in 26 patients (mean, 1.3 ± 0.8) and had minor changes in 34 (mean, 0.1 ± 0.7). Signal intensity increased in 33 patients (mean, 48 ± 19), whereas 27 patients showed almost no signal change (mean, 32 ± 24) after DO. No patient within signal intensity increase died in-hospital, whereas 2 of 27 with no signal change died soon after surgery (1 patient with increase in WM after DO, 1 patient without WM changes). Of the 33 patients with signal increase, 7 had angina, 2 heart failure, and all were alive after a 4-year follow-up. In this group, six patients had no increase in WM after DO. Of the 27 patients without signal change in the target area, 5 had angina, 13 heart failure, 5 underwent reoperation, and 5 died ($p < 0.05$). Five of the latter had significant increase in WM after DO. The authors conclude that myocardial signal change by MRI after DO infusion is a more sensitive approach to detect HM than WM analysis by cine MRI. This protocol may have a role in clinical practice to evaluate and stratify the risk of patients with suspected HM.

References

1. Pinto IMF, Pavanello R, Piegas L, et al. Dobutamine magnetic resonance imaging detection of hibernating myocardium (abstract). Circulation, 1995; 92(suppl):I-509.
2. Dendale PAC, Franken PR, Waldman GJ, et al. Low-dosage dobutamine magnetic resonance imaging as an alternative to echocardiography in the detection of viable myocardium after acute myocardial infarction. Am. Heart J., 1995; 130:134–140.

Functional Genomics of the αMHC$^{403/+}$ Mouse Model of Familial Hypertrophic Cardiomyopathy

Joanne S. Ingwall, Matthias Spindler, Kurt W. Saupe. *NMR Laboratory for Physiological Chemistry, Cardiovascular Division, Department of Medicine, Brigham and Women's Hospital, Harvard Medical School, Boston, MA*

Background and Goals: An arginine missense mutation at position 403 of the β-cardiac myosin heavy chain causes familial hypertrophic cardiomyopathy. Recently, Seidman and colleagues at Harvard Medical School bioengineered a mouse in which half of the myosin heavy chain in the heart contained this missense mutation (αMHC$^{403/+}$). Studying this mouse heart allows us to test whether this single mutation at the base of the actin-binding loop alters acto-myosin kinetics sufficiently to alter systolic and diastolic properties of the whole heart and whether these mechanical alterations are associated with changes in energetics. Although specific for this mutation, these studies illustrate the type of information it is possible to obtain defining functional genomics at the whole heart level.

The Study: We used the isolated isovolumic heart preparation so that cardiac performance could be measured simultaneously with energetics using ^{31}P-NMR spectroscopy. We observed three major alterations in the physiology and bioenergetics of the αMHC$^{+/403}$ mouse hearts. First, although there was no evidence of systolic dysfunction, diastolic function was impaired during inotropic stimulation. Diastolic dysfunction was manifest as both a decreased rate of left ventricular relaxation and an increase in end-diastolic pressure. Second, under baseline conditions, αMHC$^{+/403}$ hearts had lower phosphocreatine and increased inorganic

phosphate contents, with unchanged ATP content, resulting in a decrease in the calculated value for the free energy released from ATP hydrolysis. Third, hearts from $\alpha MHC^{+/403}$ that were studied unpaced responded to increased perfusate calcium by decreasing heart rate approximately twice as much as wild-types.

We conclude that hearts from $\alpha MHC^{403/+}$ mice demonstrate workload-dependent diastolic dysfunction resembling the human form of familial hypertrophic cardiomyopathy. These changes may be explained by a slowed release of the actin binding loop from the thin filament. Changes in high energy phosphate content suggest that an energy-requiring process contributes to the observed diastolic dysfunction.

Creatine Kinase Flux in Myocardium: Insights from Transgenic Mice

Cees J.A. van Echteld. *University Hospital, Utrecht, The Netherlands*

^{31}P-NMR magnetization transfer methods have been extensively used to study fluxes through the myocardial CK reaction. However, in general it has not been possible to determine the individual contributions of the different iso-enzymes. A kind gift of Prof. Dr. B. Wieringa, University of Nijmegen, of the transgenic mouse model, has enabled us to study in vivo enzyme kinetics of CK in isolated perfused hearts of transgenic mice lacking the cytosolic MM-CK in heart and skeletal muscle. Recently, the group of Prof. Wieringa found no NMR-detectable fluxes through the CK reaction in skeletal muscle of these MM-CK–deficient mice (1). In our study (2), we investigated whether in cardiac muscle of MM-CK–deficient mice a Mi-CK-mediated flux through the CK reaction could be observed. Isolated perfused mouse hearts were studied at 400 and 600 bpm and during K^+ arrest. ^{31}P-NMR spectra were obtained at 202 MHz on a Bruker AM 500 spectrometer. Spectra showed clearly observable magnetization transfer in these MM-CK–deficient mouse hearts. PCr/ATP ratios in wild-type and MM-CK–deficient hearts were similar. Saturation of the γ-ATP resonance for varying durations was used to determine the rate constant kfor of the PCr to ATP reaction in wild-type (n = 7) and MM-CK–deficient (n = 6) mouse hearts. At 400 bpm kfor calculated from these data was 0.43 ± 0.06 s^{-1} for wild-type and 0.22 ± 0.03 s^{-1} for MM-CK–deficient hearts. During K^+ arrest the flux through the forward CK reaction decreased by ~50% in wild-type hearts and remained unchanged in MM-CK–deficient hearts. That Mi-CK flux in hearts of MM-CK–deficient mice could be clearly observed, in contrast to Mi-CK flux in skeletal muscle of these mice, is most likely due to the much higher Mi-CK content in cardiac muscle. In vitro assessment showed that total CK activity in MM-CK–deficient hearts was 26% of total CK activity in wild-type hearts. Therefore, it appears that, in vivo, Mi-CK contributes much more than MM-CK to total CK flux in wild-type mouse hearts. It is also tempting to speculate that during K^+ arrest in wild-type hearts, total CK flux is fully explained by Mi-CK activity, although an MM-CK contribution cannot be ruled out. However, when interpreting these data, one should keep in mind that adaptations may occur in response to the genetic modifications (3,4). For instance, Ventura-Clapier et al. (3) reported that the rate constant of tension changes of skinned ventricular fibers was markedly reduced in MM-CK–deficient mice, which is not surprising in view of the absence of a local ATP-regenerating system. Veksler et al. (4) found that in MM-CK–deficient mouse heart, the K_m for ADP and the V_{max} of the mitochondrial respiration had changed substantially in the absence of creatine compared with wild-type heart, from which they conclude an adaptation of the adenine nucleotide transport system. Interestingly, no such differences were found in the presence of creatine, which is always the case for the hearts in our study. Furthermore, although not consistently found, some studies show an increased expression of BB-CK in MM-CK–deficient mouse hearts. Nevertheless, when carefully taking into account the consequences of these adaptations, these CK knockout mice will yield much valuable information on the role of the different CK iso-enzymes, which cannot be obtained otherwise.

References

1. Van Deursen J, Heerschap A, Oerlemans F, Ruitenbeek W, Jap P, Ter Laak H, Wieringa B. Skeletal muscles of mice deficient in muscle creatine kinase lack burst activity. Cell, 1993; 74:612–631.
2. Van Dorsten FA, Nederhoff MGJ, Nicolay K, Van Echteld CJA. ^{31}P NMR studies of creatine kinase flux in M-creatine kinase deficient mouse heart. Am. J. Physiol. (provisionally accepted).
3. Ventura-Clapier R, Kuznetsov AV, D'Albis A, Van Deursen J, Wieringa B, Veksler VI. Muscle creatine kinase-deficient mice. I. Alterations in myofibrillar function. J. Biol. Chem., 1995; 270:19914–19920.
4. Veksler VI, Kuznetsov AV, Anflous K, Mateo P, Van Deursen J, Wieringa B, Ventura-Clapier R. Muscle creatine kinase-deficient mice. II. Cardiac and skeletal muscle exhibit tissue-specific adaptation of the mitochondrial function. J. Biol. Chem., 1995; 270:19921–19929.

^{31}P-NMR of the Failing Heart

Stefan Neubauer. *Medizinische Universitätsklinik, Würzburg, Germany*

^{31}P-NMR spectroscopy (^{31}P-MRS) is the only method for the noninvasive investigation of cardiac energy metabolism without the need for radioactive tracers. In heart failure, ^{31}P-MRS may have three applications: study of the pathophysiology of contractile failure, diagnostic tool for grading of disease severity and prognosis assessment, and follow-up during chronic drug therapy. Whether the failing heart has limited contractile function due to impaired energy metabolism has been debated for decades (1). ^{31}P-MRS now allows the study of this hypothesis in the human heart. In principle, energy metabolism could limit performance via three mechanisms. First, simply by a reduction of ATP. Because ATP levels in heart failure are unchanged or reduced by no more than 30–40% and because the K_m (ATP) values of SERCA, myosin ATPase, and other enzymes involved in contractile function are in the μM range, reduction of steady-state ATP levels is almost certainly not a limiting factor. Second, it is likely that intracellular ATP is compartmentalized, and thus the question is whether "we get ATP where we need it" (i.e., foremost to the myofibrillar compartment). The creatine kinase (CK) shuttle is likely to serve as an energy transfer system, shuttling the high-energy phosphate bond to the sites of ATP utilization (1,2). CK reaction velocity (flux) can be measured with NMR saturation transfer. If CK flux falls below the rate of ATP synthesis (measured from oxygen consumption), then ATP transfer may be limiting performance. Third, the free energy change of ATP hydrolysis (ΔG) is a measure of the amount of energy that can be released from hydrolysis of 1 mol of ATP (3). ΔG can decrease without a major change in ATP steady-state levels. Typically, ΔG is approximately −58 kJ/mol. The minimum required ΔG for SERCA is −52 kJ/mol. If ΔG falls below this threshold, contractile dysfunction develops. Experimentally, many animal models of heart failure have been studied, including, among others, postmyocardial infarction, aortic banding, volume overload, pacing tachycardia, hereditary (Syrian hamster, SHR rat), or toxic (isoproterenol, adriamycin, furazolidone) models. Changes of energy metabolism occur uniformly in these models, independent of the etiology of heart failure. Typically, ATP levels are unchanged or slightly decreased. Phosphocreatine and total creatine levels are reduced by up to ~80% (1,4). Total CK activity decreases as does the activity of the mitochondrial CK isoenzyme. B-containing fetal CK isoenzymes increase. ATP transfer (CK flux) decreases substantially. In most models, ATP transfer remains higher than ATP synthesis and thus cannot be

limiting performance. In severe end-stage heart failure, however, ATP transfer may decrease below ATP synthesis, limiting performance (5). During inotropic simulation, ADP increases disproportionately and thus ΔG decreases in the failing heart. This is a mechanism likely to be responsible for limiting contractile reserve of the failing heart. Although experimentally all components of energy metabolism (ATP, phosphocreatine, free creatine, CK total and isoenzyme activity, ADP, ΔG) can be measured or calculated, human studies (6) were limited to measuring the PCr/ATP ratio as an "index of the energetic state of the heart." Because the CK equilibrium constant favors ATP synthesis over PCr synthesis by two orders of magnitude, any imbalance between ATP demand and supply will first decrease PCr and thus the PCr/ATP ratio. In addition, decreases of the PCr/ATP ratio in the failing human heart also reflect the loss of total creatine. Solutions to quantitate absolute levels of ATP and PCr in human heart are on the way (7). In addition, quantification of total creatine by ^{1}H-MRS (8) will allow calculation of free ADP and ΔG in human heart. Thus, future studies of human heart failure will allow us to study the contribution of energy metabolism to contractile failure in greater detail, including ADP and ΔG measurements during inotropic stimulation. Also, measurement of CK flux in human heart failure should be performed to evaluate a possible role for ATP transfer. Present data are consistent with, but do not prove, a causal role for energy metabolism in heart failure.

In heart failure of nonischemic or ischemic origin, we (9) and others (10) described a significant reduction of the PCr/ATP ratio. The reduction also correlates with the severity of heart failure and with ejection fraction. Altered energetics can be shown for post-MI hearts (11), dilated cardiomyopathy (9,11), and also valve disease (12), again demonstrating that this is a phenomenon occurring independent from the etiology of heart failure. We recently demonstrated that PCr/ATP ratios also hold prognostic information on mortality in patients with DCM (13).

^{31}P-MRS allows us to sequentially follow the energetic response of the failing heart to chronic drug therapy. Experimentally, ACE-inhibitors and beta-receptor-blockers attenuated the changes of energy metabolism in heart failure models. We reported an improvement of the PCr/ATP ratio in DCM patients during chronic therapy with ACE inhibitors, diuretics, digitalis, and beta-receptor-blockers (9). Systematic placebo-controlled clinical trials are awaited.

References

1. Ingwall JS. Is cardiac failure a consequence of decreased energy reserve? Circulation, 1993; 87(Suppl.VII):58–62.
2. Wallimann T, Wyss M, Brdiczka D, Nicolay K, Eppenberger HM. Intracellular compartmentation, structure and function of creatine kinase isoenzymes in tissues with high and fluctuating energy demands: The "phosphocreatine circuit" for cellular energy homeostasis. Biophys. J., 1992; 281:21–40.
3. Kammermeier H, Schmidt P, Jüngling E. Free energy change of ATP-hydrolysis: A causal factor of early hypoxic failure of the myocardium? J. Mol. Cell. Cardiol., 1982; 14:267–277.
4. Neubauer S, Horn M, Naumann A, et al. Impairment of energy metabolism in intact residual myocardium of rat hearts with chronic myocardial infarction. J. Clin. Invest., 1995; 95:1092–1100.
5. Liao R, Nascimben L, Friedrich J, Gwathmey JK, Ingwall JS. Decreased energy reserve in an animal model of dilated cardiomyopathy. Relationship to contractile performance. Circ. Res., 1996; 78:893–902.
6. Bottomley PA. MR spectroscopy of the human heart: The status and the challenges. Radiology, 1994; 191:593–612.
7. Bottomley PA, Atalar E, Weiss RG. Human cardiac high-energy phosphate metabolite concentrations by 1D-resolved NMR spectroscopy. Magn. Reson. Med., 1996; 35:664–670.
8. Bottomley P, Lee SYH, Weiss RG. Proton MR spectroscopy of creatine in myocardial infarction. Vol. 1. *ISMRM* 4th scientific meeting, New York; 1996.
9. Neubauer S, Krahe T, Schindler R, et al. 31P magnetic resonance spectroscopy in dilated cardiomyopathy and coronary artery disease. Altered cardiac high-energy phosphate metabolism in heart failure. Circulation, 1992; 86:1810–1818.
10. Hardy CJ, Weiss RG, Bottomley PA, Gerstenblith G. Altered myocardial high-energy phosphate metabolites in patients with dilated cardiomyopathy. Am. Heart J., 1991; 122:795–801.
11. Hardy CJ, Bottomley PA. 31P spectroscopic localization using pinwheel NMR excitation pulses. Magn. Reson. Med., 1991; 17:315–327.
12. Neubauer S, Horn M, Pabst T, et al. Cardiac high-energy phosphate metabolism in patients with aortic valve disease assessed by 31P-magnetic resonance spectroscopy. J. Invest. Med., in press.
13. Neubauer S, Horn M, Cramer M, et al. In patients with dilated cardiomyopathy the myocardial phosphocreatine-to-ATP ratio is a predictor of mortality. Circulation, 1997; 96:2190–2196.

Preliminary Experience with Multislice First-Pass Perfusion Imaging in Patients with Coronary Artery Disease

A. Moalemi,[1] S. Ding,[1] F. Epstein,[1] V. Dilsizian,[1] R. Balaban,[1] A. Arai,[1] C. Lundergan.[2] [1]*Bethesda, MD;* [2]*Washington, DC*

Purpose: To use dipyridamole thallium and cardiac catheterization to guide reading criteria for detection of significant coronary artery disease by a new multislice MRI technique.

Methods: Nine patients with history of coronary artery disease with a clinical indication for a stress thallium study underwent both dipyridamole thallium and dipyridamole perfusion MRI study. Imaging was performed on a 1.5-T GE scanner with enhanced gradients using a highly segmented cardiac-gated GRE-EPI sequence with a volumetric sat pulse preceding each image. Five to seven short-axis images of the left ventricle were acquired every heart beat during the first passage of gadopentate dimeglumine (Magnevist) 0.14 mmol/kg at 5 ml/s via an antecubital IV. The temporal resolution of each image was approximately 100–120 ms, and the spatial resolution was approximately 2.8 mm. Cardiac catheterization information was available on all patients.

Results: Nine patients with coronary artery disease (six men, three women) completed the study. Perfusion defects appeared as dark subendocardial regions with delayed enhancement relative to normal zones. These abnormal zones persist beyond the peak left ventricular cavity enhancement phase. Subendocardial artifacts in normal zones tend to be evanescent correlating in time with peak contrast in the cardiac chambers. Defining significance as ≥60% coronary stenosis, 11 of 27 coronary distributions (LAD, RCA, LCX and their corresponding major branches) were abnormal. Qualitative assessment of the MRI scans detected 11 of 11 coronary distribution abnormalities but had 3 of 16 false positives.

Discussion: First-pass MRI perfusion methods are practical in patients with known coronary artery disease. Preliminary results suggest that this technique can be calibrated to have a high sensitivity and reasonable specificity for the detection of coronary artery disease.

Predicting the Long-term Follow-up of Patients with Acute Myocardial Infarction by Gadolinium-Enhanced Magnetic Resonance Imaging

Ibraim Pinto, Ricardo Pavanello, Leopoldo Piegas, Rodrigo Barretto, Marcos Barbosa, Edson Romano, Enilton Egito, Amanda Sousa, J. Eduardo Sousa, Luis C.B. Souza. *Hospital do Coração, ASS, São Paulo, SP, Brazil.*

Preliminary work with gadolinium (GD) enhanced magnetic resonance imaging (MRI) suggested that this method could estimate myocardial viability and predict the long-term follow-up of patients with acute

myocardial infarction (AMI). There is little evidence, however, supporting its clinical utility. To evaluate if MRI may evaluate patients after an AMI and give any information regarding their evolution, we studied 70 patients undertaken to Gd-MRI within 72 hr after AMI symptoms onset. MRI included gradient-echo series to define left ventricular ejection fraction (EF) and spin-echo series acquired immediately (I) and 10 (II) and 20 min (III) after Gd injection. Due to the high affinity of Gd-DTPA to inflammatory areas, Gd uptake should be higher in AMI walls without viability, which also should have a longer washout time. Signal intensity was measured in the AMI wall in acquisitions I, II, and III. Myocardial viability was considered present if the signal intensity in series III was smaller than that of series II. The percent of necrosis was calculated by measuring all regions with high signal in series III (AHIII), divided by the left ventricular myocardial mass ((AHIII/myocardial mass) × 100). We followed the patients for 5.2 ± 2.1 yr. There were eight in-hospital deaths, all in patients with high signal in series III and percent necrosis by MRI > 30%. The baseline EF of these patients was 38.9% and the EF of the 62 discharged alive was 43.1% (p = NS). In the follow-up, heart failure developed in 6 patients (baseline percent necrosis by MRI, 25%) and there were four deaths (baseline percent necrosis by MRI, 33.4% of the AMI wall). Two patients died of cardiogenic shock and had baseline percent necrosis by MRI of 42.6%. Patients with heart failure at follow-up had a mean baseline EF of 37.6%, patients who died at follow-up had a mean EF of 40.5%, and patients wih no adverse events at follow-up had a mean EF of 44.1% (p = NS). We conclude that patients with late Gd washout present worse in-hospital and late outcome, with higher mortality rates. The method has potential to be used to identify higher risk AMI patients.

References

1. Lima JAC, Judd RM, Bazille A, et al. Regional heterogeneity of human myocardial infarcts demonstrated by contrast enhanced MRI. Potential mechanisms. Circulation, 1995; 92:1117–1125.
2. Sechtem U, et al. Assessment of residual viability in patients with myocardial infarction using magnetic resonance imaging. Int. J. Cardiac Imaging, 1993; 9:31–40.

Real-Time MR Imaging with Partial k-Space Acquisitions

Adam B. Kerr, John M. Pauly, Dwight G. Nishimura.
Department of Electrical Engineering, Stanford University, Stanford, CA

Partial k-space acquisitions reduce scan time but come at a cost of a lowered SNR and increased reconstruction complexity (1). We demonstrate the ability to reconstruct images in real time despite this additional burden. Several novel acquisition strategies are also introduced, including partial circular echo-planar (CEPI) and partial variable-density spiral (VDS).

Method: The three partial k-space acquisition strategies used are shown in Figure 1. Although the symmetric VDS trajectory has been introduced previously for fluoroscopic and partial k-space applications (2,3), the asymmetric approach is novel and offers unique advantages. A homodyne gridding reconstruction was implemented using a distributed processing approach previously described (4). On a Sun SPARC 20/71 upgraded with four ROSS 125-MHz HyperSPARC processors, 16 128 × 128 images/s can be reconstructed with a delay of only 0.5 s.

Results: A full and 60% partial CEPI acquisition were implemented on a 1.5-T GE Signa to acquire 20-cm FOV and 2.2-mm resolution images. The scan times were 5 and 7.1 images/s, respectively. Cardiac images of a normal volunteer were acquired in real time, and as expected, the partial acquisition presented noticeably fewer motion and flow-related ghosting artifacts. Symmetrical and asymmetrical VDS acquisitions providing images with the same FOV and resolution were able to acquire up to 10 images/s. Flow and motion characteristics were better than for CEPI, but partial k-space artifacts were more prevalent. Of the two, the asymmetric VDS acquisition showed the least noticeable artifacts.

Discussion: Partial k-space acquisitions offer the advantage of decreasing scan time up to 50% or increasing spatial resolution. In a real-time interactive imaging system, the choice of full or partial acquisitions on spiral or CEPI trajectories can be seamlessly made to optimize image quality.

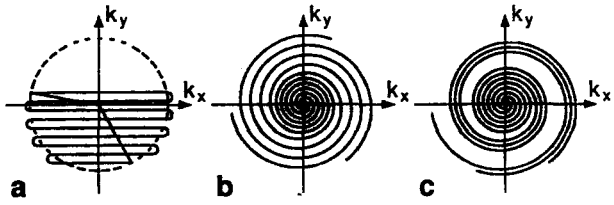

Figure 1. Partial k-space acquisitions; (a) partial CEPI, (b) symmetrical, and (c) asymmetrical variable-density spiral.

References

1. Noll D, et al. IEEE TMI, 1991; 10(2):154.
2. Spielman D, et al. MRM, 1995; 34:388.
3. Schomberg H, et al. Proc., 2nd SMR, 1994; 480.
4. Kerr A, et al. MRM, 1997; 38:355.

Combining Myocardial Perfusion and Coronary Angiography Using a New Ultrasmall Paramagnetic Iron Oxide: First Trials in Humans

L.O. Johansson,[1] A. Ragnarsson,[2] H. Ahlström,[2] P. Akeson.[3] [1]*St. Louis, MO;* [2]*Uppsala, Sweden;* [3]*Oslo, Norway*

Myocardial perfusion in humans has until now mainly been done using the T1 effect during the first pass of different gadolinium chelates. Because of the short intravascular half-life, it has not been possible to perform coronary angiography using the same injection. The purpose of this study was to use a new ultrasmall paramagnetic iron oxide (USPIO) blood-pool agent to perform myocardial perfusion imaging during the first pass of the contrast agent and coronary angiography during steady state. Nine volunteers were scanned using a 1.5-T system, Gyroscan ACS-NT (Philips Medical Systems). NC100150 injection, a new USPIO (Nycomed Imaging AS, a part of Nycomed Amersham), was injected in an antecubital vein. The different doses used were 1, 2.5, and 4 mg Fe/kg body weight with three subjects per dose. A 2D slice was positioned as a short-axis view for first-pass perfusion imaging. One slice per heartbeat was acquired. The sequence was a gradient echo with TR/TE/flip 7.7/2.6/15. Starting 30 min postinjection, coronary angiography of the left coronary system was performed using a 3D ECG-gated gradient echo with no prepulses or fat suppression. Navigator echoes were used for respiratory triggering. All injections, except one subject with the 1.0-mg Fe/kg dose, gave a signal drop during the first pass with larger signal drops for larger doses. The LM and LCX were visualized, with better result for higher doses. At the highest dose, the longest segments seen were 7 cm in all cases.

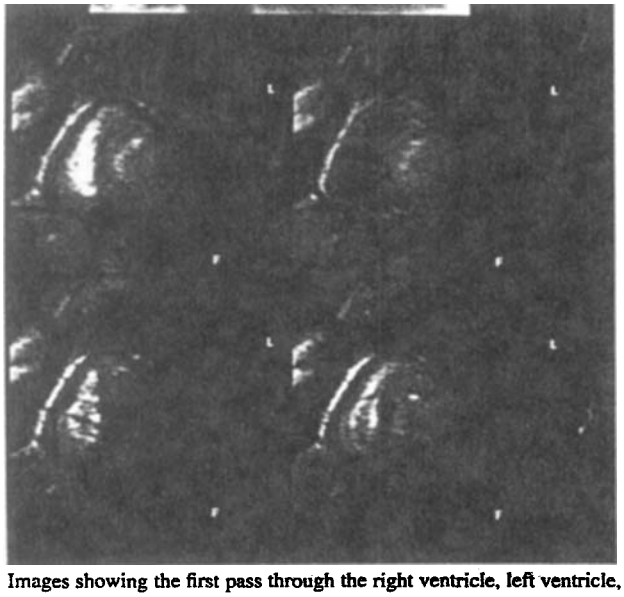

Images showing the first pass through the right ventricle, left ventricle, and myocardium.

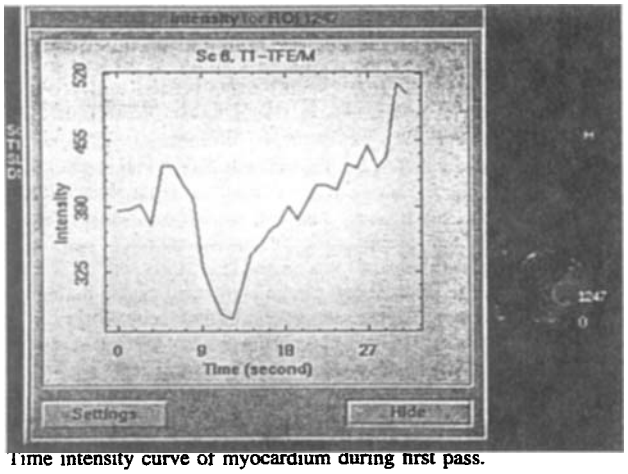

Time intensity curve of myocardium during first pass.

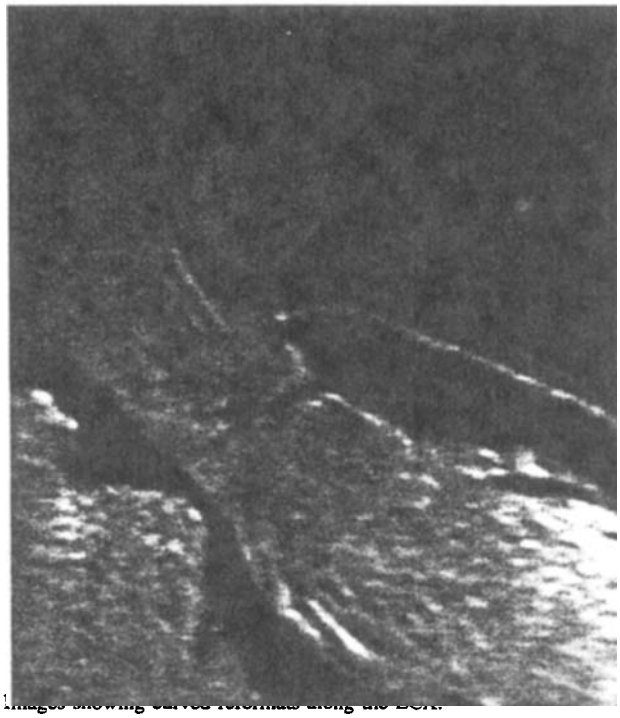

We showed that it is possible to combine myocardial perfusion imaging and coronary angiography using the same injection. We also showed that it is possible to get T2* dominant perfusion images with an echo time as short as 2.6 ms. The results also indicate that by using NC100150 injection, it is possible to perform coronary angiography without prepulses for myocardial suppression and without fat suppression.

Development of Quantitative Magnetic Resonance Perfusion Analysis in the WISE Study

A. Fuisz, M. Doyle, E. Kortright, E. Walsh, E. Martin, W. Rogers, G. Pohost, for the WISE investigators. *Birmingham, AL*

The purpose of the study is to develop quantitative algorithms to analyze MR perfusion images generated as part of the NHLBI WISE study.

In the first phase of the study, 53 women with a chest pain syndrome underwent perfusion MR imaging and cardiac catheterization. First-pass images were obtained after rapid infusion of gadolinium via a peripheral IV. Two to three short-axis slices were imaged. Rest and "stress" images were obtained (stress images after infusion of dypiridamole). The images were qualitatively read in a blinded fashion and compared with angiographic results. Initial sensitivity and specificity for MR imaging for the detection of coronary stenosis > 70% was 59% and 62%, respectively. Retrospective unblinded subgroup analysis of these patients demonstrated a population of patients who had a prominent increase in the slope of myocardial signal intensity after dipyridamole (53% of patients). To allow comparison between different patients and account for temporal changes, the slope of the intensity rise in the myocardial segment was divided by the slope of the intensity rise in the left ventricular cavity. The sensitivity and specificity for the detection of coronary disease was then calculated separately for the two groups identified. Patients in this "prominent increase" group demonstrated improved sensitivity and specificity for the detection of coronary stenosis (75% and 81%, respectively) compared with the remaining patients without evidence of increase in slope postdipyridamole, with sensitivity and specificity of 67% and 40%, respectively. Analysis of hemodynamic variables collected during the study did not distinguish between the two groups. Quantitative MR perfusion imaging has great potential as a method to diagnose coronary artery disease. The degree of coronary vasodilatation in response to dipyridamole seems to have a substantial effect on the accuracy of the technique.

Noninvasive Quantification of Absolute Myocardial Blood Flow with an Extracellular Tracer

M. Jerosch-Herold, N. Wilke, Y. Wang, A.E. Stillman. *Minneapolis, MN*

Purpose: We investigated the noninvasive quantification of absolute myocardial blood flow in ml/min per g of tissue with magnetic resonance (MR) imaging during the first pass of an extracellular bolus-injected contrast agent. We used a sensitivity analysis in combination with a tracer kinetic model to determine if one can distinguish with an extracellular MR contrast agent between changes in blood flow and changes of other physiological parameters such as blood volume and capillary permeability.

Methods: We used the closed-chest instrumented porcine model of chronic ischemia ($n = 6$). Multislice MR first-pass images were acquired for every heart beat on a 1.5-T whole body MR system with a saturation recovery prepared FLASH imaging sequence (1) during rest and inotropic stimulation with dobutamine (up to 5 mg/kg/min iv.). THe effects of water exchange on the measured signal were minimized by using a high α flip angle for FLASH readout. Gadopentetate dimeglumine (Gd-DTPA) (0.025 mmol/kg) was injected through a right atrial catheter. Regional absolute myocardial blood flow in ml/min per g of tissue was quantified independently from the MR measurements with radioisotope-labeled microspheres. Region of interest (ROI) residue curves were analyzed with a multipath, spatially distributed model (2), and the parameters for blood flow, vascular volume, and leakage was optimized by least-squares minimization.

Results: Blood flows covered a range from 0.05 to 3.0 ml/min/g. The coefficient of variation for the differences between MR and microsphere data in 175 ROIs averaged 0.33 ± 0.13. MR measurements agreed with microsphere data (slope of 1.12 and correlation coefficient of $r = 0.82$).

Conclusions: Myocardial blood flow can be determined noninvasively with rapid first-pass imaging and an extracellular contrast agent. Signal enhancement during the first pass allows distinction between blood flow and transcapillary leakage of the extracellular contrast agent.

References

1. Jerosch-Herold M, Wilke N. MR first pass imaging: Quantitative assessment of transmural perfusion and collateral flow. Int. J. Cardiac Imaging, 1997; 13:205–218.
2. Bassingthwaighte JB, Chan IS, Wang CY, King RB. MMID4—multi-path, multi-indicator dilution, 4-region model (XSIM Version: 2.07). National Simulation Resource, Seattle; 1997.

Advantage of GD-Enhanced MRI in Leakage Detection After Composite Graft Replacement of the Ascending Aorta

R. Fattori, B. Descovich, F. Celletti, G. Napoli, P. Bertaccini, A. Pierangeli, G. Gavelli. *Institute of Radiology and Cardiac Surgery, University of Bologna, Italy*

Objective: Composite graft replacement of the ascending aorta may have a high risk of leakage and false aneurysm formation, mostly related to the reimplanted coronary arteries (1,2). The purpose of this study was to assess the value of magnetic resonance imaging (MRI) in the detection of postoperative complications after composite graft insertion.

Methods: Fifty-two patients underwent MRI follow-up (0.5–200 months) after composite graft replacement of the ascending aorta (22 for dissection, 30 for aneurysm). In all patients, prosthetic aortic segment, distal and proximal anastomosis, morphology, and diameter of the reimplanted coronary arteries were evaluated by spin-echo and gradient-echo sequences. In case of abnormal perigraft thickening (3), an additional spin-echo sequence was performed after gadolinium injection.

Results: The proximal portion of both reimplanted coronary arteries was visualized in 50 patients and was moderately dilated in five cases. Normal postoperative perigraft thickening (≤10 mm) was observed in 41 patients. Eleven patients showed a periprosthetic thickening ranging from 15 to 52 mm. Gadolinium-enhanced MRI demonstrated a leackage in five patients. The lack of enhancement excluded the presence of bleeding in the remaining six patients (three chronic hematomas, one perioperative bleeding, one infection, and one case of granulation tissue). These findings were confirmed at surgery or by subsequent MRI follow-up exams.

Conclusion: MRI was demonstrated to be an optimal imaging modality to evaluate the morphology of composite grafts and reimplanted coronary arteries. With the use of gadolinium, MRI represents a simple, accurate, and noninvasive method to detect a leakage, requiring urgent reoperation.

References

1. Kouchoukos NT, Marshall WG, Wedige-Stecher TA. Eleven-year experience with composite graft replacement of the ascending aorta and aortic valve. Thorac. Cardiovasc. Surg., 1986; 92:691–705.
2. Svensson LG. Approach to the insertion of composite valve graft. Ann. Thorac. Surg., 1992; 54:376–378.
3. Gaubert JY, Moulin G, Mesana T, Chagnaud C, Caus T, Delannoy L, Blin D, Bartoli JM, Kasbarian M. Type A dissection of the thoracic aorta: Use of MR imaging for long-term follow-up. Radiology, 1995; 196:363–369.

MR Breathhold Flow Measurement in Venous and Arterial Coronary Grafts: Comparison with Intraoperative Doppler Measurement

T. Voigländer,[1] K.-F. Kreitner,[2] M. Dahm,[3] T. Wittlinger,[1] P. Kalden,[1] C. Frick,[1] J. Meyer,[1] W. Nitz.[4] [1]*2nd Medical Clinic,* [2]*Clinic for Radiology, and* [3]*Clinic for Heart Surgery, University of Mainz, Germany;* [4]*Siemens, Erlangen, Germany*

Recently, noninvasive evaluation of coronary bypass grafts using MR angiography has been reported. MR flow measurement in venous and arterial coronary grafts provides an important contribution to morphological assessment (1,2). The aim of this study was to evaluate the reliability of breathhold MR flow measurement early after coronary bypass grafting, comparing it with the results of the intraoperatively performed Doppler measurement.

Methods: In 21 patients (mean age 57 yr, range 43–78 yr) with 12 internal mammarial grafts (IMA) and 13 venous grafts (VG), flow was measured intraoperatively using the transit time Doppler (TTF) method (Cardio Med., Norway, one measurement/4 ms). MR flow measurement (Siemens Vision, 1.5 T) was performed after 8 ± 3 days. After visualization of the course of the bypass grafts (HASTE, seven to nine slices, breathhold, acquisition time 10–15 s), flow measurements (phase-change technique, breathhold, TR 110–125 ms) perpendicular to the course of the grafts were performed.

Results: All grafts evaluated intraoperatively were visualized by MR, and flow measurement could be performed. The mean flow for VG and IMA was not significantly different.

	Mean Flow/min		
	All (n = 25)	VG (n = 12)	IMA (n = 13)
TTF (ml/min)	44.91 ± 26.6	47.84 ± 29.65	41.73 ± 23.91
MR (ml/min)	45.37 ± 26.84	50.52 ± 30.98	39.8 ± 21.43
r value	0.81	0.80	0.83

Conclusion: MR flow measurement in coronary grafts correlated well with intraoperatively derived mean flow values. The prerequisite for these promising results is optimized MR flow measurement after visualization of the bypass course by HASTE sequence.

References

1. Sakuma H. Breath-hold MR measurement of blood flow velocity in internal mammary arteries and coronary bypass grafts. JMRI, 1996; 1: 219–222.

2. Van Rossum. The role of MR in the evaluation of functional results after CABG/PTCA. Int. J. Cardiac Imaging, 1993; 9:59–69.

MR Assessment of Blood Flow and Flow Reserve in Internal Mammary Artery Graft

H. Sakuma,[1] N. Kawada,[1] K. Takeda,[1] B.P. Cruz,[1] I. Yada,[1] C.B. Higgins.[2] [1]*Tsu, Mie, Japan;* [2]*San Francisco, CA*

Purpose: We assessed the internal mammary artery (IMA) graft function by measuring the flow pattern and vasodilator flow reserve using fast-velocity-encoded cine (VEC) MR imaging.

Methods: Eleven patients who had undergone IMA graft surgery and 13 healthy volunteers were studied. The time interval between IMA bypass graft surgery and MR imaging was 24.6 ± 11.0 days (mean ± SD). Selective x-ray angiography of the IMA graft was performed in all patients. Fast VEC MR images were acquired on imaging planes that were perpendicular to the vessels within a single breathhold time using k-space segmentation (TR/TE 14/5 ms, VENC ±1 m/s). Fast VEC MR images of the IMA grafts were obtained in the basal state and after administration of dipyridamole. In five healthy volunteers, flow measurement in the native IMA was performed in the basal state. Flow velocities in the native coronary artery were assessed in the basal state and after dipyridamole injection in eight healthy volunteers.

Results: The IMA graft was patent at x-ray angiography in all patients. Graft flow was characterized by a biphasic forward-flow pattern, with one peak in early systole and another in early diastole. In nine patients without graft stenosis, the diastolic/systolic peak velocity ratio in the IMA graft was 2.17 ± 0.30, which was significantly higher than that in the native IMA in healthy volunteers (0.23 ± 0.02, $p < 0.01$). In early postoperative state, the CFR ratio in the nonstenotic IMA grafts (1.67 ± 0.17) was lower than the normal CFR ratio in the native coronary artery (3.11 ± 0.48, $p < 0.01$). VEC MRI showed a decrease in the diastolic flow in two patients with stenotic IMA grafts.

Conclusions: Fast VEC MR imaging is a noninvasive technique that can provide assessment of the functional adequacy of the IMA to coronary artery bypass grafts.

Analysis and Display of Phase-Contrast Data by Computational Fluid Dynamics Methods

B.R. Cowan, G.D. Mallinson. *Auckland, New Zealand*

Computational fluid dynamics (CFD) is the discipline concerned with the prediction of fluid motion by numerical solution of the fundamental equations of physics. These techniques have found wide application in areas such as flow over aircraft, around yacht keels, and in many industrial processes. In clinical applications where vessels are curved in a complex manner such as the aortic arch, clustered in a complex way as is commonly found in congenital heart disease or blood flow has a complex structure as may be encountered at the site of a stenosis, good visualization is essential. It is advantageous to obtain a three-dimensional velocity data set and to be able to view and analyze it in a single animated display format. Phase-contrast MR imaging (PCI) produces images containing a rectangular grid of velocity data that is similar in many respects to the output from CFD solutions. The aim of this study was to develop a visualization package based on CFD techniques that would accept four-dimensional PCI data and analyze and display these data in an intuitive and clinically useful format. PCI data containing multiple slices, each acquired with three orthogonal velocity sensitizing directions and gated over the cardiac cycle, were automatically read from storage into the software and the header information used to assemble the data correctly. Although still evolving in response to clinical need, current capabilities include maps of vectors indicating the direction (as a three-dimensional projection) and speed (by length and/or colour) of flow; simultaneous displays of single or multiple image planes, which may also be time varying or interpolated; calculated streamlines that indicate the path taken by a notional red blood cell; time varying absolute speed plots at interactively user defined location; and flow rates through user-defined regions of interest.

Visualization results are presented for a 20-year-old man who underwent surgery for coarctation of the aorta at 6 months of age. Five parasagittal slices were obtained to encompass the ascending arch and descending aorta. An asymmetrical jet of blood is demonstrated at the site of the repair with a peak velocity of 2.0 m/s. Because of the three-dimensional nature of the software, it was possible to display the data in any plane and to systematically investigate the three-dimensional nature of the flow. Finally, quantitative flow rates, velocity information, and streamlines representing the path of notional red cells were extracted at representative locations in the data set. The results presented demonstrate the utility of the application of computational fluid dynamics flow visualization approaches to the display and analysis of complex three-dimensional PCI data sets.

MR Assessment of Myocardial Viability

Christopher M. Kramer. *Allegheny University of the Health Sciences, Allegheny General Hospital, Pittsburgh, PA*

I. Definitions of viability
  A. Normal resting function
  B. Normal thallium uptake
  C. Normal FDG uptake
  D. Normal dobutamine response
II. Viability in acute myocardial infarction
  A. Contrast-enhanced MRI
    1. First-pass imaging
      i. Hypoenhancement—delayed wash-in of contrast
    2. Delayed imaging
      i. Hypoenhancement—represents part of the no-reflow zone, little functional return
      ii. Hyperenhancement—delayed wash-out of contrast, larger than infarct zone, some functional return
      iii. Combinations of enhancement patterns
    3. ^{23}Na imaging, T2 imaging
  B. Dobutamine MRI
    1. Cine MRI—compared with dobutamine echo
    2. MR tagging
III. Viability in chronic ischemic heart disease
  A. Contrast-enhanced MRI—rate of enhancement
  B. Dobutamine MRI
    1. Compared with FDG-PET
    2. Compared with dobutamine echo and TEE

1. Acute myocardial infarction

A. Contrast-enhanced MRI

Saeed M, Wendland MF, Yu KK, Lauersma K, Li H-T, Derugin N, Cavagna FM, Higgins CB. Identification of myocardial reperfusion with echo planar magnetic resonance imaging: Discrimination between occlusive and reperfused infarctions. Circulation, 1994; 90: 1492–1501.

Yakota C, Nonogi H, Miyazaki S, Miyazaki S, Goto Y, Maeno M, Daikoku S, Itoh A, Haze K, Yamada N. Gadolinium-enhanced magnetic resonance imaging in acute myocardial infarction. Am. J. Cardiol., 1995; 75:577.

Lima JAC, Judd RM, Bazille A, Schulman SP, Atalar E, Zerhouni EA. Regional heterogeneity of human myocardial infarcts demonstrated by contrast enhanced MRI: Potential mechanisms. Circulation, 1995; 92:1117–1125.

Judd RM, Lugo-Olivieri CH, Arai M, Kondo T, Croisille P, Lima JAC, Mohan V, Becker LC, Zerhouni EA. Physiological basis of myocardial contrast enhancement in fast magnetic resonance images of two-day-old reperfused canine infarcts. Circulation, 1995; 92:1902–1910.

Pinto I, Pavanello R, Abizaid A, Piegas L, Abib MH, Barbosa M, Romano E, Egito E, Barreto R, Sousa A, Sousa E. Predictors of left ventricular function recovery after an acute myocardial infarction by magnetic resonance imaging. Circulation, 1995; 92:I-509 (abstract).

Kim RJ, Chen EL, Lima JAC, Judd RM. Myocardial Gd-DTPA kinetics determine MRI contrast enhancement and reflect the extent and severity of myocardial injury after acute reperfused infarction. Circulation, 1996; 94:3318–3326.

Rogers WJ, Kramer CM, Geskin G, Hu Y-L, Theobald TM, Petruolo SM, Reichek N. Contrast enhanced MRI early after reperfused MI predicts late functional recovery. Circulation, 1996; 94:I-541 (abstract).

Pereira RS, Prato FS, Wisenberg G, Sykes J. The determination of myocardial viability using Gd-DTPA in a canine model of acute myocardial ischemia and reperfusion. Magn. Reson. Med., 1996; 36:684–693.

Kim RJ, Lima JAC, Chen E-L, Reeder SB, Klocke FJ, Zerhouni EA, Judd RM. Fast ^{23}Na magnetic resonance imaging of acute reperfused myocardial infarction: Potential to assess myocardial viability. Circulation, 1997; 95:1877–1885.

Asanuma T, Tanabe K, Ochiai K, Yoshitomi H, Nakamura K, Murakami Y, Sano K, Shimada T, Murakami R, Moriaka S, Beppu S. Relationship between progressive microvascular damage and intramyocardial hemorrhage in patients with reperfused anterior myocardial infarction. Circulation, 1997; 96:448–453.

B. Dobutamine MRI

Dendale PAC, Franken PR, Waldman G-J, De Moor DGE, Tombeur DAM, Block PFC, De Roos A. Low-dosage dobutamine magnetic resonance imaging as an alternative to echocardiography in the detection of viable myocardium after acute infarction. Am. Heart J., 1995; 130:134–140.

Shigeru W, Isao S, Miharu U, Yasuyoshi H, Toshihis I, Yamamoto T, Yoshiaki I, Hitoshi I, Akira M, Yoshiaki. Detection of viable myocardium by tagging with magnetic resonance imaging during dobutamine infusion in patients with acute myocardial infarction. Circulation, 1996; 94:I-540 (abstract).

Kramer CM, Geskin G, Rogers WJ, Theobald TM, Hu Y-L, Reichek N. Assessment of myocardial viability after reperfused first infarction by low dose dobutamine MR tagging. Proc. Int. Soc. Magn. Res. Med., 1997, 387 (abstract).

2. Chronic myocardial ischemia

A. Contrast-enhanced MRI

Lauersma K, Virtanen KS, Sipila LM, Hekali P, Aronen HJ. Multislice MRI in assessment of myocardial perfusion in patients with single-vessel proximal left anterior descending coronary artery disease before and after revascularization. Circulation, 1997; 96:2859–2867.

B. Dobutamine MRI

Baer FM, Voth E, Schneider CA, Theissen P, Schicha H, Sechtem U. Comparison of low-dose dobutamine gradient-echo magnetic resonance imaging and positron emission tomography with [^{18}F]-fluorodeoxyglucose in patients with chronic coronary artery disease. Circulation, 1995; 81:1006–1015.

Sayad DE, Willett DL, Hundley WG, Grayburn PA, Peshock RM. Dobutamine magnetic resonance imaging with myocardial tagging predicts quantitative improvement in regional function after revascularization. Circulation, 1995; 92:I-507 (abstract).

Cubukcu AA, Ridgway JP, Sivananthan UM, Cooke A, Nair UR, Tan LB. Detection of contractile reserve by tagged cine MRI during low-dose dobutamine infusion. Circulation, 1995; 92:I-509 (abstract).

Baer FM, Voth E, LaRosee K, Schneider CA, Theissen P, Deutsch HJ, Schicha H, Erdmann E, Sechtem U. Comparison of dobutamine transesophageal echocardiography and dobutamine magnetic resonance imaging for detection of residual myocardial viability. Am. J. Cardiol., 1996; 78:415–419.

Isao S, Shigeru W, Yoshiaki M. Detection of hibernating myocardium with dobutamine stress MRI by automatic trace method. Proc. Int. Soc. Magn. Res. Med., 1997; 897 (abstract).

Methods and Clinical Importance of Magnetic Resonance Imaging in the Diagnosis of Coronary Bypass Grafts

T. Wittlinger,[1] T. Voigtländer,[1] K.F. Kreitner,[2] P. Kalden,[2] K. Grauvogel,[1] M. Thelen,[2] J. Meyer.[1] [1]*2nd Medical Clinic and Policlinic and* [2]*Department of Radiology, University Clinic, Mainz, Germany*

The aim of this study was to evaluate the reliability of magnetic resonance imaging (MRI) in the assessment of coronary bypass grafts, we investigated 44 patients with a total of 113 bypass grafts. With 87 venous and 26 arterial bypasses (IMA). Target vessel was in 41 cases the LAD, in 26 cases the RCA, in 8 cases the RCX, and in 38 cases side branches of the LAD or RCX. MRI (1.5 T Vision, Siemens AG, Erlangen) was performed using a multislice, electrocardiogram-gated, T2-weighted breathhold turbo spin-echo sequence (HASTE), a 3D angiography sequence with navigator echo-based respiratory gating (NAVIGATOR), and a 3-D contrast-agent-enhanced angiography sequence (FISP). Standardized scan directions consisted of axial scans, long axis views parallel to the interventricular septum, and of tangential scans directed to the anterior wall of the left ventricle simulating the 50° left anterior oblique view of the coronary angiography. After MRI in all patients, coronary angiography was performed within 1 week. The HASTE-sequence served as a fast orientation of the vessel course and as basis for planning flow quantitative measurements. A feature of the 3D angiography in navigator technique is the registration of the diaphragm of the free-breathing patient. The FISP angiography sequence is characterized by short repetition and echo times. This sequence allows an investigation time of 25–32 seconds the imaging of the proximal anastomosis and of the vessel course and of the distal anastomosis in about 80% of the cases.

Results:

Sequence	Sensitivity	Reliability	Pos. Prognostic Value
HASTE	92%	97%	97%
NAVIGATOR	82%	87%	100%
3D and contrast media	92%	94%	100%

These results show that coronary bypass grafts can reliably be detected using MRI. A total imaging of the vessel course is possible in most cases by combining different investigation techniques. The distal anastomosis can be detected in 80% of the bypass grafts.

References

1. Pennel DJ, Bogren HG, Keegan J, Firmin DN, Underwood SR. Assessment of coronary artery stenosis by magnetic resonance imaging. Heart, 1996; 127–133.

2. Buser PT, Higgins CB. Coronary artery graft disease: Diagnosis of graft failure by magnetic resonance imaging. In: Lüscher TF, Turina M, Braunwald E eds. Coronary Artery Graft Disease: Mechanisms and Prevention. Berlin: Springer Verlag; 1994: 99–112.

3D Coronary Imaging with Phase Reordering for Optimal Scan Efficiency

P. Jhooti, J. Keegan, P.D. Gatehouse, A.M. Taylor, S. Collins, D.N. Firmin. *Magnetic Resonance Unit, Royal Brompton Hospital, London, UK*

3D coronary imaging techniques are limited by long acquisition times and respiratory motion artifacts. The purpose of this study was to investigate the potential of applying phase encode reordering to 3D segmented acquisitions to allow larger navigator acceptance windows to be used to reduce the acquisition time while retaining image quality.

Methods: The mapping algorithm used was based on the hybrid ordered phase encoding method. This method, which was developed for 2D imaging, has shown to be reliable and robust against variable respiratory patterns and patient motion. The reordering method uses a 10-mm window with the most frequent 5-mm range of positions used for the central 50% of k-space. The method was compared with the acceptance rejection algorithm (ARA) using a window of 5 mm, the diminishing variance algorithm (DVA) with its scan time set to that of the phase reordered scan, and retrospective respiratory gating (RRG). To test the methods in vitro, a specially designed coronary phantom was built. In vivo studies were also carried out in 10 volunteers.

Results/Discussion: Studies in vitro have shown the method to produce a consistent image quality that was comparable or better than the other methods, with a considerable increase in scan efficiency. Results in vivo are also very promising. Statistical analysis of image quality showed no significant difference between phase reordering and ARA ($p = 0.85\%$). However, a significant improvement was observed between phase reordering and both DVA ($p = 0.03$) and RRG ($p = 0.03$). For scan efficiency, analysis showed a significant improvement between the phase reordering method and both ARA (72% vs. 48% respectively, $p < 0.001$) and RRG (72% vs. 20% respectively, $p < 0.001$).

Conclusion: The method presented improves image quality while maintaining a short acquisition time, compared with other currently applied respiratory compensation methods.

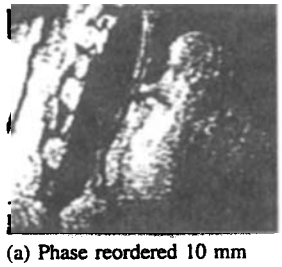

(a) Phase reordered 10 mm (efficiency = 73%)

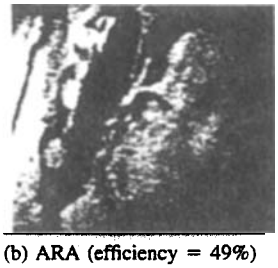

(b) ARA (efficiency = 49%)

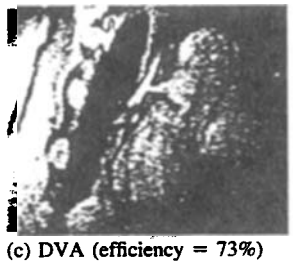

(c) DVA (efficiency = 73%)

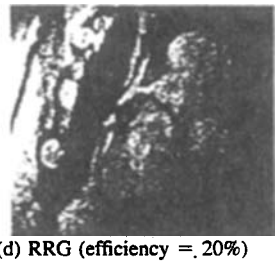

(d) RRG (efficiency = 20%)

Magnetic Resonance Angiography of Coronary Arteries with Gadolinium Enhancement

J. Zheng, D. Li, K.T. Bae, E.M. Haacke. *St. Louis, MO*

Purpose: We evaluated the feasibility of magnetic resonance (MR) imaging of coronary arteries during first pass of gadolinium injection.

Methods: A three-dimensional (3D) segmented gradient-echo sequence was developed to image the coronary arteries within a single breathhold (TR 4 ms, flip angle 25° data acquisition matrix 124 × 256, FOV 140 × 300 × 16 mm^3, breathhold time 30 s). ECG triggering was used to minimize cardiac motion. An anterior-posterior four-element phased array coil was used as the signal receiver, and the two posterior elements were turned off to avoid wrap-around artifacts when a small rectangular FOV was used. Every subject was first given a test bolus to determine the time of peak enhancement. Based on our experience, a delay of 10 s was expected between peaks of test bolus and a 20-s full-dose injection. A 35-ml gadolinium-DTPA contrast agent was then injected over 20 s and the 3D MR angiography sequence was initialized

at a predetermined time so that the central k-space of data acquisition coincided with the peak concentration of gadolinium. Ten volunteers were studied.

Results: Roughly 1 × 1 mm² in-plane resolution was achieved with this segmented 3D sequence. Signal-to-noise ratio and contrast-to-noise ratio were dramatically improved by injection of gadolinium. The figure shows pre- and postcontrast images of a right coronary artery in a double oblique section from one subject.

Conclusion: Gadolinium-enhanced MR angiography improved the visualization of coronary arteries and may have potential utility to better detect coronary artery stenoses.

Precontrast

Postcontras

Real-Time Navigator Gated and Corrected Three-Dimensional Coronary Magnetic Resonance Angiography Using T2 Preparation Prepulses for Contrast Enhancement

R.M. Botnar, M. Stuber, K.V. Kissinger, P.G. Danias, W.J. Manning. *Boston, MA*

Coronary arteries are subject to cardiac and respiratory motion, which limits the spatial resolution of breathhold coronary MRA. 2D selective navigator pulses can be used for respiratory gating and/or correction to allow for free-breathing coronary MRA (1–3). Despite motion artifacts, the contrast behavior between blood, cardiac muscle, and epicardial fat is crucial for proper visualization of the coronary arteries. Fat signal is usually suppressed using a frequency selective prepulse. However, coronary arteries may be embedded or rest adjacent to cardiac muscle that T1 relaxation time is close to blood. Therefore, a series of T2 preparation prepulses was applied to suppress signal of cardiac muscle (5).

Methods: Five healthy adult subjects were examined in the supine position with a real-time respiratory navigator gated/corrected and ECG-gated 3D TFE imaging sequence. All measurements were performed on a 1.5-T Philips Gyroscan ACS/NT MR scanner (Philips Medical Systems, Best, The Netherlands) using a five-element phased array research cardiac coil. Imaging parameters were FOV 360 × 305 mm², matrix 512 × 304, slice thickness 3 mm, resulting in an in-plane resolution of 0.7 × 1.0 mm² and volume coverage of 30 mm. The scan time was approximately 10–20 min. To shorten the acquisition window and to minimize flow artifacts, TR as the TE were set to their minimum values. Inflow was enhanced by acquiring data at middiastole (trigger delay 500–600 ms), a period of minimal cardiac motion, and rapid coronary flow. Before the 2D selective navigator pulse and before the frequency selective fat suppression prepulse, T2 preparation was performed using a series of nonselective 90°, 180°, 180°, 180°, 180°, and 90° prepulses.

Results: All five subjects were examined successfully without any evidence of respiratory motion artifacts, which allowed visualization of the proximal and midportions of the LAD and the LCX. Without T2 preparation, cardiac muscle and blood had a similar signal level. In all cases, application of T2 preparation prepulses helped to reduce signal of cardiac muscle, yielding an improved contrast behavior between coronary blood and cardiac muscle. The efficiency of the T2 preparation prepulses could be improved by lowering the acquisition window from 120 to 60 ms.

Conclusions: The application of a respiratory navigator together with a short acquisition window of 60 ms allows acquisition of respiratory artifact free images. T2 preparation prepulses improve the contrast between the coronary arteries and cardiac muscle, which is crucial for proper visualization of the left coronary arteries. Further improvements toward a higher resolution have to overcome the limited signal-to-noise ratio of a noncontrast agent sequence.

References

1. Ehman RL, Felmlee JP. Radiology, 1989; 173:255–263.
2. Danias PG, et al. Radiology, 1997; 203:733–736.
3. McConnell MV, et al. Magn. Reson. Med., 37: 148–152.
4. Wang Y, et al. Magn. Reson. Med., 1995; 33:713–719.
5. Brittain JH, et al. Magn. Reson. Med., 1995; 33:689–696.

Real-Time Interactive Non–Breathheld Coronary MRA Using Three-Dimensional Diminishing Variance Algorithm

T. Sachs, C. Meyer, J. Pauly, D. Nishimura, A. Macovski. *Stanford, CA*

Respiratory motion remains a major challenge to overcome in coronary MRA (1). Cardiac-triggered breathheld exams are possible but require substantial patient cooperation. We present a real-time technique, the interactive three-dimensional diminishing variance algorithm (DVA), which allows MR imaging of the coronary arteries without the use of breathholds. The DVA uses navigator echoes to measure organ displacement due to respiration. Three orthogonal navigators are acquired close in time to a spiral interleaf image acquisition. After each interleaf is acquired, displacements are calculated in real-time from each of the navigator echoes using a cross-correlation technique. These displacements are stored in histograms during the first pass through the scan. After one complete pass through the scan, a reacquisition interval begins, starting with the spiral interleaf whose measured displacements are furthest from the most common position as determined from the histograms. The histograms are then updated, and this process is repeated until all the measured displacements fall within a specified range or until the user interactively stops the scan. At this point, the data set consists of interleaves acquired from as stationary a respiratory position as possible given the scan time constraints. To interact with the DVA during a scan, a Java graphical user interface (GUI) was designed. In addition to starting and stopping the scan, the GUI controls navigator placement and DVA parameters. Real-time position plots and histograms are displayed for each of the navigator echoes. An image display window shows an updated image every 3 s during the reacquisition interval, so that the user can stop the scan when suitable image quality is achieved. Results obtained using the interactive 3D DVA have consistently shown dramatic reduction in motion artifacts over the course of a reacquisition interval. With this technique, delineation of coronary arteries on normal volunteers has routinely been achieved.

Reference

1. Ehman R. Influence of physiological motion on the appearance of tissue in MR. Radiology, 1986; 159:777–782.

Evaluation of Reactive Hyperemic Response in the Leg by MR Velocity Mapping

E.M. Pedersen, A. Lombardi, J. Laustsen. *Aarhus, Denmark*

With the increased use—and concurrent decrease in examination time—of peripheral MR-angiography, it is becoming realistic to establish MR-based techniques for hemodynamic evaluation along with angiography. It was the aim of this study to explore the feasibility of establishing a setup for creating and measuring the reactive hyperemic response in the leg by use of fast MR phase velocity mapping techniques. Nonmagnetic pressure cuffs were placed around both thighs in nine young volunteers. After initial baseline left common femoral flow measurements, the cuff around the left thigh was pressurized with 300 mm Hg for 4 min. After the first 3 min the opposite cuff was also pressurized to prevent any "steal phenomenon" when the left cuff was released. Immediately after release, a series of 10 common femoral flow measurements were performed immediately after each other. The cuff on the right leg was then released, and finally measurements were performed 5 and 10 min after release of the left cuff. Measurements were performed on a Philips Gyroscan NT 1.5-T scanner using cardiac patch release five (CPR5) software and an 8-cm circular surface coil. Initially, a standard gradient-echo flow measurement with NSA 2, FOV 128 mm, matrix 128 mm, and TR 30 ms was performed as a reference measurement in the left common femoral artery 4–6 cm proximal to the femoral bifurcation. For the rest of the flow measurements, a hybrid segmented k-space technique with EPI readouts (TFEPI) was used at the same location. The parameters were TE 8–9.5 ms, HPI 34–36 ms, ST 10 mm, rectangular FOV 40%, FOV 192 × 237 mm, matrix 128, EPI factor 3, giving a total measurement time of 14 heart beats for each flow measurement. Central k-space was acquired first. V_{max} was 100 cm/s for the "before" scan and 200 cm/s for the scans after cuff pressure release. Phase correction and manual segmentation were performed off-line using dedicated software. The reference FFE scans and the TFEPI scan taken immediately after revealed correlation with mean difference of 0.0% and 95% confidence limits of ±4%. In all nine volunteers, consistent quality measurements were obtained with the TFEPI sequence both before, during, and after pressurizing the cuff. In Figure 1 the flow and heart rate parameters from before to 10 min after induction of reactive hyperemia are shown. Please note the delayed peak in heart rate relative to the peak flow, the fast decrease in flow, and the high minimum (and thus high end diastolic) flows in the first 14 heart beats nearly reaching the same level as peak flow before reactive hyperaemia ("before"). This study demonstrated that the TFEPI sequence is capable of providing consistent, fast, and accurate flow measurements in the femoral artery. The reactive hyperemia situation was easy to induce and control in the scanner, and the hyperemic response was shown to diminish very fast, emphasizing the need for fast flow measurements. Data from the literature suggest that patients have a lower hyperemic flow and a prolonged response, thus making the volunteers an extreme situation. In conclusion, it seems realistic to develop an objective MR-based hemodynamic stress test in the leg.

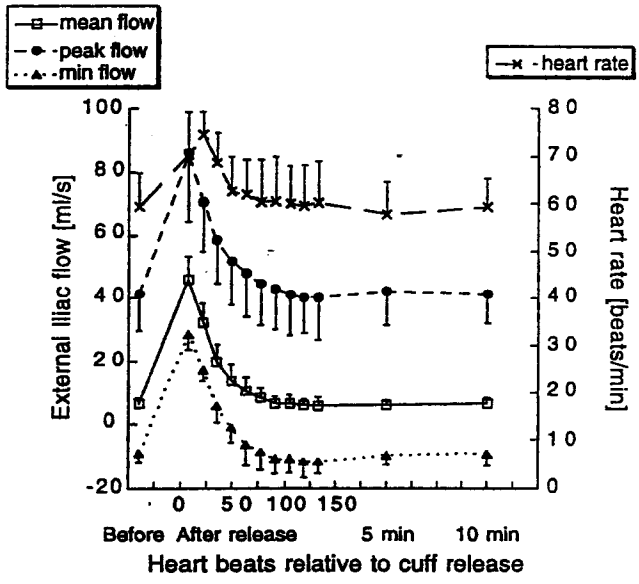

Figure 1. Reactive hyperemic common femoral flow with standard deviations

Improved Coronary Visualization Using a Slow Infusion of Low-Molecular-Weight Gadolinium

W.J. Rogers, C.M. Kramer, N. Reichek. *Pittsburgh, PA*

Three-dimensional navigator echo coronary imaging methods have improved the evaluation of proximal coronary arteries by eliminating the need for breathholding. However, available signal is still too low to

permit spatial resolution of an order that is clinically required. Gadolinium-based contrast agents improve signal by means of their T1 shortening effect. Because of the extended acquisition period, often as long as 10 min, and the extravascular fate of currently approved contrast agents, effective coronary signal enhancement has not been achieved. The purpose of the current study was to evaluate the combined use of slow regulated gadolinium administration with centric ordered 3D navagator coronary acquisition as a means of improving coronary signal. Eight volunteers (three male, mean age 31 ± 2 yr) without evidence of coronary disease were imaged on a Siemens 1.5-T scanner. An axial 3D volume was positioned to cover the proximal coronary arteries with acquisition timed to late diastole. 1D data were acquired along the inferior-superior direction in the region of the right hemidiaphragm. Data were saved only when diaphagm position was within a predefined ±1 pixel window and the cardiac cycle was in late diastole. Image parameters included 24 partitions, variable flip angle, band width 244, centric k-space ordering, TR 230 ms, TE 2.7 ms, FOV 250 × 250 mm, 128 phase lines, 256 frequency lines. After acquisition of a 3D baseline set, infusion of 20 ml of Magnavist (Berlex Laboratories, Wayne, NJ) was started at a rate of 0.1 ml/s using a Spectris MR power injector (Medrad, Pittsburgh, PA). 2D short-axis flow compensated segmented (7 segs/RR) images were acquired to track myocardial and LV blood pool signal enhancement (see graph). Regions of interest were placed within the LV cavity and myocardium and normalized to a subcutaneous fat region. Peak blood enhancement was 147% of baseline and occurred 4 min after infusion was started. Peak myocardial enhancement was 165% also at 4 min. Visual assessment of 3D coronary images showed that six volunteers displayed moderate coronary enhancement and two displayed dramatic enhancement. Thus, slow metered infusion of low-molecular-weight gadolinium produces significant extended blood signal enhancement that when combined with centric acquisitions may improve visualization of coronary arteries during non–breathhold imaging.